1969

Load distribution in simply supported concrete box girder highway bridges

James Grant Arendts
Iowa State University

LOAD DISTRIBUTION IN SIMPLY SUPPORTED CONCRETE BOX GIRDER HIGHWAY BRIDGES

by

James Grant Arendts

A Dissertation Submitted to the
Graduate Faculty in Partial Fulfillment of
The Requirements for the Degree of
DOCTOR OF PHILOSOPHY

Major Subject: Structural Engineering

Approved:

Signature was redacted for privacy.

In Charge of Major Work

Signature was redacted for privacy.

Head of Major Department

Signature was redacted for privacy.

Dean of Graduate College

Iowa State University
Ames, Iowa

1969

TABLE OF CONTENTS

SYNOPSIS

A method is presented for the complete determination of forces, moments, and deflections in simply supported concrete box girder highway bridges due to externally applied vertical loads. The method is used for a behavioral study of a representative sample of structures whose geometries conform to those found in commonly built bridges. The results of the behavioral study are used to illustrate the range of internal force quantities and deflections that may be expected for these structures. In addition, recommendations are made concerning the use of different bridge geometric configurations to optimize the distributions of the force quantities and deflections.

NOTATION

a	Half of the width of the structure
A_{in}, A_{in}'	Constants used in the solution of the governing equations
da	Differential element of area
B	Denotes integration around the entire boundary of the equivalent plate
b	Half of the span of the structure
B_{in}, B_{in}'	Constants used in the solution of the governing equations
c	Longitudinal position of applied load
C_{in}, C_{in}'	Constants used in the solution of the governing equations
D	Flexural rigidity of the equivalent plate
d	Depth of the actual structure from the center of the top flange to the center of the bottom flange
D_y	Measure of the shearing rigidity of the equivalent plate
E	Modulus of elasticity of the structure
e	Distance of the applied load from the centerline of the structure
f	Half of the width of the applied load
F_{in}, F_{in}'	Constants used in the solution of the governing equations
G	Modulus of rigidity of the structure
G_y	Shearing rigidity of the equivalent plate in the transverse direction
h	Depth of the core media for the equivalent plate

H_n Fourier constant for the loading function

I_e Total moment of inertia of an exterior beam element

I_i Total moment of inertia of an interior beam element

I_w Moment of inertia per unit width of a web plate

K_w Stiffness constant of a unit width of web plate

L Total span of the structure

ℓ_i Limit of integration used in the evaluation of coefficients per beam

M_{in}, M_{in}' Constants used in the solution of the governing equations

M_x Longitudinal bending moment per unit width used in the derivation of the governing equations

M_{xa} Longitudinal bending moment per unit width of the cylindrically bent plate

M_{xi} Longitudinal bending moment per unit width of the equivalent plate

M_{xy} Twisting moment per unit width used in the derivation of the governing equations

M_{xyi} Twisting moment per unit width of the equivalent plate

M_y Transverse bending moment per unit length used in the derivation of the governing equations

M_{yi} Transverse bending moment per unit length of the equivalent plate

$\bar{M}_{xb}, \bar{M}_{xb_k}$ Longitudinal bending moment coefficient per beam

$\bar{m}_{xb_{kn}}$ Y dependent part of the longitudinal bending moment coefficient per beam

$\bar{M}_x$, $\bar{M}_{xi}$ Longitudinal bending moment coefficient per unit width

$\bar{m}_{xin}$ Y dependent part of the longitudinal bending moment coefficient per unit width

$\bar{M}_{xyb}$, $\bar{M}_{xyb_k}$ Twisting moment coefficient per beam

$\bar{m}_{xyb_{kn}}$ Y dependent part of the twisting moment coefficient per beam

$\bar{M}_{xy}$, $\bar{M}_{xyi}$ Twisting moment coefficient per unit width

$\bar{m}_{xyin}$ Y dependent part of the twisting moment coefficient per unit width

$\bar{M}_y$, $\bar{M}_{yi}$ Transverse bending moment coefficient per unit length

$\bar{m}_{yin}$ Y dependent part of the transverse bending moment coefficient per unit length

N Number of girders in the actual structure

N_{bl} Left bottom normal flange force

N_{br} Right bottom normal flange force

N_{in}, N_{in}' Constants used in the solution of the governing equations

N_{tl} Left top normal flange force

N_{tr} Right top normal flange force

$\vec{n}_x$ X component of the outward directed unit normal vector on the boundary of the equivalent plate

$\vec{n}_y$ Y component of the outward directed unit normal vector on the boundary of the equivalent plate

$p(x,y)$, p Arbitrary load intensity acting on the equivalent plate

$q(c)$ Specific load intensity acting on the equivalent plate

Q_x Longitudinal shearing force per unit width used in the derivation of the governing equations

Q_{xa} Longitudinal shearing force per unit width of the cylindrically bent plate

Q_{xi} Longitudinal shearing force per unit width of the equivalent plate

Q_y Transverse shearing force per unit length used in the derivation of the governing equations

Q_{yi} Transverse shearing force per unit length of the equivalent plate

$\overline{Q}_{xb}$, $\overline{Q}_{xb_k}$ Longitudinal shearing force coefficient per beam

$\overline{q}_{xb_{kn}}$ Y dependent part of the longitudinal shearing force coefficient per beam

$\overline{Q}_x$, $\overline{Q}_{xi}$ Longitudinal shearing force coefficient per unit width

$\overline{q}_{xin}$ Y dependent part of the longitudinal shearing force coefficient per unit width

$\overline{Q}_y$, $\overline{Q}_{yi}$ Transverse shearing force coefficient per unit length

$\overline{q}_{yin}$ Y dependent part of the transverse shearing force coefficient per unit length

R Denotes integration over entire horizontal area of the equivalent plate

r_b Ratio of the stiffness of a unit width of the bottom flange to the stiffness of a unit width of the web

R_d Equivalent distributed shearing rigidity of the diaphragms

R_f Equivalent distributed shearing rigidity of the web and flanges

r_t Ratio of the stiffness of a unit width of the top flange to the stiffness of a unit width of the web

s_d Diaphragm spacing

s_e Equivalent width of an exterior girder

s_w Web spacing

S_m Infinite sum part of the longitudinal bending moment per unit width of the cylindrically bent plate

S_{qx} Infinite sum part of the longitudinal shearing force per unit width of the cylindrically bent plate for use in longitudinal shearing force coefficients

S_{qy} Infinite sum part of the longitudinal shearing force per unit length of the cylindrically bent plate for use in the transverse shearing force coefficient

ds Differential element of arc length

t_{bf} Bottom flange thickness

t_d Diaphragm thickness

t_f Flange thickness used in the derivation of the governing equations

t_{tf} Top flange thickness

t_w Web thickness

u_i Limit of integration used in the evaluation of coefficients per beam

V Total shearing force on the equivalent shear block

v_b Shearing force on the bottom flange

v_t Shearing force on the top flange

V_{xi} Longitudinal reactive force per unit width

V_{yi} Transverse reactive force per unit length

$\bar{V}_{xi}$ Longitudinal reactive force coefficient per unit width

$\bar{v}_{xin}$	Y dependent part of the longitudinal reactive force coefficient per unit width
$\bar{v}_{yi}$	Transverse reactive force coefficient per unit length
$\bar{v}_{yin}$	Y dependent part of the transverse reactive force coefficient per unit length
dv	Differential element of volume
W	Width of the structure
w(x,y), w	Deflection of the equivalent plate
w_a	Deflection of the cylindrically bent plate
W_e	Equivalent width of the structure
w_{hi}	Homogeneous part of the deflection of the equivalent plate
w_i	Total deflection of the equivalent plate
w_{pi}	Particular part of the deflection of the equivalent plate
$\bar{w}$, $\bar{w}_i$	Deflection coefficient
$\bar{w}_{in}$	Y dependent part of the deflection coefficient
x	Ordinate denoting longitudinal position
x_1	Ordinate at which the deflection, longitudinal bending moment, and transverse bending moment coefficients are evaluated
x_2	Ordinate at which the longitudinal shearing force and reactive force coefficients are evaluated
x_3	Ordinate at which the transverse shearing force and reactive force coefficients are evaluated
x_4	Ordinate at which the twisting moment coefficients are evaluated
y	Ordinate denoting transverse position

α_n $n\pi/2a$

β_n $\alpha_n b$

Γ Complementary energy

γ Total transverse shear deformation

Γ_o Modified complementary energy density function

γ_1 Shear deformation of flanges

γ_2 Shear deformation of web

$\bar{\Gamma}$ Modified complementary energy

δ_{ij} Kronecker's delta

δM_x Variation taken on the longitudinal unit bending moment

δM_{xy} Variation taken on the unit twisting moment

δM_y Variation taken on the transverse unit bending moment

δQ_y Variation taken on the transverse unit shearing force

δw Variation taken on the deflection

$\delta \Gamma_o$ Variation taken on the modified complementary energy density function

$\delta \bar{\Gamma}$ Variation taken on the modified complementary energy

$\delta \lambda$ Variation taken on the Lagrange Multiplier, λ

ζ Non-dimensional transverse location of the left side of the applied load

η Non-dimensional ordinate denoting transverse position

η_j Boundaries of equivalent plate regions

$\eta 1_k$, $\eta 2_k$ Boundaries of the beam elements

θ_n $\left[\phi_n(1+\nu) - (1-\nu) \right] /2$

i Moment of inertia of the structure per unit width

$\lambda(x,y)$, λ Lagrange Multiplier used in the derivation of the governing equations

ν Poisson's Ratio for the structure

ξ Non-dimensional transverse location of the right side of the applied load

σ Dummy transverse ordinate

σ_x Normal stress acting in the longitudinal direction

σ_y Normal stress acting in the transverse direction

σ_z Normal stress acting in the vertical direction

τ Horizontal shearing stress acting on the flanges

τ_x Vertical shearing stress acting on the core media normal to the longitudinal direction

τ_{xy} General shearing stress acting normal to the vertical direction

τ_{xz} General shearing stress acting normal to the transverse direction

τ_y Vertical shearing stress acting on the core media normal to the transverse direction

τ_{yz} General shearing stress acting normal to the longitudinal direction

ϕ Stiffness parameter

ϕ_n $\phi(n\pi)^2$

$\Phi(y)_{in}$ Arbitrary functions of class C^4 dependent on y

ψ Ratio of the shear modulus, G, to the equivalent transverse shear modulus G_y

INTRODUCTION

Introductory Remarks

The determination of internal stresses or forces existing in bridge structures subjected to externally applied loads is generally called load distribution. This thesis presents a method for the complete determination of load distribution in simply supported concrete box girder highway bridges. In addition, the method is used for a comprehensive study of the behavior of these structures with geometrical configurations representing the majority of commonly built box girder bridges.

Other procedures are currently available for the determination of load distribution in the class of structures studied (10,11,12). However, these procedures are complex and require considerable computer programming and operation time for the complete determination of load distribution in box girder bridge structures. In addition, the description of a box girder structure which is to be analyzed by presently available means requires the description of the specific geometric and elastic properties of the individual elements that make up the complete structure. Thus, a behavioral study of a number of structures encompassing a wide range of possible geometric configurations becomes complex and costly when the existing methods of analysis are used. The study presented herein was undertaken to provide a relatively simple, accurate,

and rapid method for the determination of load distribution in box girder bridges and to study the behavior of commonly built structures of this type.

Object and Scope of the Investigation

The objectives of the study are:

1. Development of a simple general method of analysis for concrete box girder bridges: A method of analysis is developed which replaces the actual structure by a structurally equivalent uniform plate. Governing equations for the equivalent plate are obtained and solutions to these equations are found for the boundary conditions and loading considered. Expressions for internal shears and moments are obtained, and parameters which govern the behavior of the equivalent plate or box girder structure are developed.

2. Verification of the analysis procedure developed: Internal force quantities predicted by the proposed analysis are compared with corresponding quantities measured in field tests conducted by other investigators (4). Since available field test results are very limited, internal forces and deflections predicted by the proposed analysis are further compared with similar quantities predicted by other analytical procedures (1,8,9).

3. Study of the effect of governing parameters on behavior: The range of governing parameters associated with the

range of geometries found in common bridge configurations is determined. The complete description of forces, moments, and deflections is presented for structures with combinations of parameters representing the range of common bridge configurations.

4. Discussion of results of the behavioral study: The range of each of the internal force quantities and deflections presented in the behavioral study is discussed and the parameters associated with these ranges are outlined. In addition, the parameter values which lead to the most optimum load distribution are discussed.

The scope of the study includes the majority of commonly built concrete box girder highway bridge cross-sections. However, certain restrictions are made so that the actual structure may be modelled by an equivalent uniform plate. These are: the top and bottom flanges are of constant thickness, the vertical web elements are equally spaced and have the same thicknesses, and the web and flange elements are monolithically constructed. No restrictions are placed on edge beam configurations in the theory development.

Transverse interior diaphragms with finite shearing rigidities may be considered. No restriction is placed on the number of interior diaphragms that may be considered in the theory development. Included is the case of no interior diaphragms.

Because of the existence of a wide variety of concrete box girder highway bridge overall geometries, some geometrical restrictions were desirable to limit the scope of the study. The bridges studied conform to the following overall geometrical conditions:

1. The longitudinal axis of the bridge is at right angles to the piers or abutments.

2. The bridge spans between adjacent piers or abutments are simple or non-continuous.

3. Span lengths are of the range 50 to 130 feet and the overall widths are of the range 30 to 75 feet.

Loading is restricted to statically applied vertical loads. The loads approximate truck wheel loads and may be applied anywhere on the horizontal top surface of the structure.

Definition of Concrete Box Girder Highway Bridges

Figure 1 illustrates three typical concrete box girder bridge cross-sections. It is seen that each of the three structures shown represents a common configuration where only the edge geometries differ. Referring to the terminology shown in the figure, each of the structures shown is characterized by the rectangular multi-celled configuration formed by the top flange, bottom flange, and webs. The webs are equally spaced and are all of the same thickness. However, the thickness of

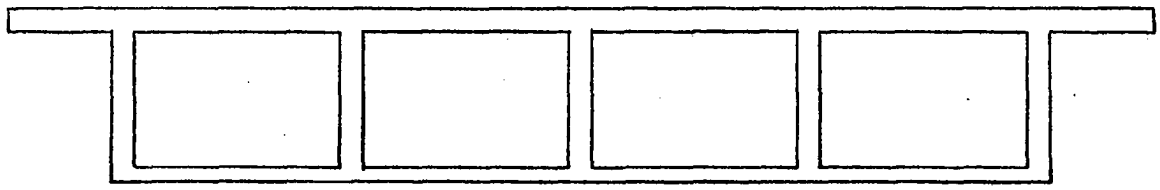

Cantilevered top flange configuration

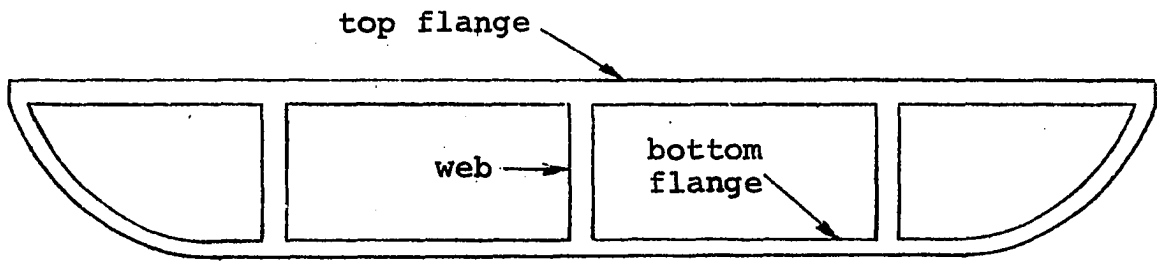

Curved soffit configuration

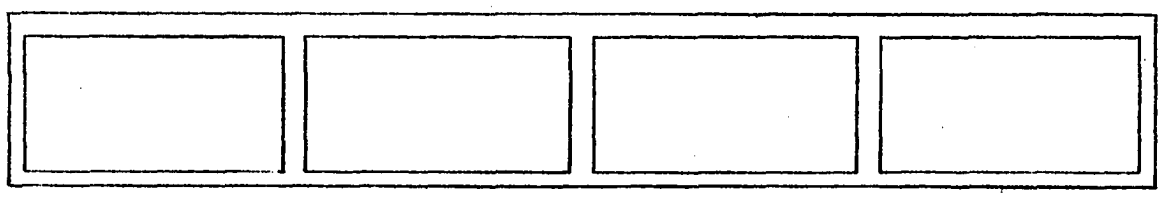

Basic rectangular configuration

Figure 1. Typical concrete box girder highway bridge cross-sections

the top flange may be different than the bottom flange thickness. Also, many concrete box girder bridges possess plate elements which are perpendicular to the axis of the cells and may be located at various positions along the span of the structure. These elements are commonly termed diaphragms.

So that no confusion exists between the class of bridge structures studied herein and two other similarly named bridge types, the constructional and behavioral differences between these three similarly named bridge types is discussed. The first of these bridge types is commonly referred to as a composite concrete-steel box girder bridge. This class of bridge is characterized by a concrete deck slab which is supported by and is continuous over composite steel girders. The girders are formed of welded thin steel plates compositally constructed with the deck slab such that the resulting overall configuration is separated composite closed-section girders. The second class of highway bridges with a name similar to the bridge type studied herein is commonly referred to as a box girder beam bridge or separated box girder beam bridge. This structure is similar to the composite box girder bridge except that instead of composite closed-section girders, the supporting beams are concrete box beams. In both of these structures, the

transverse[a] flexural stiffness of the bridge is supplied only by the deck slab, whereas the longitudinal[a] flexural stiffness is supplied by the girders or beams. Hence, these structures possess orthogonally anisotropic flexural stiffnesses. It may be assumed that concrete box girder bridges possess nearly isotropic flexural stiffnesses. Thus, composite box girder and separated box beam bridges differ from concrete box girder bridges in both construction and structural behavior.

Review of Previous Studies

Investigations of the behavior of many types of highway bridges are numerous. For example, Sanders and Elleby (9) cite approximately 300 references directly concerned with load distribution in general types of highway bridges. However, due to the relatively recent use of box girder highway bridges and their complex structural behavior, literature concerned with load distribution in these structures is relatively scarce.

Perhaps the first comprehensive investigations to determine the load distributing characteristics of concrete box girder highway bridges were conducted by Little and Rowe (6,7,8). The earliest investigations by Little and Rowe (6,7) were primarily experimental in nature. Tests were conducted on small plastic models subjected to statically applied

---

[a]The term longitudinal refers to the axis of the structure parallel to the axis of the beams or cells and transverse refers to the direction perpendicular to the axis of the beams or cells.

concentrated vertical loads. Deflections and strains were measured for various load positions and the strains were converted to internal transverse and longitudinal bending moments. These measured moments and deflections were then compared with corresponding results predicted by orthotropic plate theory (1,8,9). The conclusions obtained by Little and Rowe were that the deflections and longitudinal bending moments could be predicted with reasonable accuracy, but the transverse bending moments were inaccurately predicted by the theory. In addition, a satisfactory method of calculating torsional rigidities, which are required for the orthotropic plate theory, was not found. A semi-empirical method was used for the calculation of these quantities.

Another investigation of a similar nature to that described above was conducted by Campbell-Allen and Lee (2). In this case, the effect of transverse interior diaphragms was investigated. In addition to testing three small plastic models, a one-fifth scale prestressed concrete box girder structure was tested. In these tests, emphasis was placed on measuring deflections of the structures under applied vertical concentrated loads. The measured deflections were compared with similar results predicted by orthotropic plate theory. It was found, as in the Little and Rowe investigations, that a semi-empirical method of calculating torsional rigidities was necessary for satisfactory comparisons of measured

and theoretical results. In addition, discrepancies existed in the measured deflections that could not be accounted for by the theory. The discrepancies were attributed to the effects of local deformations and a procedure was developed to predict these deformations. It was concluded that the deflections of concrete box girder bridges could be reasonably predicted by the orthotropic plate theory, provided that local deformations were taken into account.

A series of extensive investigations of the behavior of concrete box girder bridges has been recently initiated at the University of California at Berkeley. The first of these investigations is a report by Davis et al. (4) dealing with the full-scale testing of a concrete box girder bridge. The structure investigated was a simple-span bridge 80 feet long and 34 feet wide. Loading was accomplished by means of a single heavily loaded vehicle moving parallel to the longitudinal axis of the bridge at creep speeds (0 to 5 mph). Instrumentation of the structure was very complete and the results of the tests were well documentated. Strains and deflections were measured and the strains were converted to stresses and longitudinal bending moments. Folded plate theory was used to develop an analytical procedure which was then used to predict stresses and bending moments analogous to the quantities measured in the tests. It was found that the theory predicted the test results with excellent accuracy, and it was concluded

that the method developed from folded plate theory could accurately predict the behavior of concrete box girder bridges.

The initial experimental and analytical study described above was followed by a series of analytical studies of concrete box girder highway bridges conducted at the University of California at Berkeley by Scordelis (10,11) and Scordelis and Meyer (12).

The first of these reports (11) contains a comprehensive survey of existing box girder bridges in the state of California. In addition, two methods of analyzing simply supported concrete box girder bridges are given which include the effects of transverse interior diaphragms. Again, these methods are based on the theory of folded plates. The diaphragms are assumed to be infinitely rigid in their planes and perfectly flexible normal to their planes. Analytically predicted stresses are given in each of the elements of several hypothetical structures to illustrate the results of the theories.

The second report in the series cited above is an analytical study of continuous concrete box girder highway bridges. This investigation (10) represents an extension of the previous work conducted at the University of California (4,11) and is concerned with the analysis of continuous box girder bridge structures. Three methods are presented for the analysis of the continuous structures. Two are based on the theory of folded plates, and the third is founded on the

theory of finite elements. The purpose and results of the study are primarily intended to compare the three methods and to ascertain their strengths, weaknesses, and accuracy.

The final report of the series of investigations conducted at the University of California (12) is concerned with developing design criterion for simply supported and continuous concrete box girder highway bridges. The theoretical methods developed in the previous studies from the University of California were used in an extensive study of the effect of variations of geometrical properties of the structures on their behavior under design loadings. Empirical relationships are presented which represent the bridge's behavior under the design loadings and recommendations are made for design criteria incorporating these relationships.

Sanders and Elleby (9) have presented an extensive investigation concerned with the development of design criteria for a wide range of highway bridge types. Included in this investigation is a study of simply supported concrete box girder highway bridges. Sanders and Elleby used the method of analysis developed by Scordelis (11) for a parameter analysis of a wide variety of the geometric variables for design loadings. Presented is an empirical relationship derived from the parameter analysis for the determination of design moments in simply supported structures under design loading conditions.

It is seen from the review presented above that, basically, two approaches have been used for the analytical prediction of load distribution in concrete box girder highway bridges. These are: a uniform equivalent plate approach based on the theory of orthotropic plates, and a method of analysis based on the theory of folded plates. The first method of analysis represents a relatively non-complex analysis. However , it was found by the investigators who used this method that the predictions were relatively inaccurate and that semi-empirical methods were required for the calculation of rigidity parameters used to describe the structure. The second method of analysis was found to predict the behavior of the structures with good accuracy. However, this method, based on the theory of folded plates, is relatively complex, requires considerable programming and computer operation time for some combinations of geometric variables (11), and requires considerable geometric information for the complete description of the structure to be studied.

Selection and Basis of the Method of Analysis

It is seen from the review of previous studies that a method of analysis of concrete box girder highway bridges that combines both accuracy and relative simplicity is not available. So that the relative simplicity requirement is fulfilled, the method of analysis developed herein is based on the concept of

modelling the behavior of the actual structure by an equivalent plate. However, as seen from the previous studies (2,6,7), the use of an equivalent orthotropic plate to represent the behavior of a box girder bridge is not satisfactory. Thus, another type of equivalent plate must be used.

Two requirements must be fulfilled for the equivalent plate approach to be a valid method of analysis. The first requirement is that the actual structure must be geometrically uniform. The second requirement is that the equivalent plate must represent the structural properties of the actual structure. The first requirement is met since, except for the edge beams, a typical concrete box girder bridge is composed of uniform beam elements. It will be shown later that the non-uniformity of the edge beams may be accounted for in the equivalent plate analysis by the use of a special width parameter. So that structural equivalence is maintained, the structural behavior of the box girder bridge is intuitively examined, and the corresponding assumed behavior of the equivalent plate is assumed.

In cellular structures, such as a box girder bridge, the flexural and torsional rigidities are derived primarily from the outermost elements of the structure. In the case of a box girder bridge, these elements are the top and bottom flanges and the edge webs. Thus, it is seen that for a typical interior element of a box girder bridge, the flexural and torsional rigidities should be nearly isotropic since the top and bottom

flanges represent equal rigidities in any horizontal direction. Thus, it is assumed that the equivalent plate used to represent the structure is isotropic with respect to flexure and torsion. In addition, the equivalent plate must possess the same shear characteristics as the actual structure. In the longitudinal direction, it may be assumed that the webs contribute most of the shearing rigidity. Since for practical structures the webs are relatively closely spaced and possess a relatively large cross-sectional area, the longitudinal shearing rigidity may be assumed large, and, hence, shearing deformations are assumed small. In the transverse direction, however, shearing deformations may not be small since for the case of no internal diaphragms, shearing deformation would be produced by bending of, and relative horizontal slip between the top and bottom flanges. Also, for structures which have diaphragms, transverse shearing deformations might not be small since for practical structures the diaphragms are few in number and are widely spaced. Thus, it is assumed that the equivalent plate possesses infinite shearing rigidity in the longitudinal direction and finite shearing rigidity in the transverse direction.

In summary, the equivalent plate used herein to represent the behavior of concrete box girder highway bridges has the following structural properties: isotropic flexural and torsional rigidities, infinite shearing rigidity in one orthogonal

direction, and finite shearing rigidity in the other orthogonal direction. This equivalent plate is termed an orthogonally shear anisotropic plate.

DEVELOPMENT OF THE PROPOSED ANALYSIS

The complete development of the analysis procedure for an equivalent plate which represents the behavior of the actual bridge structure is presented in this section. As was discussed in the previous section, a plate which has finite orthogonally anisotropic shearing rigidities is used as a model to represent the behavior of the actual structure. This equivalent plate, which is a form of a sandwich plate, is herein termed an orthogonally shear anisotropic plate. A derivation of the governing general equations for the case of bending of a sandwich plate has been obtained by Cheng (3). A similar type of derivation of governing equations for the specific equivalent plate used herein is carried out. The derivation is shown for the purpose of illustrating the assumptions that are made relating the actual structure to the orthogonally shear anisotropic plate. Also, the derivation helps achieve a physical feeling for the governing equations. However, it should be noted that under special conditions, the equations derived by Cheng (3) correspond to the equations developed herein.

Derivation of the Governing Equations

Summation of the forces and moments acting on a typical plate element, as shown in Figure 2, leads to the following well known equations of equilibrium for a plate element:

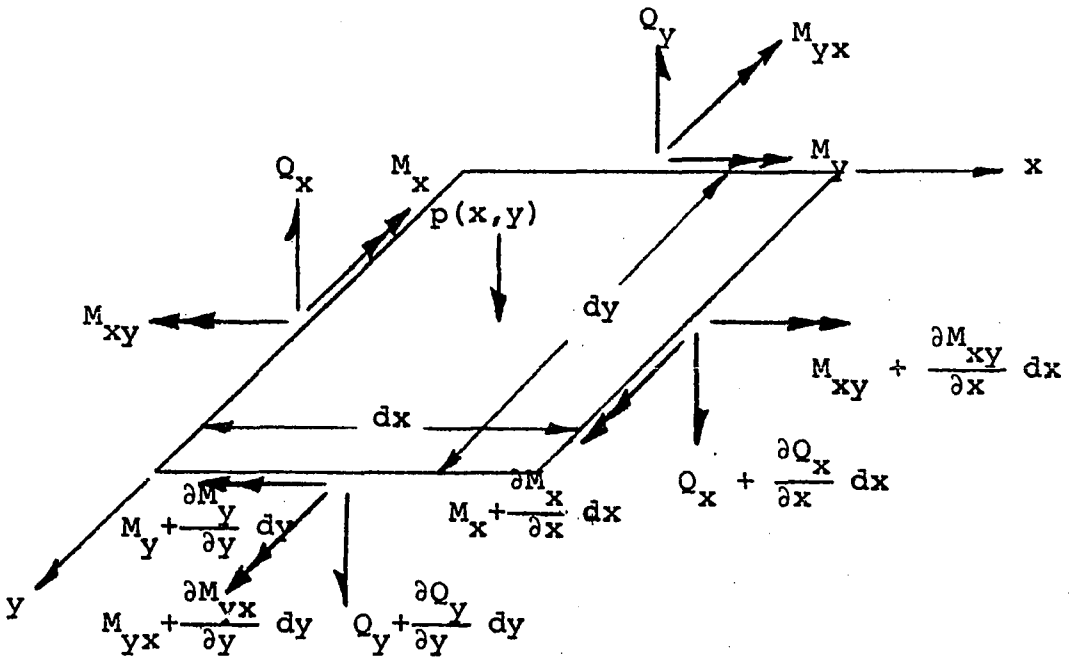

Figure 2. Force nomenclature for a typical plate element

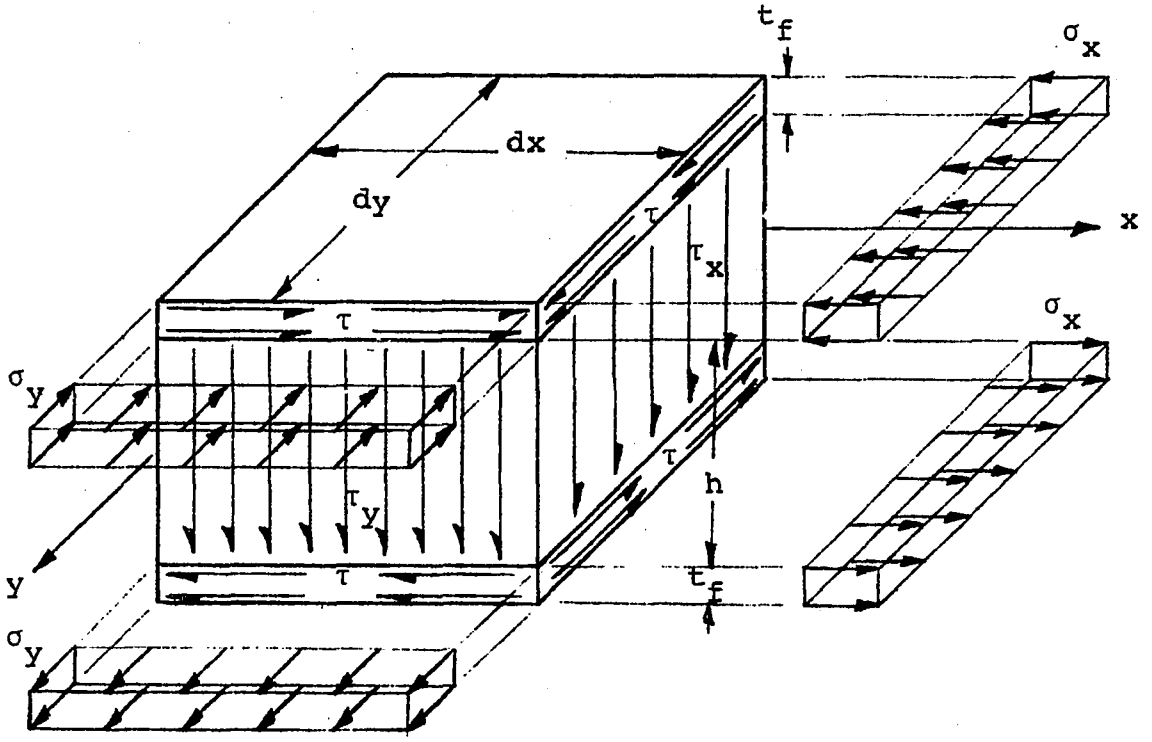

Figure 3. Assumed stress distribution on a typical plate element

$$\frac{\partial Q_x}{\partial x} + \frac{\partial Q_y}{\partial y} + p(x,y) = 0, \tag{1}$$

$$\frac{\partial M_{xy}}{\partial x} - \frac{\partial M_y}{\partial y} + Q_y = 0, \tag{2}$$

$$\frac{\partial M_{yx}}{\partial y} + \frac{\partial M_x}{\partial x} - Q_x = 0 \ . \tag{3}$$

Since the shearing force, Q_x, is not of primary importance in the following derivation, it can be eliminated from the equilibrium equations by differentiating equation 3 with respect to x and substituting $\frac{\partial Q_x}{\partial x}$ into equation 1, which results in the following expression when it is observed that $M_{xy} = -M_{yx}$:

$$\frac{\partial^2 M_x}{\partial x^2} - \frac{\partial^2 M_{xy}}{\partial x \partial y} + \frac{\partial Q_y}{\partial y} + p(x,y) = 0 \ . \tag{4}$$

The equilibrium of the plate element can now be completely represented by equations 2 and 4.

The following assumptions regarding the relationship of the geometry and rigidities of the equivalent plate to the actual structure are made:

1. The equivalent plate is composed of two flange sections separated by a core section with different stiffnesses than the flanges. In the actual structure, the top and bottom slabs are represented by the flanges, and the longitudinal webs and

transverse diaphragms are represented by the core material in the equivalent plate.

2. The thicknesses of the top and bottom flanges are small compared to the total depth of the plate. This assumption follows from the geometry of the actual structure.

3. The horizontal plane stiffnesses of the core material are small compared to the in-plane flange stiffnesses. Conversely, the vertical shear stiffnesses of the flanges are assumed to be small compared to the vertical shear stiffnesses of the core material. In addition, the vertical shear stiffness of the core material in one direction is of the same order of magnitude as an isotropic plate. It can be seen that the assumed stiffness properties of the equivalent plate should approximate the stiffness properties of the actual structure when the stiffnesses of the slabs are compared with the stiffnesses of the webs and diaphragms. Also, it can be seen that the vertical shearing stiffness of the longitudinal webs should be relatively large.

The assumed stress distribution in a typical plate element, as shown in Figure 3, is outlined as follows:

1. The normal stresses, σ_x and σ_y, are carried by the flanges. Thus, there are no net horizontal plane normal forces acting on the element, and the normal stresses are constant over the area of the flanges. If the flanges are assumed to have the same thickness, then the no net normal force assumption

implies that the normal stresses on the top flange are equal to the normal stresses on the bottom flange. This stress distribution follows from the assumed rigidity properties, the small flange thickness assumption, and the assumption, as found in classical plate theory, that no net horizontal normal forces exist.

2. The vertical shearing stresses, τ_x and τ_y, are carried by the core medium. In the longitudinal direction this follows from the rigidity characteristics of the actual structure. However, for the transverse direction, this assumption requires a special relationship since in the real structure the vertical shearing stresses, τ_y, are carried partly or entirely by the flanges. A homogeneous core medium with shear characteristics equivalent to the real web-diaphragm system is used in this case and the shearing stresses are assumed to act through this medium. The structural equivalence of the assumed core medium to the actual structure is taken up in a succeeding section dealing with the determination of the governing stiffness parameter.

3. The horizontal shearing stresses, τ, are carried by the flanges only. This follows from the assumed stiffness properties of the equivalent plate. In addition, the horizontal shearing stresses are constant across the flanges. This follows from the small flange thickness assumption. It can also be seen that due to the small horizontal plane stiffness components

of the core medium, the horizontal plane stress components of the core stress tensor are small. Therefore, stress equilibrium of the core medium requires that $\frac{\partial \tau_x}{\partial z} = 0$ and $\frac{\partial \tau_y}{\partial z} = 0$ across the core medium. Thus, the vertical shearing stresses are constant with respect to the depth of the core medium.

The principle of minimum complementary energy is now used to derive force-displacement relationships for the equivalent plate. The complementary energy of a general elastic isotropic body may be expressed as (5)

$$\Gamma = \iiint_V \frac{1}{2E}\Big[\sigma_x^2 + \sigma_y^2 + \sigma_z^2 - 2\nu\left(\sigma_x\sigma_y + \sigma_x\sigma_z + \sigma_y\sigma_z\right) + 2(1+\nu)\left(\tau_{xy}^2 + \tau_{xz}^2 + \tau_{yz}^2\right)\Big] dv \ .$$

If, in addition to the previous assumptions, the stress, σ_z, is assumed small and, therefore, contributes negligibly to the total energy, the expression for the complementary energy for the equivalent plate considered herein becomes

$$\Gamma = \iiint_V \left[\frac{1}{2E}\left(\sigma_x^2 + \sigma_y^2 - 2\nu\sigma_x\sigma_y\right) + \frac{1}{2G}\tau^2 + \frac{1}{2G_y}\tau_y^2\right] dv \qquad (5)$$

where E is Young's modulus for the flange material,

G is the shear modulus of the flange material,

G_y is the equivalent shear modulus of the core media,

V is the total volume of the equivalent plate,

and σ_x, σ_y, τ, τ_y are the normal and shearing stresses as shown in Figure 3.

The unit forces, M_x, M_y, M_{xy}, and Q_y can be expressed in terms of the stresses through the following relationships:

$$M_x = \int_{-(h/2+t_f)}^{h/2+t_f} \sigma_x \, z\,dz \quad , \qquad M_y = \int_{-(h/2+t_f)}^{h/2+t_f} \sigma_y \, z\,dz \quad , \qquad (6,7)$$

$$M_{xy} = \int_{-(h/2+t_f)}^{h/2+t_f} \tau \, z\,dz \quad , \qquad Q_y = \int_{-(h/2+t_f)}^{h/2+t_f} \tau_y \, dz \quad . \qquad (8,9)$$

As noted earlier, the normal and shearing stresses used in equations 5 through 9 are assumed to act only on specific areas of the cross-section and are assumed constant over the areas on which they act. If these assumptions regarding the distribution of stresses on the plate element, as shown in Figure 3, are used, equation 5 may be integrated with respect to the z direction. In addition, equations 6 through 9 may also be integrated if the above assumptions are utilized. If

the integrated forms of equations 6 through 9 are solved for the stresses, σ_x, σ_y, τ, and τ_y, and these results substituted into the integrated form of equation 5, the following form for the complementary energy is obtained:

$$\Gamma = \iint_R \left\{ \frac{1}{t_f(h+t_f)^2} \left[\frac{1}{E} \left(M_x^2 + M_y^2 - 2\nu M_x M_y \right) + \frac{1}{G} M_{xy}^2 \right] + \frac{1}{2hG_y} Q_y^2 \right\} da \qquad (10)$$

where R denotes the total horizontal area of the equivalent plate.

According to the principle of minimum complementary energy, a necessary condition for the total complementary energy of the system to be a minimum is that an expression containing the complementary energy, as shown in equation 10, is an extremal. This expression is the difference of the complementary energy, Γ, and a line integral expression for work done along the boundary of the equivalent plate. However, for the purpose of determining force displacement relations in the region, R, only the expression for Γ needs to be extremalized since extremalizing the appended line integral expression leads only to natural boundary condition expressions along the boundary (5). In addition to the condition that the complementary energy be an extremal, the principle of minimum complementary energy requires

that equilibrium must also be satisfied. Both conditions may be satisfied by introducing the Lagrange multipliers, $w(x,y)$ and $\lambda(x,y)$ (3). The Lagrange multipliers may be introduced into a modified form of the complementary energy such that the constraints of equilibrium are satisfied when the modified form of complementary energy is extremalized. The modified form of the complementary energy is:

$$\overline{\Gamma} = \iint_R \Gamma_o da, \tag{11}$$

$$\Gamma_o = \frac{1}{t_f(h+t_f)^2}\left[\frac{1}{E}\left(M_x^2 + M_y^2 - 2\nu M_x M_y\right) + \frac{1}{G}M_{xy}^2\right]$$

$$+ \frac{1}{2hG_y}Q_y^2 + \left(\frac{\partial^2 M_x}{\partial x^2} - \frac{\partial^2 M_{xy}}{\partial x \partial y} + \frac{\partial Q_y}{\partial y} + p(x,y)\right)w$$

$$+ \lambda\left(\frac{\partial M_{xy}}{\partial x} - \frac{\partial M_y}{\partial y} + Q_y\right) \quad . \tag{12}$$

The physical interpretation of the Lagrange multiplier, w, can be seen from the above expression. The energy term,

$$\iint_R w\, p(x,y)\, da,$$

is seen to represent the virtual work done by the external loads. Therefore, it can be seen that w represents the deflection of the equivalent plate.

The extremal of $\bar{\Gamma}$ may be found by setting the first variation, $\delta\bar{\Gamma}$, of the modified complementary energy equal to zero. According to the calculus of variations, the first variation of the modified complementary is shown by the following expression:

$$\delta\bar{\Gamma} = \iint_R \left(\frac{\partial \Gamma_o}{\partial M_x} \delta M_x + \frac{\partial \Gamma_o}{\partial M_y} \delta M_y + \frac{\partial \Gamma_o}{\partial M_{xy}} \delta M_{xy} + \frac{\partial \Gamma_o}{\partial Q_y} \delta Q_y + \frac{\partial \Gamma_o}{\partial w} \delta w + \frac{\partial \Gamma_o}{\partial \lambda} \delta \lambda \right) da. \tag{13}$$

After performing the indicated differentiations, the expression for the first variation of the modified complementary becomes

$$\delta\bar{\Gamma} = \iint_R \left\{ \left[\frac{2}{t_f (h+t_f)^2 E} (M_x - \nu M_y) + w \frac{\partial^2}{\partial x^2} \right] \delta M_x \right.$$

$$+ \left[\frac{2}{t_f (h+t_f)^2 E} (M_y - \nu M_x) - \lambda \frac{\partial}{\partial y} \right] \delta M_y$$

$$+ \left[\frac{2}{t_f (h+t_f)^2 G} M_{xy} - w \frac{\partial^2}{\partial x \partial y} + \lambda \frac{\partial}{\partial x} \right] \delta M_{xy}$$

$$+ \left[\frac{1}{hG_y} Q_y + w \frac{\partial}{\partial y} + \lambda \right] \delta Q_y$$

$$\left. + \left[\frac{\partial^2 M_x}{\partial x^2} - \frac{\partial^2 M_{xy}}{\partial x \partial y} + \frac{\partial Q_y}{\partial y} + p(x,y) \right] \delta w \right.$$

$$+ \left[\frac{\partial M_{xy}}{\partial x} - \frac{\partial M_y}{\partial y} + Q_y \right] \delta\lambda \Big\} \, da \, . \tag{14}$$

Using Green's theorem and integration by parts, the following identities can be derived which will be used to simplify the above expression:

$$\iint_R w \frac{\partial^2}{\partial x^2} \delta M_x \, da = \iint_R \frac{\partial^2 w}{\partial x^2} \delta M_x \, da + \oint_B \left(w \frac{\partial}{\partial x} \delta M_x - \frac{\partial w}{\partial x} \delta M_x \right) \vec{n}_x \, ds, \tag{15}$$

$$\iint_R w \frac{\partial^2}{\partial x \partial y} \delta M_{xy} \, da = \iint_R \frac{\partial^2 w}{\partial x \partial y} \delta M_{xy} \, da$$

$$+ \oint_B \left(w \frac{\partial}{\partial y} \delta M_{xy} \vec{n}_x - \frac{\partial w}{\partial x} \delta M_{xy} \vec{n}_y \right) ds, \tag{16}$$

$$\iint_R \lambda \frac{\partial}{\partial y} \delta M_y \, da = - \iint_R \frac{\partial \lambda}{\partial y} \delta M_y \, da + \oint_B \lambda \delta M_y \, \vec{n}_y \, ds, \tag{17}$$

$$\iint_R \lambda \frac{\partial}{\partial x} \delta M_{xy} \, da = - \iint_R \frac{\partial \lambda}{\partial x} \delta M_{xy} \, da + \oint_B \lambda \delta M_{xy} \vec{n}_x \, ds, \tag{18}$$

$$\iint_R w\frac{\partial}{\partial y}\,\delta Q_y\,da = -\iint_R \frac{\partial w}{\partial y}\,\delta Q_y\,da + \int_B w\delta Q_y\,\vec{n}_y\,ds \qquad (19)$$

where R refers to the horizontal plane boundary of the equivalent plate and $\vec{n}_x$ and $\vec{n}_y$ are, respectively, the x and y components of the outward directed unit normal vector on the boundary of the equivalent plate. If the identities represented by equations 15 through 19 are substituted into equation 14, the following expression results:

$$\begin{aligned}\delta\bar{\Gamma} = \iint_R \Bigg\{ &\left[\frac{2}{t_f(h+t_f)^2E}\left(M_x - \nu M_y\right) + \frac{\partial^2 w}{\partial x^2}\right]\delta M_x \\ &+ \left[\frac{2}{t_f(h+t_f)^2E}\left(M_y - \nu M_x\right) + \frac{\partial \lambda}{\partial y}\right]\delta M_y \\ &+ \left[\frac{2}{t_f(h+t_f)^2G}M_{xy} - \frac{\partial^2 w}{\partial x\partial y} - \frac{\partial \lambda}{\partial x}\right]\delta M_{xy} \\ &+ \left[\frac{1}{hG_y}Q_y - \frac{\partial w}{\partial y} + \lambda\right]\delta Q_y \\ &+ \left[\frac{\partial^2 M_x}{\partial x^2} - \frac{\partial^2 M_{xy}}{\partial x\partial y} + \frac{\partial Q_y}{\partial y} + p(x,y)\right]\delta w \\ &+ \left[\frac{\partial M_{xy}}{\partial x} - \frac{\partial M_y}{\partial y} + Q_y\right]\delta\lambda \Bigg\}\,da\end{aligned}$$

$$+ \oint_B \left[\left(w \vec{n}_x \frac{\partial}{\partial x} - \frac{\partial w}{\partial x} \vec{n}_x \right) \delta M_x - \lambda \vec{n}_y \delta M_y + \left(\frac{\partial w}{\partial x} \vec{n}_y - w \vec{n}_x \frac{\partial}{\partial y} \right.\right.$$

$$\left.\left. + \lambda \vec{n}_x \right) \delta M_{xy} + w \vec{n}_y \delta Q_y \right] ds. \qquad (20)$$

Since the variations, δM_x, δM_y, δM_{xy}, δQ_y, δw, and $\delta \lambda$, are arbitrary, a necessary condition that $\delta \bar{\Gamma}$ vanish is that each of the coefficients of these variations vanish. Setting each of the coefficients to be zero corresponds to writing the Euler equations for this variational problem. It can be seen that a second necessary condition such that $\delta \bar{\Gamma} = 0$ is the requirement that the line integral vanish. However, this condition, together with the condition that the first variation of the appended line integral vanishes, leads to the natural boundary conditions of the problem. Since it is not the purpose of this study to outline the natural boundary conditions, the second necessary condition will not be pursued further. It can be seen that the coefficients of the variations of w and λ identically vanish since these are the equilibrium constraints that were originally imposed. By equating the coefficients of the remaining variations to zero, the Euler equations are found which can be shown as follows:

$$\frac{2}{t_f (h+t_f)^2 E} \left(M_x - \nu M_y \right) + \frac{\partial^2 w}{\partial x^2} = 0, \qquad (21)$$

$$\frac{2}{t_f(h+t_f)^2E}\left(M_y - \nu M_x\right) + \frac{\partial \lambda}{\partial y} = 0, \tag{22}$$

$$\frac{2}{t_f(h+t_f)^2G} M_{xy} - \frac{\partial^2 w}{\partial x \partial y} - \frac{\partial \lambda}{\partial x} = 0, \tag{23}$$

$$\frac{1}{hG_y} Q_y - \frac{\partial w}{\partial y} + \lambda = 0 \ . \tag{24}$$

Equations 21 through 24 can be solved simultaneously for M_x, M_y, and M_{xy} in terms of w and Q_y. The resulting equations, shown below, are the force-displacement expressions for the equivalent plate.

$$M_x = -D\left(\frac{\partial^2 w}{\partial x^2} + \nu \frac{\partial^2 w}{\partial y^2}\right) + \frac{2\nu D_y}{1-\nu} \frac{\partial Q_y}{\partial y} \tag{25}$$

$$M_y = -D\left(\frac{\partial^2 w}{\partial y^2} + \nu \frac{\partial^2 w}{\partial x^2}\right) + \frac{2\ D_y}{1-\nu} \frac{\partial Q_y}{\partial y} \tag{26}$$

$$M_{xy} = D\ (1-\nu)\ \frac{\partial^2 w}{\partial x \partial y} - D_y \frac{\partial Q_y}{\partial x} \tag{27}$$

where $D = \dfrac{t_f(h+t_f)^2E}{2(1-\nu^2)}$, the flexural rigidity of the equivalent plate,

$D_y = \dfrac{D(1-\nu)}{2hG_y}$, a measure of the shearing rigidity of the equivalent plate.

It can be seen in the above expressions that as the transverse shear modulus, G_y, becomes large, the force-displacement relationships are identical with those of classical plate theory (15) when the flexural rigidity, D, is replaced by the corresponding rigidity of a homogeneous plate.

Equations 25 through 27 can now be used in conjunction with the equations of equilibrium to establish the governing equations of the equivalent plate. If equation 27 is differentiated with respect to x, equation 26 differentiated with respect to y, and the resulting values of

$$\frac{\partial M_{xy}}{\partial x} \quad \text{and} \quad \frac{\partial M_y}{\partial y}$$

substituted into equation 2, then, after simplification, the following expression results:

$$\left[D_y \left(\frac{2}{1-\nu} \frac{\partial^2}{\partial y^2} + \frac{\partial^2}{\partial x^2} \right) - 1 \right] Q_y = D \frac{\partial}{\partial y} \nabla^2 w. \tag{28}$$

If equation 25 is differentiated twice with respect to x and equation 27 differentitated twice with respect to x and y, the following equations are obtained:

$$\frac{\partial^2 M_x}{\partial x^2} = -D \frac{\partial^4 w}{\partial x^4} - \nu D \frac{\partial^4 w}{\partial x^2 \partial y^2} + \frac{2\nu D_y}{1-\nu} \frac{\partial^3 Q_y}{\partial x^2 \partial y}, \tag{29}$$

$$\frac{\partial^2 M_{xy}}{\partial x \partial y} = D (1-\nu) \frac{\partial^4 w}{\partial x^2 \partial y^2} - D_y \frac{\partial^3 Q_y}{\partial x^2 \partial y}. \tag{30}$$

Equation 28 can be differentiated with respect to y and, together with equations 29 and 30, substituted into equation 4. The resulting expression, upon simplification, becomes

$$\frac{2D_y}{1-\nu} \frac{\partial}{\partial y} \nabla^2 Q_y = D\nabla^4 w - p(x,y). \tag{31}$$

If equations 29 and 30 are again substituted into expression 4 and the result differentiated with respect to y, the following result is seen:

$$\frac{\partial^2 Q_y}{\partial y^2} = D \frac{\partial^3}{\partial x^2 \partial y} \nabla^2 w - D_y \left(\frac{1+\nu}{1-\nu}\right) \frac{\partial^4 Q_y}{\partial x^2 \partial y^2} - \frac{\partial}{\partial y} p(x,y). \tag{32}$$

Now, equation 28 can be differentiated twice with respect to x and added to equation 32 which results in

$$\left(1 - D_y \frac{\partial^2}{\partial x^2}\right) \nabla^2 Q_y = - \frac{\partial}{\partial y} p(x,y). \tag{33}$$

The last equation can be modified by multiplying through by D_y and differentiating with respect to y which yields

$$D_y \frac{\partial}{\partial y} \nabla^2 Q_y - D_y^2 \frac{\partial^3}{\partial x^2 \partial y} \nabla^2 Q_y = -D_y \frac{\partial^2}{\partial y^2} p(x,y). \tag{34}$$

The governing equation for the equivalent plate can now be found by multiplying equation 31 by D_y and differentiating it twice with respect to x. The result of this operation along with the

original form of equation 31 can now be substituted into expression 34. The result, after simplification, can be written as follows:

$$\left(1 - D_y \frac{\partial^2}{\partial x^2}\right) D\nabla^4 w = \left[1 - D_y \left(\frac{\partial^2}{\partial x^2} + \frac{2}{1-\nu} \frac{\partial^2}{\partial y^2}\right)\right] p(x,y). \qquad (35)$$

The above expression is the governing equation for the equivalent plate considered herein. As in the case of the force-displacement equations, this expression is seen to reduce to the governing equation found in classical plate theory when D_y and D are set, respectively, equal to zero and to the flexural rigidity of a homogeneous plate. Equations 28 and 35, together with the force-displacement expressions and boundary conditions, must be satisfied stepwise for the complete solution to the problem. It should also be mentioned that satisfying equations 31 and 33, although they are not independent of the governing equation, will be helpful in forming the complete solution.

Solution of the Governing Equations

The geometry of the equivalent plate conforms to the range of geometries selected for the actual structures. That is, the equivalent plate is rectangular with variable length sides. The boundary conditions of the equivalent plate also conform to the boundary conditions of the actual structure in that two opposite

sides of the equivalent plate are simply supported, and the other sides are free. As shown in Figure 4, the free sides are set parallel to the x axis and are of length 2a. The simply supported sides are parallel to the y axis and are of length 2b.

A wheel load acting on the actual structure is approximated by a finite length line load acting on the equivalent plate. As seen in Figure 4, the load acts parallel to the y axis and has length 2f. The centroid of the load is located on the equivalent plate by the coordinates (c,e). Only one equivalent load need be considered since the effect of multiple loads acting on the actual structure may be handled by superimposing the effects of the loads considered individually.

Assuming the loading shown;

$$p(x,y) = 0 \text{ for all } y \text{ when } x \neq c,$$

$$p(c,y) = q/2f \text{ for } e-f \leq y \leq e+f,$$

$$p(c,y) = 0 \text{ for } -b \leq y < e-f \text{ and } e+f < y \leq b.$$

In the region, $e-f \leq y \leq e+f$, the load, p, may be expressed as the Fourier series

$$p = \sum_{n=1}^{\infty} H_n \sin \alpha_n x \tag{36}$$

where $\alpha_n = \frac{n\pi}{2a}$, and

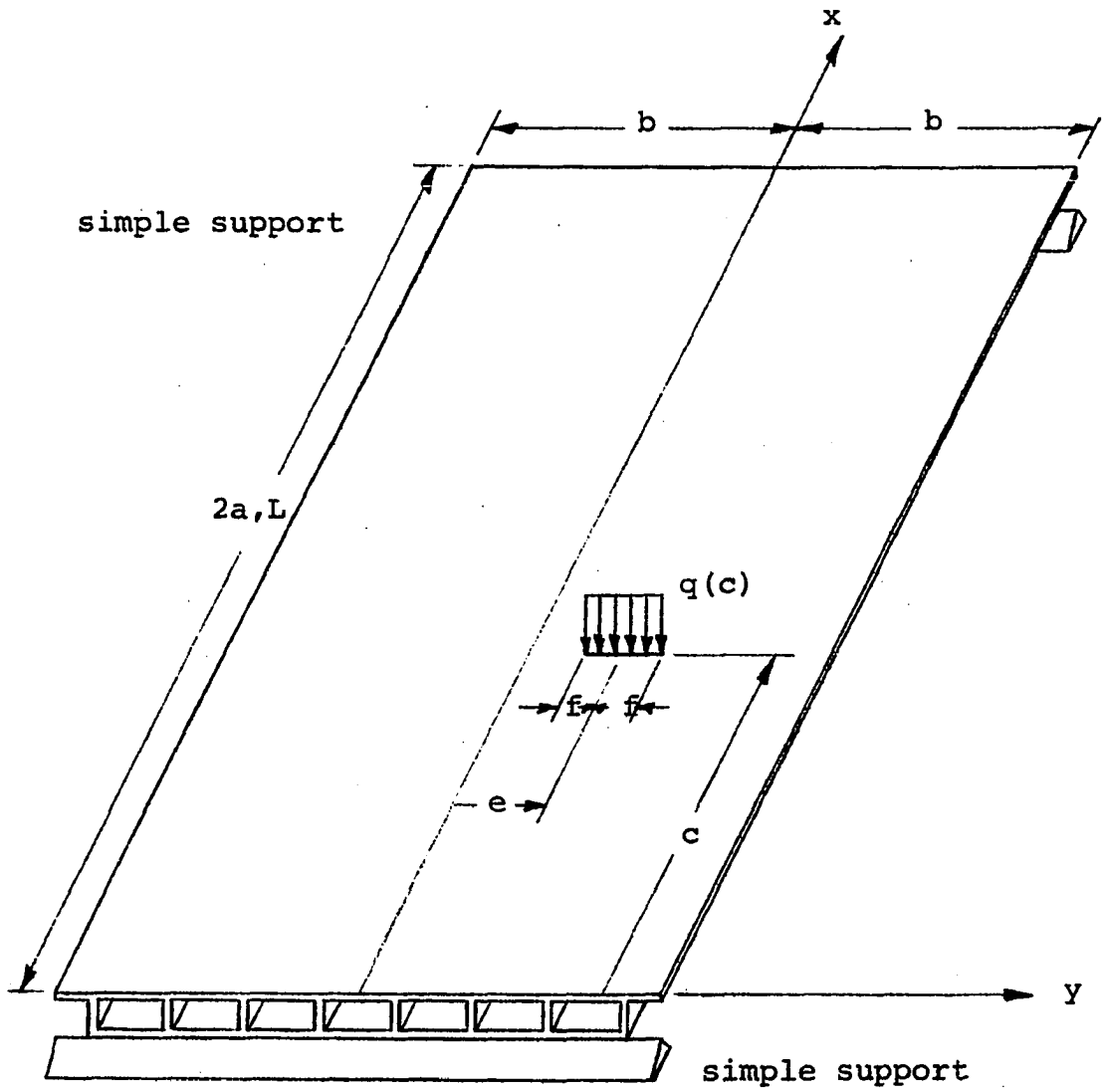

Figure 4. Dimension and load nomenclature for the structure

$H_n = \frac{q}{a} \sin \alpha_n c$, the Fourier coefficient of the load function.

The region of the plate will now be divided into three separate subregions with boundaries parallel to the x axis. In the succeeding work, these regions will be denoted by the subscript, i, where the regions are defined as follows:

$$i = 1 \text{ when } -b \leq y < e-f,$$

$$i = 2 \text{ when } e-f \leq y \leq e+f,$$

$$i = 3 \text{ when } e+f < y \leq b.$$

The solution for w will be found by considering separately the solution of the homogeneous form of the governing equation, and a particular integral which satisfies the governing equation. The complete solution will then be the sum of the homogeneous and particular solutions. In each of the three regions, the following Levy series form of the homogeneous portion of w is assumed:

$$w_{hi} = \sum_{n=1}^{\infty} \Phi(y)_{in} \sin \alpha_n x \tag{37}$$

where i = 1, 2, 3 and $\Phi(y)_{in}$ are continuous functions of class C^4 and are dependent on the regions, i, and the series term, n.

Assuming the above series to be uniformly convergent[a], equations 37 may be differentiated termwise and substituted into the homogeneous form of equation 35 which results in the following series:

$$\sum_{n=1}^{\infty} D(1 + \phi_n)\left[\frac{d^4}{dy^4}\Phi(y)_{in} - 2\frac{d^2}{dy^2}\Phi(y)_{in}\alpha_n^2 + \Phi(y)_{in}\alpha_n^4\right] \cdot \sin \alpha_n x = 0 \tag{37a}$$

where $\phi_n = D_y\alpha_n^2$. It can be seen that $\Phi(y)_{in}$ must have the following form such that the above relationship is satisfied for all x and n:

$$\Phi(y)_{in} = A_{in}'\sinh \alpha_n y + B_{in}'\cosh \alpha_n y + C_{in}'\alpha_n y \sinh \alpha_n y + F_{in}'\alpha_n y \cosh \alpha_n y \tag{38}$$

where A_{in}', B_{in}', C_{in}', and F_{in}' are arbitrary constants dependent on the region, i, and the series term, n, and the values of y take on the range assigned to each value of i.

It should be noted that the above solution for w_{hi} is a solution to $\nabla^4 w_{hi} = 0$. Since equation 35 is of the sixth

---

[a]Uniform convergence is assumed for all series in succeeding work so that termwise differentiation and integration is valid.

order, two additional integrals for w_{hi} are required for the complete determination of the homogeneous portion of w. However, the effect of these additional integrals on the complete solutions is assumed to be negligible due to the presence of simple support boundary conditions at x = 0 and 2a. It is pointed out, however, that for other boundary conditions such as clamped or cantilevered edges, the omission of the additional integrals of w_{hi} may lead to erroneous solutions.

The particular solution for w can be taken as

$$w_{pi} = \delta_{2i} \sum_{n=1}^{\infty} \frac{H_n}{\alpha_n{}^4 D} \sin \alpha_n x \tag{39}$$

where $\delta_{2i} = 0$ for i = 1,3

$= 1$ for i = 2.

It can be seen that the above expression satisfies the governing equation for all values of x and y.

The complete solution for w may be expressed as follows by combining equations 37, 38, and 39:

$$w_i = \sum_{n=1}^{\infty} \frac{H_n}{\alpha_n{}^4 D(1-\nu)} \left[A_{in} \sinh \alpha_n y + B_{in} \cosh \alpha_n y \right.$$

$$+ C_{in}\,\alpha_n y \sinh \alpha_n y + F_{in}\,\alpha_n y \cosh \alpha_n y + \delta_{2i}\,(1-\nu)\Big]$$

$$\cdot \sin \alpha_n x \qquad (40)$$

where the constants have been redefined as

$$\left[A_{in}' \;\ldots\; F_{in}'\right] = \frac{H_n}{\alpha_n{}^4 D(1-\nu)} \left[A_{in} \;\ldots\; F_{in}\right] \quad .$$

For the loading series and complete solution for w assumed thus far, it is seen that $\frac{\partial}{\partial y}p = 0$ and $D\nabla^4 w_i = p$ for i = 1, 2, and 3. Thus, equations 31 and 33 are homogeneous. Therefore, a part of the solution for Q_y is harmonic. In general, the homogeneous form of equation 31 requires that Q_y is partly harmonic with an added integral. Similarly, the homogeneous form of equation 33 shows that the complete solution for Q_y is partly harmonic with two added integrals. However, as in the case of the homogeneous solution for w, the effect of the added integrals on the final solutions is assumed negligible due to the simple support boundary conditions at x = 0 and 2a. Thus, Q_y is assumed to be harmonic.

In particular, Q_y is assumed to be of the following form:

$$Q_{yi} = \sum_{n=1}^{\infty} \left[M_{in}'\sinh \alpha_n y + N_{in}'\cosh \alpha_n y \right] \sin \alpha_n x. \qquad (41)$$

Equation 28 is now the only expression remaining to be satisfied. If expressions 40 and 41 are substituted into equation 28, the following relationships are found between the constants:

$$C_{in} = \theta_n M_{in} \text{ , and } F_{in} = \theta_n N_{in}$$

$$\text{where } \theta_n = \frac{(1-\nu)\left[\phi_n\left(\frac{1+\nu}{1-\nu}\right) - 1 \right]}{2} ,$$

$$M_{in}' = \frac{H_n}{\alpha_n} M_{in} \text{ , and}$$

$$N_{in}' = \frac{H_n}{\alpha_n} N_{in} .$$

The expressions for w and Q_y can now be written in terms of the twelve constants, A_{in}, B_{in}, M_{in}, and N_{in}, in the following forms:

$$w_i = \sum_{n=1}^{\infty} \frac{H_n}{\alpha_n{}^4 D(1-\nu)} \Big[A_{in} \sinh \alpha_n y + B_{in} \cosh \alpha_n y$$

$$+ M_{in}\theta_n \alpha_n y \sinh \alpha_n y + N_{in}\theta_n \alpha_n y \cosh \alpha_n y$$

$$+ \delta_{2i} (1-\nu) \Big] \sin \alpha_n x \qquad (42)$$

$$Q_{yi} = \sum_{n=1}^{\infty} \frac{H_n}{\alpha_n} \Big[M_{in} \sinh \alpha_n y + N_{in} \cosh \alpha_n y \Big] \sin \alpha_n x \qquad (43)$$

The reactive force, V_{yi}, is required for the evaluation of the constants. This force is (15)

$$V_{yi} = Q_{yi} - \frac{\partial M_{xyi}}{\partial x} . \qquad (44)$$

The unit forces, M_x, M_y, M_{xy}, and V_y, can now be found by substituting equations 42 and 43 into expression 44 and the force-displacement relations. It is convenient for coefficient evaluation and computational purposes to express the unit force expressions in the following dimensionless forms:

$$M_{xi} = \sum_{n=1}^{\infty} \frac{H_n}{\alpha_n^2} \left\{ A_{in} \sinh \beta_n \eta + B_{in} \cosh \beta_n \eta \right.$$

$$+ M_{in} \left[\theta_n \beta_n \eta \sinh \beta_n \eta + \nu(\phi_n + 1) \cosh \beta_n \eta \right] \qquad (45)$$

$$+ N_{in} \left[\theta_n \beta_n \eta \cosh \beta_n \eta + \nu(\phi_n + 1) \sinh \beta_n \eta \right]$$

$$\left. + \delta_{2i} \right\} \sin \alpha_n x$$

$$M_{yi} = \sum_{n=1}^{\infty} - \frac{H_n}{\alpha_n^2} \left\{ A_{in} \sinh \beta_n \eta + B_{in} \cosh \beta_n \eta \right.$$

$$+ M_{in} \left[\theta_n \beta_n \eta \sinh \beta_n \eta - (\phi_n + 1) \cosh \beta_n \eta \right] \qquad (46)$$

$$+ N_{in} \left[\theta_n \beta_n \eta \cosh \beta_n \eta - (\phi_n + 1) \sinh \beta_n \eta \right] - \nu \delta_{2i} \Big\}$$

$$\cdot \sin \alpha_n x$$

$$M_{xyi} = \sum_{n=1}^{\infty} \frac{H_n}{\alpha_n^2} \left\{ A_{in} \cosh \beta_n \eta + B_{in} \sinh \beta_n \eta \right.$$

$$+ M_{in}\left[\theta_n\beta_n\eta \cosh \beta_n\eta + (\theta_n - \phi_n) \sinh \beta_n\eta\right]$$

$$+ N_{in}\left[\theta_n\beta_n\eta \sinh \beta_n\eta + (\theta_n - \phi_n) \cosh \beta_n\eta\right]\Big\} \qquad (47)$$

$$\cdot\cos \alpha_n x$$

$$V_{yi} = \sum_{n=1}^{\infty} \frac{H_n}{\alpha_n}\Big\{A_{in} \cosh \beta_n\eta + B_{in} \sinh \beta_n\eta$$

$$+ M_{in}\left[\theta_n\beta_n\eta \cosh \beta_n\eta + (\theta_n - \phi_n + 1) \sinh \beta_n\eta\right] \qquad (48)$$

$$+ N_{in}\left[\theta_n\beta_n\eta \sinh \beta_n\eta + (\theta_n - \phi_n + 1) \cosh \beta_n\eta\right]\Big\}$$

$$\cdot\sin \alpha_n x$$

where $\beta_n = \alpha_n b$ and $\eta = \frac{y}{b}$.

In addition to the above unit forces, a complete solution to the problem should also contain expressions for the longitudinal shear and reactive forces. Upon substitution of the appropriate force displacement relationships into the third equation of equilibrium, the expression for the longitudinal unit shearing force can be found. This force is:

$$Q_{xi} = -D\frac{\partial}{\partial x} \nabla^2 w_i + D_y \left(\frac{1+\nu}{1-\nu}\right)\frac{\partial^2 Q_{yi}}{\partial x \partial y} \quad . \qquad (49)$$

Also, the longitudinal reactive force is (15)

$$V_{xi} = Q_{xi} - \frac{\partial M_{xyi}}{\partial y} \quad . \tag{50}$$

If equations 42, 43, and 47 are substituted into expressions 49 and 50, the following expressions for the longitudinal shear and reactive force result:

$$Q_{xi} = \sum_{n=1}^{\infty} \frac{H_n}{\alpha_n} \left[M_{in} \cosh \beta_n \eta + N_{in} \sinh \beta_n \eta + \delta_{2i} \right] \cos \alpha_n x, \tag{51}$$

$$\begin{aligned} V_{xi} = \sum_{n=1}^{\infty} - \frac{H_n}{\alpha_n} \Big\{ & A_{in} \sinh \beta_n \eta + B_{in} \cosh \beta_n \eta \\ & + M_{in} \left[\theta_n \beta_n \eta \sinh \beta_n \eta + (2\theta_n - \phi_n - 1) \cosh \beta_n \eta \right] \\ & + N_{in} \left[\theta_n \beta_n \eta \cosh \beta_n \eta + (2\theta_n - \phi_n - 1) \sinh \beta_n \eta \right] \\ & - \delta_{2i} \Big\} \cos \alpha_n x \ . \end{aligned} \tag{52}$$

If the solution derived thus far is to be a true solution, then it must satisfy the boundary conditions. The boundary conditions for the simply supported sides, x = 0 and 2a, are

$w = 0$ and $M_x = 0$ for all y values (15). It can be seen that these conditions are identically satisfied by virtue of the sine series used. For the sides, $y = \pm b$, the following conditions must hold for all values of x (15):

$$M_{y1}\Big|_{\eta = -1} = 0 \tag{53}$$

$$V_{y1}\Big|_{\eta = -1} = 0 \tag{54}$$

$$M_{y3}\Big|_{\eta = 1} = 0 \tag{55}$$

$$V_{y3}\Big|_{\eta = 1} = 0 \tag{56}$$

In addition to the boundary conditions, compatibility and force continuity conditions must be maintained in the domain at the boundaries of the three regions specified previously. For this purpose it is convenient to define the non-dimensional parameters, ζ and ξ, such that $\zeta = (e-f)/b$ and $\xi = (e+f)/b$. Sufficient conditions such that compatibility and force continuity are maintained at $\eta = \zeta$ and $\eta = \xi$ may be listed as follows:

$$w_j\Big|_{\eta = \eta_j} = w_{j+1}\Big|_{\eta = \eta_j} \tag{57}$$

$$\frac{\partial w_j}{\partial y}\Big|_{\eta = \eta_j} = \frac{\partial w_{j+1}}{\partial y}\Big|_{\eta = \eta_j} \tag{58}$$

$$M_{yj}\Big|_{\eta = \eta_j} = M_{y\ j+1}\Big|_{\eta = \eta_j} \tag{59}$$

$$Q_{yj}\Big|_{\eta = \eta_j} = Q_{y\ j+1}\Big|_{\eta = \eta_j} \tag{60}$$

where $j = 1, 2$ and $\eta_1 = \zeta$ and $\eta_2 = \xi$. If the appropriate expressions are substituted into the four boundary condition and eight compatibility and force continuity equations, and the resulting expressions satisfied termwise, a set of twelve simultaneous equations is obtained. The solution of these equations results in the unique determination of the twelve constants, A_{in}, B_{in}, M_{in}, and N_{in}. This procedure must be repeated for each series term considered when numerical computations are performed. The resulting set of simultaneous equations is shown as follows:

$$A_{1n} \sinh \beta_n - B_{1n} \cosh \beta_n - M_{1n}\left[\theta_n\beta_n \sinh \beta_n - (\phi_n + 1) \cosh \beta_n\right] + N_{1n}\left[\theta_n\beta_n \cosh \beta_n - (\phi_n + 1) \sinh \beta_n\right] = 0 \tag{61}$$

$$A_{1n} \cosh \beta_n - B_{1n} \sinh \beta_n - M_{1n}\left[\theta_n\beta_n \cosh \beta_n + (\theta_n - \phi_n + 1) \sinh \beta_n\right] + N_{1n}\left[\theta_n\beta_n \sinh \beta_n + (\theta_n - \phi_n + 1) \cosh \beta_n\right] = 0 \tag{62}$$

$$(A_{1n} - A_{2n}) \sinh \beta_n\zeta + (B_{1n} - B_{2n}) \cosh \beta_n\zeta + (M_{1n} - M_{2n}) \theta_n\beta_n\zeta \cdot\sinh \beta_n\zeta + (N_{1n} - N_{2n}) \theta_n\beta_n\zeta \cosh \beta_n\zeta = 1 - \nu \quad (63)$$

$$(A_{1n} - A_{2n}) \cosh \beta_n\zeta + (B_{1n} - B_{2n}) \sinh \beta_n\zeta + (M_{1n} - M_{2n}) \cdot\theta_n (\beta_n\zeta \cosh \beta_n\zeta + \sinh \beta_n\zeta) + (N_{1n} - N_{2n}) \theta_n (\beta_n\zeta \sinh \beta_n\zeta + \cosh \beta_n\zeta) = 0 \quad (64)$$

$$(A_{2n} - A_{1n}) \sinh \beta_n\zeta + (B_{2n} - B_{1n}) \cosh \beta_n\zeta + (M_{2n} - M_{1n}) \cdot \left[\theta_n\beta_n\zeta \sinh \beta_n\zeta - (\phi_n + 1) \cosh \beta_n\zeta\right] + (N_{2n} - N_{1n}) \left[\theta_n\beta_n\zeta \cosh \beta_n\zeta - (\phi_n + 1) \cdot\sinh \beta_n\zeta\right] = \nu \quad (65)$$

$$(M_{1n} - M_{2n}) \sinh \beta_n\zeta + (N_{1n} - N_{2n}) \cosh \beta_n\zeta = 0 \quad (66)$$

$$(A_{3n} - A_{2n}) \sinh \beta_n\xi + (B_{3n} - B_{2n}) \cosh \beta_n\xi + (M_{3n} - M_{2n}) \cdot\theta_n\beta_n\xi \sinh \beta_n\xi + (N_{3n} - N_{2n}) \theta_n\beta_n\xi \cosh \beta_n\xi = 1 - \nu \quad (67)$$

$$(A_{3n} - A_{2n}) \cosh \beta_n\xi + (B_{3n} - B_{2n}) \sinh \beta_n\xi + (M_{3n} - M_{2n})$$
$$\cdot\theta_n (\beta_n\xi \cosh \beta_n\xi + \sinh \beta_n\xi) + (N_{3n} - N_{2n}) \theta_n$$
$$\cdot(\beta_n\xi \sinh \beta_n\xi + \cosh \beta_n\xi) = 0 \qquad (68)$$

$$(A_{2n} - A_{3n}) \sinh \beta_n\xi + (B_{2n} - B_{3n}) \cosh \beta_n\xi + (M_{2n} - M_{3n})$$
$$\cdot\left[\theta_n\beta_n\xi \sinh \beta_n\xi - (\phi_n + 1) \cosh \beta_n\xi\right] + (N_{2n} - N_{3n})$$
$$\cdot\left[\theta_n\beta_n\xi \cosh \beta_n\xi - (\phi_n + 1) \sinh \beta_n\xi\right] = \nu \qquad (69)$$

$$(M_{3n} - M_{2n}) \sinh \beta_n\xi + (N_{3n} - N_{2n}) \cosh \beta_n\xi = 0 \qquad (70)$$

$$A_{3n} \sinh \beta_n + B_{3n} \cosh \beta_n + M_{3n}\left[\theta_n\beta_n \sinh \beta_n\right.$$
$$\left. - (\phi_n + 1) \cosh \beta_n\right] + N_{3n}\left[\theta_n\beta_n \cosh \beta_n\right.$$
$$\left. - (\phi_n + 1) \sinh \beta_n\right] = 0 \qquad (71)$$

$$A_{3n} \cosh \beta_n + B_{3n} \sinh \beta_n + M_{3n}\left[\theta_n\beta_n \cosh \beta_n + (\theta_n - \phi_n + 1)\right.$$
$$\left.\cdot\sinh \beta_n\right] + N_{3n}\left[\theta_n\beta_n \sinh \beta_n + (\theta_n - \phi_n + 1)\right.$$
$$\left.\cdot\cosh \beta_n\right] = 0 \ . \qquad (72)$$

Since the exact solution of the above equations is seen to be practically impossible, numerical techniques are used for computational purposes.

Definition of Distribution Coefficients

So that the previously derived expressions for the deflection and unit force quantities are more readily usable, distribution coefficients are defined such that the resulting coefficients are non-dimensional and normalized. All coefficients are based on the behavior of an infinitely wide cylindrically bent plate of length 2a and flexural rigidity D. The coefficients are defined such that the deflections or unit force quantities existing in the equivalent plate are divided by corresponding quantities in the cylindrically bent plate for similar external loading. Given a unit force or deflection coefficient thus defined, the span and rigidity of the structure, and the total external load and longitudinal load position, the calculation of the actual unit force or deflection is easily done. This results from the fact that a deflections and unit force quantities in a cylindrically bent plate may be found by simple beam theory.

If the infinitely wide plate is loaded with an infinitely long line load of magnitude $\frac{qf}{b}$ located at x=c, the infinite plate will undergo cylindrical bending. In this case, the total load acting on a 2b width of the infinite plate must

equal the total load on the equivalent plate. The deflection and unit force quantities of the infinite plate will represent the average deflection and unit forces of the equivalent plate.

The deflection, w_a, of the infinite plate can be written as

$$w_a = \sum_{n=1}^{\infty} \frac{f}{b} \frac{H_n}{\alpha_n{}^4 D} \sin \alpha_n x$$

or

$$w_a = \frac{f}{bD} \left(\frac{2a}{\pi}\right)^4 S_w$$

where $S_w = \sum_{n=1}^{\infty} \frac{H_n}{n^4} \sin \alpha_n x_1$,

and x_1 is the ordinate at which the deflection is to be evaluated. Also, the longitudinal unit shearing force, Q_{xa}, and longitudinal unit moment, M_{xa}, in the cylindrically bent plate are

$$Q_{xa} = -D \frac{d^3 w_a}{dx^3} = \frac{f}{b} \frac{2a}{\pi} S_{qx},$$

$$M_{xa} = -D \frac{d^2 w_a}{dx^2} = \frac{f}{b} \left(\frac{2a}{\pi}\right)^2 S_m$$

$$\text{where} \quad S_{qx} = \sum_{n=1}^{\infty} \frac{H_n}{n} \cos \alpha_n x_2,$$

$$S_m = \sum_{n=1}^{\infty} \frac{H_n}{n^2} \sin \alpha_n x_1,$$

and x_2 is the ordinate at which the longitudinal unit shearing force is to be evaluated. It is seen that the longitudinal unit bending moments will be evaluated at the same location as the deflections. It is convenient for later use to define the following quantity:

$$Q_{xa}' = \frac{f}{b} \frac{2a}{\pi} S_{qy}$$

$$\text{where } S_{qy} = \sum_{n=1}^{\infty} \frac{H_n}{n} \cos \alpha_n x_3,$$

and x_3 is an arbitrary ordinate to be defined later.

Distribution coefficients per unit width

The following coefficients will be defined such that the overall behavior of the equivalent plate and hence the actual structure can be studied in detail. The following definitions

of the various coefficients, as discussed previously, are convenient for behavioral studies and design purposes. The deflection coefficient per unit width is defined as

$$\bar{w}_i = \frac{w_i}{w_a} .$$

If expression 42 for w_i is written as

$$w_i = \frac{1}{D} \left(\frac{2a}{\pi}\right)^4 \sum_{n=1}^{\infty} \frac{H_n}{n^4} \bar{w}_{in} \sin \alpha_n x_1 ,$$

then the deflection coefficient per unit width becomes

$$\bar{w}_i = \frac{b}{f} \frac{\sum_{n=1}^{\infty} \frac{H_n}{n^4} \bar{w}_{in} \sin \alpha_n x_1}{S_w} . \qquad (73)$$

In a similar manner, the moment coefficients per unit width for M_{xi}, M_{yi}, and M_{xyi} can respectively be defined as

$$\bar{M}_{xi} = \frac{M_{xi}}{M_{xa}} ,$$

$$\bar{M}_{yi} = \frac{M_{yi}}{M_{xa}} ,$$

$$\bar{M}_{xyi} = \frac{M_{xyi}}{M_{xa}} .$$

If expressions 45, 46, and 47 are respectively defined as

$$M_{xi} = \left(\frac{2a}{\pi}\right)^2 \sum_{n=1}^{\infty} \frac{H_n}{n^2} \bar{m}_{xin} \sin \alpha_n x_1 ,$$

$$M_{yi} = \left(\frac{2a}{\pi}\right)^2 \sum_{n=1}^{\infty} \frac{H_n}{n^2} \bar{m}_{yin} \sin \alpha_n x_1 ,$$

$$M_{xyi} = \left(\frac{2a}{\pi}\right)^2 \sum_{n=1}^{\infty} \frac{H_n}{n^2} \bar{m}_{xyin} \cos \alpha_n x_4$$

where x_4 is the ordinate at which the unit twisting moment is to be evaluated, then the moment coefficients per unit width become

$$\bar{M}_{xi} = \frac{b}{f} \frac{\sum_{n=1}^{\infty} \frac{H_n}{n^2} \bar{m}_{xin} \sin \alpha_n x_1}{S_m} \qquad (74)$$

$$\bar{M}_{yi} = \frac{b}{f} \frac{\sum_{n=1}^{\infty} \frac{H_n}{n^2} \bar{m}_{yin} \sin \alpha_n x_1}{S_m} \tag{75}$$

$$\bar{M}_{xyi} = \frac{b}{f} \frac{\sum_{n=1}^{\infty} \frac{H_n}{n^2} \bar{m}_{xyin} \cos \alpha_n x_4}{S_m} \quad . \tag{76}$$

It is seen from the above definitions that the reference moment used for the transverse and twisting moment coefficients is the longitudinal moment in the cylindrically bent plate. This follows since the transverse and twisting moments in the cylindrically bent plate are identically zero. In addition, it can be seen that the x ordinate selected for twisting moment coefficient evaluation is, in general, different from the ordinate used for longitudinal and transverse moment coefficient evaluation. This follows from the behavior of simply supported plates. It can be expected that maximum longitudinal and transverse moments will be obtained at mid-span when the load is located at mid-span. However, for this loading position, the maximum twisting moments will not occur at midspan; hence, the ordinate for twisting moment coefficient evaluation is not taken at

midspan and is, in general, different from the ordinate for the bending moment coefficient evaluations.

Longitudinal unit shear and reactive force coefficients are defined as follows:

$$\overline{Q}_{xi} = \frac{Q_{xi}}{Q_{xa}}$$

$$\overline{V}_{xi} = \frac{V_{xi}}{Q_{xa}} \quad .$$

It is seen that the average longitudinal unit shearing force is used in the definition of the longitudinal reactive force coefficient. This follows since the longitudinal reactive force is identically equal to the longitudinal unit shearing force in the cylindrically bent plate. If expressions 51 and 52 are, respectively, redefined as

$$Q_{xi} = \frac{2a}{\pi} \sum_{n=1}^{\infty} \frac{H_n}{n} \overline{q}_{xin} \cos \alpha_n x_2$$

and

$$V_{xi} = \frac{2a}{\pi} \sum_{n=1}^{\infty} \frac{H_n}{n} \overline{v}_{xin} \cos \alpha_n x_2 \ ,$$

then the expressions for the longitudinal unit shear and reactive force coefficients become

$$\bar{Q}_{xi} = \frac{b}{f} \frac{\sum_{n=1}^{\infty} \frac{H_n}{n} \bar{q}_{xin} \cos \alpha_n x_2}{S_{qx}} \tag{77}$$

and

$$\bar{V}_{xi} = \frac{b}{f} \frac{\sum_{n=1}^{\infty} \frac{H_n}{n} \bar{v}_{xin} \cos \alpha_n x_2}{S_{qx}} \quad . \tag{78}$$

Finally, the transverse unit shear and reactive force coefficients can respectively be defined as

$$\bar{Q}_{yi} = \frac{Q_{yi}}{Q_{xa}'}$$

and

$$\bar{V}_{yi} = \frac{V_{yi}}{Q_{xa}'} \quad .$$

The average longitudinal unit shear force, Q_{xa}', is used in the above definitions since the transverse unit shear and reactive forces are zero in the cylindrically bent plate. As before, the unit force expressions for Q_{yi} and V_{yi} will be simplified by redefining expressions 43 and 48 to be

$$Q_{yi} = \frac{2a}{\pi} \sum_{n=1}^{\infty} \frac{H_n}{n} \bar{q}_{yin} \sin \alpha_n x_1$$

and $$V_{yi} = \frac{2a}{\pi} \sum_{n=1}^{\infty} \frac{H_n}{n} \bar{v}_{yin} \sin \alpha_n x_1 \quad .$$

Thus, the transverse unit shear and reactive force coefficients become

$$\bar{Q}_{yi} = \frac{b}{f} \frac{\sum_{n=1}^{\infty} \frac{H_n}{n} \bar{q}_{yin} \sin \alpha_n x_1}{S_{qy}} \tag{79}$$

and $$\bar{V}_{yi} = \frac{b}{f} \frac{\sum_{n=1}^{\infty} \frac{H_n}{n} \bar{v}_{yin} \sin \alpha_n x_1}{S_{qy}} \quad . \tag{80}$$

Distribution coefficients per beam

Distribution coefficients per unit width, as defined above, are useful for the study of the behavior of the structure. However, design practice requires the determination of force quantities for beam elements. Figure 5 illustrates a typical

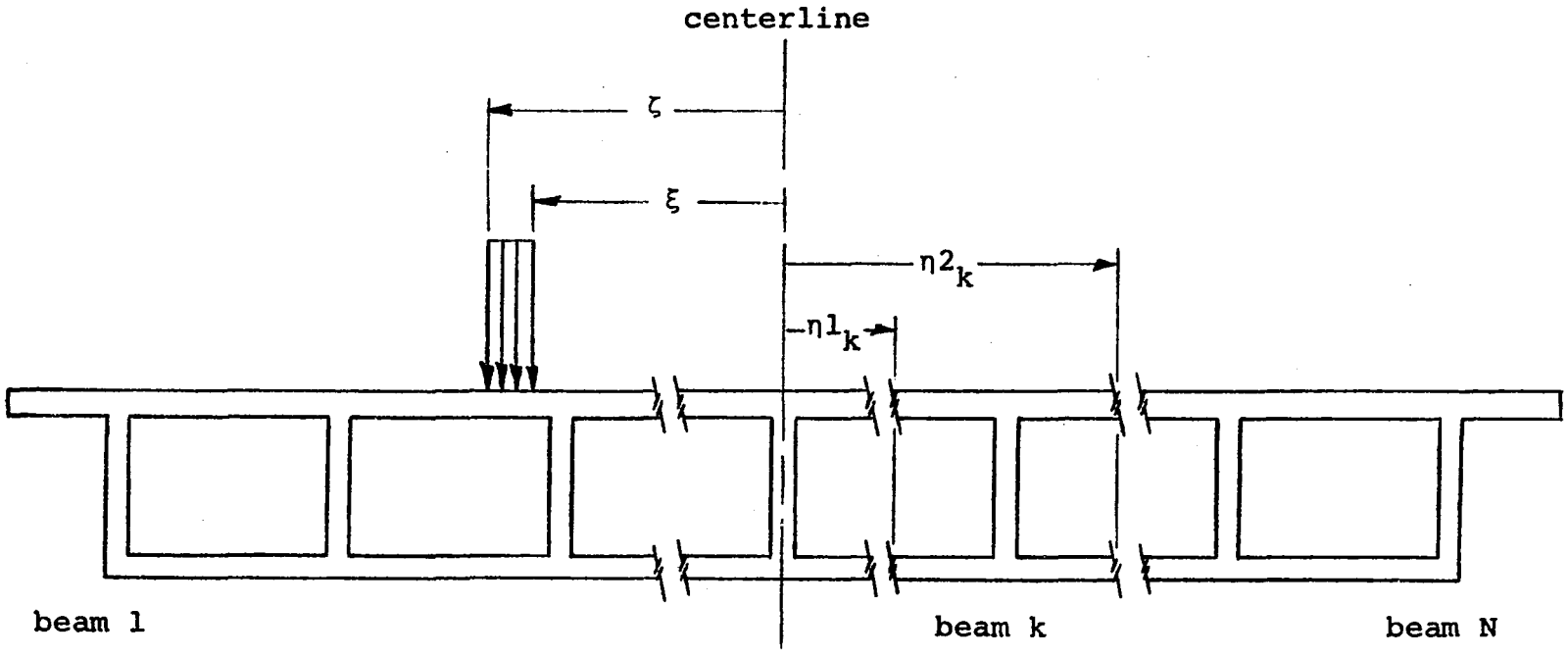

Figure 5. Typical cross-section with a beam element delineated

section of the structure with the commonly assumed beam element delineated. To find the total forces and moments acting on the beam element, it is necessary to integrate the unit force expressions across the width of the beam element. In order to design the beam element, it is necessary to know the vertical shearing force, normal bending moment, and twisting moment which act on the element. As in the case of the various coefficients per unit width, the beam element forces are conveniently described in coefficient form. The moment and shearing force coefficients per beam thus become:

$$\bar{M}_{xb_k} = \frac{\int_{\eta 1_k}^{\eta 2_k} M_x\,(\sigma)\,d\sigma}{\frac{1}{N}\int_{-1}^{1} M_x\,(\sigma)\,d\sigma},$$

$$\bar{M}_{xyb_k} = \frac{\int_{\eta 1_k}^{\eta 2_k} M_{xy}\,(\sigma)\,d\sigma}{\frac{1}{N}\int_{-1}^{1} M_x\,(\sigma)\,d\sigma}, \text{ and}$$

$$\bar{Q}_{xb_k} = \frac{\int_{\eta 1_k}^{\eta 2_k} Q_x\,(\sigma)\,d\sigma}{\frac{1}{N}\int_{-1}^{1} Q_x\,(\sigma)\,d\sigma}$$

where $\bar{M}_{xb_k}$ is the longitudinal bending moment coefficient per beam,

$\bar{M}_{xyb_k}$ is the twisting moment coefficient per beam,

$\bar{Q}_{xb_k}$ is the longitudinal shear coefficient per beam,

N is the total number of beam elements in the structure,

k is a subscript referring to the particular beam element studied, and

$\eta 1_k$ and $\eta 2_k$ are the limits of integration for the k-th beam element as shown in Figure 5.

The above expressions can be simplified in form if it is observed that the following identities must hold from overall equilibrium:

$$\int_{-1}^{1} M_x(\sigma)\, d\sigma = 2M_{xa} ,$$

and

$$\int_{-1}^{1} Q_x(\sigma)\, d\sigma = 2Q_{xa} .$$

If the numerators in the coefficient expressions are integrated termwise and the above identities are utilized, the following coefficients per beam result:

$$\bar{M}_{xb_k} = \frac{NLb}{\pi W f} \frac{\sum_{n=1}^{\infty} \frac{H_n}{n^3} \bar{m}_{xb_{kn}} \sin \alpha_n x_1}{S_m} , \qquad (81)$$

$$\bar{M}_{xyb_k} = \frac{NLb}{\pi Wf} \frac{\sum_{n=1}^{\infty} \frac{H_n}{n^3} \bar{m}_{xyb_{kn}} \sin \alpha_n x_1}{S_m}, \tag{82}$$

$$\bar{Q}_{xb_k} = \frac{NLb}{\pi Wf} \frac{\sum_{n=1}^{\infty} \frac{H_n}{n^2} \bar{q}_{xb_{kn}} \cos \alpha_n x_2}{S_{qx}} \tag{83}$$

where W is the width and L is the span of the structure.

The quantities, $\bar{m}_{xb_{kn}}$, $\bar{m}_{xyb_{kn}}$, and $\bar{q}_{xb_{kn}}$, will depend on the limits of integration for the k-th beam element and the series term n. In order to write concise expressions for these quantities, the following cases, which depend on the location of the limits of integration $\eta 1_k$ and $\eta 2_k$, are defined:

i. $-1 \leq \eta 1_k < \zeta \Rightarrow j = 1,\ \ell_1 = \eta 1_k$

ii. $\zeta \leq \eta 1_k < \xi \Rightarrow j = 2,\ \ell_2 = \eta 1_k$

iii. $\xi \leq \eta 1_k < 1 \Rightarrow j = 3,\ \ell_3 = \eta 1_k$

a. $-1 < \eta 2_k \leq \zeta \Rightarrow p = 1,\ u_1 = \eta 2_k$

b. $\zeta < \eta 2_k \leq \xi \Rightarrow p = 2,\ u_2 = \eta 2_k$

c. $\xi < \eta 2_k \leq 1 \Rightarrow p = 3,\ u_3 = \eta 2_k$

where, in addition, if

i and b, or i and c, then $u_1 = \ell_2 = \zeta$, and

i and c, or ii and c, then $u_2 = \ell_3 = \xi$.

The expressions for the coefficients per beam can now be completed by writing

$$\bar{m}_{xb_{kn}} = \sum_{i=j}^{p} \Big\{ A_{in} \left(\cosh \beta_n u_i - \cosh \beta_n \ell_i\right) + B_{in} \left(\sinh \beta_n u_i - \sinh \beta_n \ell_i\right) + M_{in} \Big[\theta_n \beta_n \left(u_i \cosh \beta_n u_i - \ell_i \cosh \beta_n \ell_i\right) + \left(\nu(\phi_n+1)-\theta_n\right)\left(\sinh \beta_n u_i - \sinh \beta_n \ell_i\right)\Big] + N_{in} \Big[\theta_n \beta_n \left(u_i \sinh \beta_n u_i - \ell_i \sinh \beta_n \ell_i\right) + \left(\nu(\phi_n+1)-\theta_n\right)\left(\cosh \beta_n u_i - \cosh \beta_n \ell_i\right)\Big] + \delta_{2i} \beta_n \left(u_i - \ell_i\right) \Big\}$$

$$\bar{m}_{xyb_{kn}} = \sum_{i=j}^{p} \Big\{ A_{in} \left(\sinh \beta_n u_i - \sinh \beta_n \ell_i\right) + B_{in} \left(\cosh \beta_n u_i - \cosh \beta_n \ell_i\right) + M_{in} \Big[\theta_n \beta_n \left(u_i \sinh \beta_n u_i - \ell_i \sinh \beta_n \ell_i\right)$$

$$- \phi_n \left(\cosh \beta_n u_i - \cosh \beta_n \ell_i\right)\Big] + N_{in}\Big[\theta_n \beta_n \left(u_i \cosh \beta_n u_i$$

$$- \ell_i \cosh \beta_n \ell_i\right) - \phi_n \left(\sinh \beta_n u_i - \sinh \beta_n \ell_i\right)\Big]\Big\}$$

$$\bar{q}_{xb_{kn}} = \sum_{i=j}^{p} \Big\{ M_{in} \left(\sinh \beta_n u_i - \sinh \beta_n \ell_i\right) + N_{in} \left(\cosh \beta_n u_i$$

$$- \cosh \beta_n \ell_i\right) + \delta_{2i} \beta_n \left(u_i - \ell_i\right)\Big\} \quad .$$

Significance of the distribution coefficients

The primary significance of the distribution coefficients, as they are defined above, lies in the ease of describing the complete behavior of an actual bridge structure by the use of these coefficients.

All of the previously defined coefficients are based on the behavior of a cylindrically bent plate with the same flexural rigidity as the equivalent plate and the actual structure. In the case where the coefficients are defined per unit width, the unit forces and deflections in the equivalent cylindrically bent plate may be easily found by calculating moments, shears, and deflections assuming the structure to be a simple beam and then dividing the simple beam forces by the width of the equivalent plate or the equivalent width of the structure. The complete behavior of the structure may now be described by multiplying

the appropriate cylindrical or average unit forces and deflections by the corresponding coefficients.

In the case where the moments or shears are desired for beam elements of the actual structure, the simple beam moments or shears are divided by the number of beam elements and then are multiplied by the corresponding beam coefficients to obtain the moments or shears for each beam element.

Governing Parameters and their Determination

Aspect ratio, W/L

The aspect ratio of the structure, defined as the ratio of the width, W, to the span, L, is a measure of the effect of the overall geometry of the bridge on its behavior. As shown in equation 48, width and span appear in the variable, β_n, as the ratio W/L. In addition, this ratio appears in expressions 73 through 80 for the distribution coefficients per unit width and in expressions 81 through 83 for the distribution coefficients per beam. In addition to the aspect ratio, the depth of the core medium, h, is a measure of the effect of overall geometry on behavior. However, h appears in the rigidity variables D and D_y and will be discussed in connection with the rigidity parameter, ϕ.

Rigidity parameter, ϕ

The rigidities of the structure are expressed in terms of the flexural rigidity, D, and the variable, D_y, which is

the measure of the structure's shearing rigidity. As previously derived, the flexural rigidity is

$$D = \frac{E}{1 - \nu^2} \cdot \frac{t_f \left(h+t_f\right)^2}{2} \quad .$$

It is seen that the last term in the above expression is the moment of inertia per unit length of the composite structure when the effect of the inertia of the webs or diaphragms is not considered. If the moment of inertia per unit length of the composite structure is termed i, the expression for flexural rigidity becomes

$$D = \frac{Ei}{1 - \nu^2} \quad . \tag{84}$$

In the above form, the rigidity is in a form that is general enough to be used for any plate structure which has orthogonally isotropic flexural rigidity. In this sense, the restriction of equal thickness top and bottom flanges that was used in the derivation of the governing equations can be generalized to include the case of non-equal flanges. It can be seen that if unequal top and bottom flange thicknesses were originally allowed for in the derivation of the governing equations, only the mechanics of the derivation and the expression for D would change. However, D would be expressible as shown in equation 84. The original assumption that the webs and diaphragms contribute negligibly toward the total composite

inertia must remain unchanged since the inclusion of the web and diaphragm inertias would violate the condition of orthogonally isotropic flexural rigidity. In succeeding work, the general form of D will be used such that flanges of differing thicknesses may be considered.

Due to the use of distribution coefficients, the flexural rigidity appears only in the expression for the variable D_y. In addition, D_y occurs only in the variable ϕ_n in the final expressions for the distribution coefficients. This variable, originally defined as $D_y\alpha_n^2$, may be redefined as

$$\phi_n = \phi(n\pi)^2 \tag{85}$$

where $\phi = \frac{D_y}{L^2}$. It is seen that ϕ is a dimensionless parameter that specifies the rigidity characteristics of the structure. When the previously derived expression for D_y is used in the definition of ϕ, the following expression results:

$$\phi = \frac{D(1 - \nu)}{2hL^2G_y} .$$

If E is expressed in terms of G in equation 84, and this expression substituted into the above form for ϕ, the following expression results upon rearrangement of terms:

$$\phi = \psi \frac{i}{h^3} \left(\frac{h}{L}\right)^2 \tag{86}$$

where $\psi = \frac{G}{G_y}$.

The transverse shear modulus, G_y, must now be defined for the complete description of the rigidity characteristics of the structure. It can be seen that since the structure is non-homogeneous, G_y must be defined as an equivalent shear modulus. This may be accomplished by examining the transverse shear behavior of a typical element of the structure. However, the transverse shear behavior or a bridge which contains transverse diaphragms may be expected to differ from the behavior of a structure which does not contain diaphragms. Therefore, the definition of G_y will be treated separately for each case.

For the case of no diaphragms, the transverse shear behavior of a typical element of the structure is shown in Figure 6. Although the actual deformations which take place in the structure are flexural, the net deformation of the element considered is seen to be purely shear deformation. It is also seen from the figure that the general deformation may be simplified by rigid body rotation of the element.

A basic assumption used in the derivation of the governing equations was that the vertical shearing stresses act through an equivalent core medium which has shear modulus G_y. Figure 7 illustrates the equivalency between the actual frame type deformation of the structure and the shearing deformation of the equivalent core medium. It is also seen that the depth

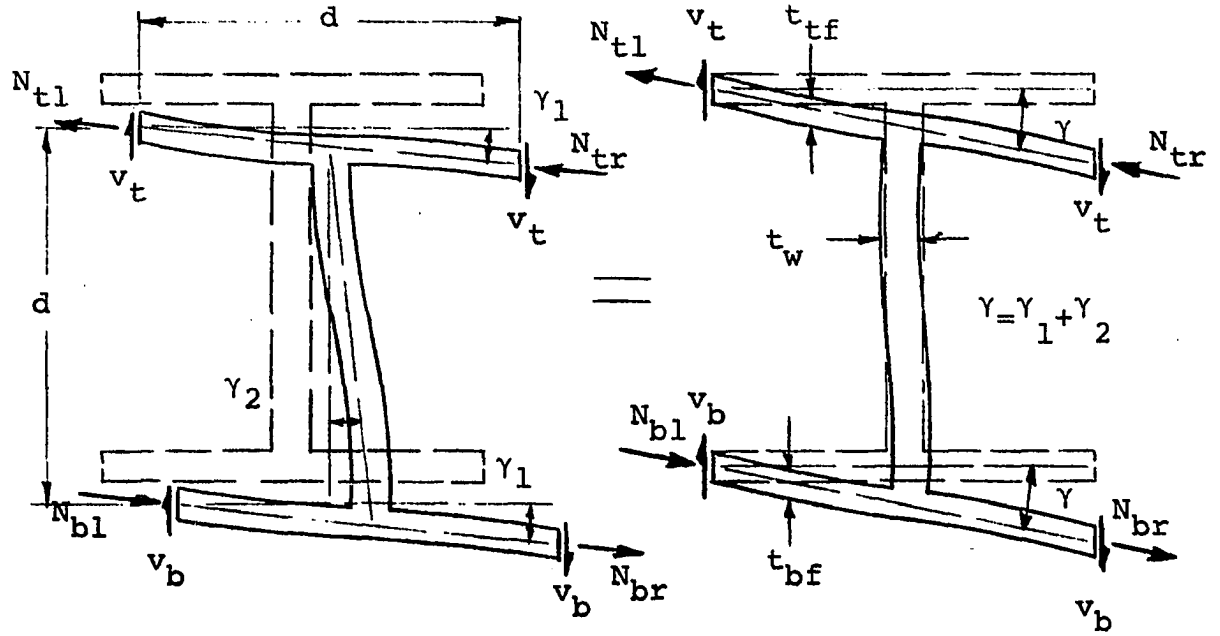

Figure 6. Transverse shear behavior of a typical structural element

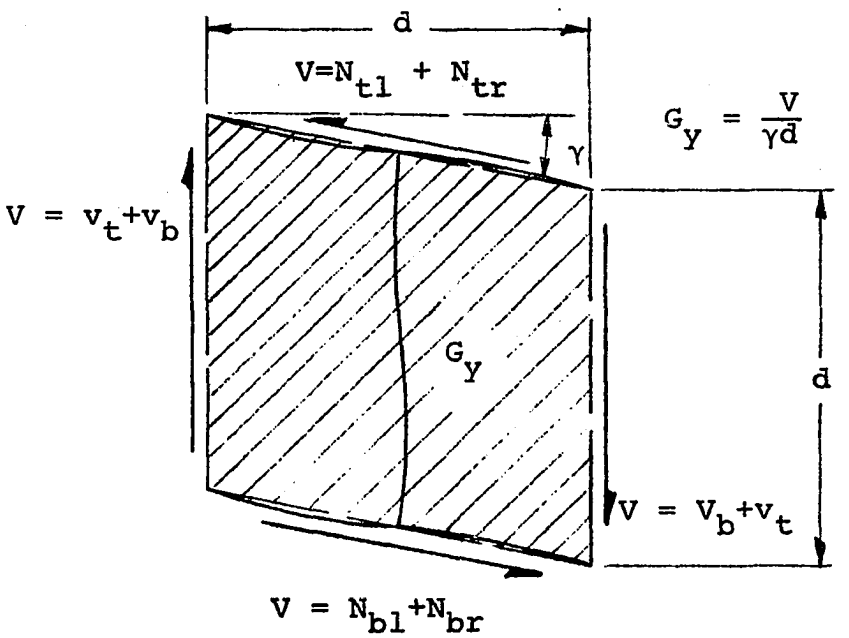

Figure 7. Idealized transverse shear behavior of a typical structural element

dimension, d, has been defined to be the center to center distance between the top and bottom flanges.

The definition of the equivalent transverse shear modulus thus becomes

$$G_y = \frac{V}{\gamma d} \tag{87}$$

where V is the total shearing force per unit width and γ is the shearing deformation of the element as shown in Figure 7.

If the structure shown in Figures 6 and 7 is given an arbitrary shear deformation, γ, the corresponding shearing force, V, may be found by means of a stiffness analysis of the frame. However, before the force is found, the equivalent stiffness of the web member for the shear block must be found. If the web spacing, s_w, is equal to the depth, d, the equivalent web stiffness will be equal to the stiffness of a unit length of the web. In general, it can be seen that the equivalent web stiffness may be expressed as

$$K_w = \frac{d}{s_w} \cdot \frac{EI_w}{d}$$

where I_w is the moment of inertia of a unit length of the web. A stiffness analysis of the frame shown in Figure 6 yields the following relationship between the shearing force and deflection:

$$V = \frac{18K_w\gamma}{d} \left[\frac{6r_b r_t + r_b + r_t}{(3r_t+2)(3r_b+2)-1} \right] \tag{88}$$

where $r_t = \frac{2s_w}{d}\left(\frac{t_{tf}}{t_w}\right)^3$,

$r_b = \frac{2s_w}{d}\left(\frac{t_{bf}}{t_w}\right)^3$,

s_w is the web spacing,

t_{tf} is the top flange thickness,

t_{bf} is the bottom flange thickness, and

t_w is the web thickness.

If I_w is expanded in the expression for K_w, equations 88 and 87 substituted into the expression for ψ, and E is expressed in terms of G, then the expression for ψ may be written as

$$\psi = \frac{1}{3(1+\nu)}\left(\frac{s_w}{d}\right)\left(\frac{d}{t_w}\right)^3\left[\frac{(3r_t+2)(3r_b+2)-1}{6r_tr_b + r_t + r_b}\right] . \qquad (89)$$

In the case where diaphragms are present, the equivalent shear modulus must take into account the effect of both shearing deformation of the diaphragms and the frame shearing deformations of the web and flanges. As simplifying assumptions, the shearing rigidity of the diaphragms is assumed to be uniformly distributed over the entire span of the bridge and no interactive forces are assumed to exist between the distributed diaphragm medium and the flanges or web. Although the second of the above assumptions appears to be unrealistic, it must be remembered

that in actual structures the number of diaphragms is small and interactive forces are highly localized. The first assumption is necessary since the basic philosophy of the investigation is to replace the actual structure by an equivalent homogeneous core medium.

The shearing deformation of a diaphragm is

$$\gamma = \frac{V_d}{Gd}$$

where V_d is the portion of the total unit shearing force transmitted to the diaphragm. When the diaphragm shearing rigidity is considered distributed over the diaphragm spacing, the above expression becomes

$$\gamma = \frac{V_d s_d}{G d t_d} \tag{90}$$

where s_d is the diaphragm spacing and t_d is the diaphragm thickness. The distribution of the total shearing force, V, to the distributed diaphragms and frame will be proportional to their respective rigidities. This may be shown by means of the following expressions:

$$V_f = \frac{R_f}{R_f+R_d} \; V \; ,$$

$$V_d = \frac{R_d}{R_d+R_f} \; V$$

where V_f is the portion of the total shearing force taken by the frame,

$R_f = 3dG(1+\nu)\left(\frac{d}{s_w}\right)\left(\frac{t_w}{d}\right)^3\left[\frac{6r_tr_b + r_t + r_b}{(3r_t+2)(3r_b+2)-1}\right]$, the equivalent shearing rigidity of the frame, and

$R_d = dG\frac{t_d}{s_d}$, the equivalent shearing rigidity of the distributed diaphragm medium.

Since the shear deformation, γ, is common to both the frame and the diaphragm medium, equation 90 may be used to express the shear deformation in equation 87. The latter equation defines the equivalent shear modulus. In addition, if the expressions for V_d and R_d are substituted into equation 87, the following form for the equivalent shear modulus results:

$$G_y = \frac{R_f+R_d}{d} \quad .$$

If the above expression is substituted into the definition of ψ together with the expressions for R_f and R_d, the following result is found for the case when diaphragms are present:

$$\psi = \frac{1}{\frac{t_d}{s_d} + 3(1+\nu)\left(\frac{d}{s_w}\right)\left(\frac{t_w}{d}\right)^3\left[\frac{6r_tr_b + r_t + r_b}{(3r_t+2)(3r_b+2)-1}\right]} \quad . \qquad (91)$$

Load width

Implicitly, load width is important to the solution since the regions defined in the solution of the governing equations are determined by the load width. Explicitly, the load width appears in each of the various coefficients as the ratio of the load width to the bridge width. The variation of this ratio, which appears as b/f in the expressions for the distribution coefficients, may be expected to affect the coefficients for points in the vicinity of the load and not have much effect on the coefficients for points which are remote from the load. In the case where loads corresponding to truck wheel loads are investigated, f will have a constant value corresponding to half of the width of a wheel. However, the bridge width is an important variable and therefore the ratio, b/f, should be expected to be a parameter which has an effect on the behavior of the structure.

Effective width and edge unstiffening

It was assumed in the derivation and solution of the governing equations that the rigidities of the structure are constant over the entire domain. However, in actual structures, this assumption is violated when the edge beam geometry is different than the geometry of a typical interior beam. In the case where the geometries are different, an effective width may be defined where the flexural rigidity remains constant within

the effective width. Figure 8 illustrates a typical structure where the edge beam is flexurally less stiff than the interior beams. As shown in the figure, the effective width is found in the following manner. First, i is found by determining the total inertia of an interior beam, I_i, and dividing this inertia by the web spacing, s_w. Next, the total inertia of the exterior beam is found which is used in the following definition of the effective exterior beam width, s_e:

$$i = \frac{I_e}{s_e} \quad \Rightarrow \quad s_e = \frac{I_e}{i} = \frac{I_e}{I_i} s_w$$

where I_e is the moment of inertia of the exterior beam element. Finally, the equivalent width of the structure may be found by summing the widths of all beam elements. The equivalent width, W_e, is thus

$$W_e = s_w \left(N-2+2\frac{I_e}{I_i}\right) \quad . \tag{92}$$

In addition, it should be pointed out that the definition of effective width, as shown above, does not insure continuity of the equivalent transverse shear modulus. However, it will be shown later in the verification of the proposes analysis that the small variation of shearing rigidity in the region of the edge beams has little effect on the ability of the theory to predict behavior accurately.

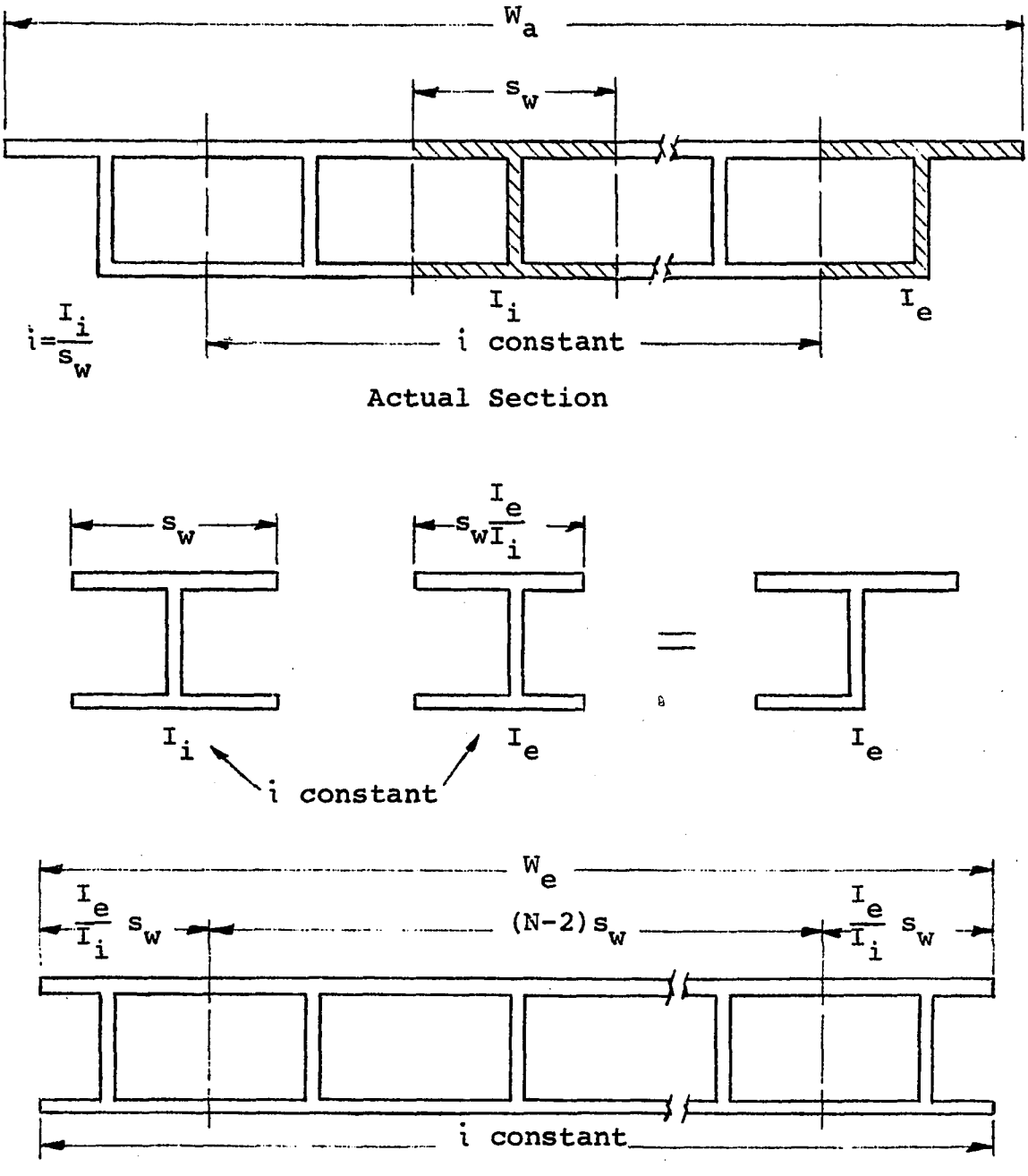

Figure 8. Relation of the effective width to the actual width of the structure

The use of effective width has an important effect on the distribution of the coefficients per beam. This effect is illustrated in Figure 9 for the case of the longitudinal moment coefficient per beam. In the figure, the two extreme possibilities for the effective width are shown for a typical five beam bridge. The subscript, j, refers to either of the two cases shown. When $j = 1$, $W_e = 4s_w$ as shown in the upper part of the figure. When $j = 2$, $W_e = 5s_w$ as shown in the lower part of the figure. The subscript, i, refers to the beam element considered for each distribution coefficient. In the figure, only the central and exterior beam coefficients are considered because the illustration is intended for qualitative purposes. From the definition, the coefficients are found by taking the ratios of the two integrals shown at the top of the figure. These integrals are represented by the two differently delineated areas. It is easily seen that for exterior beams, the coefficients are larger in the case of the greater effective width. Conversely, the interior beam coefficients are smaller in the case of the greater effective width. Since the two cases shown in the figure represent extremes, the true effective width, and hence the true distribution of the coefficients will lie between the two cases shown.

Summary of the governing parameters

External geometry is represented by the aspect ratio of the structure, W/L. When the edge beams are flexurally less stiff

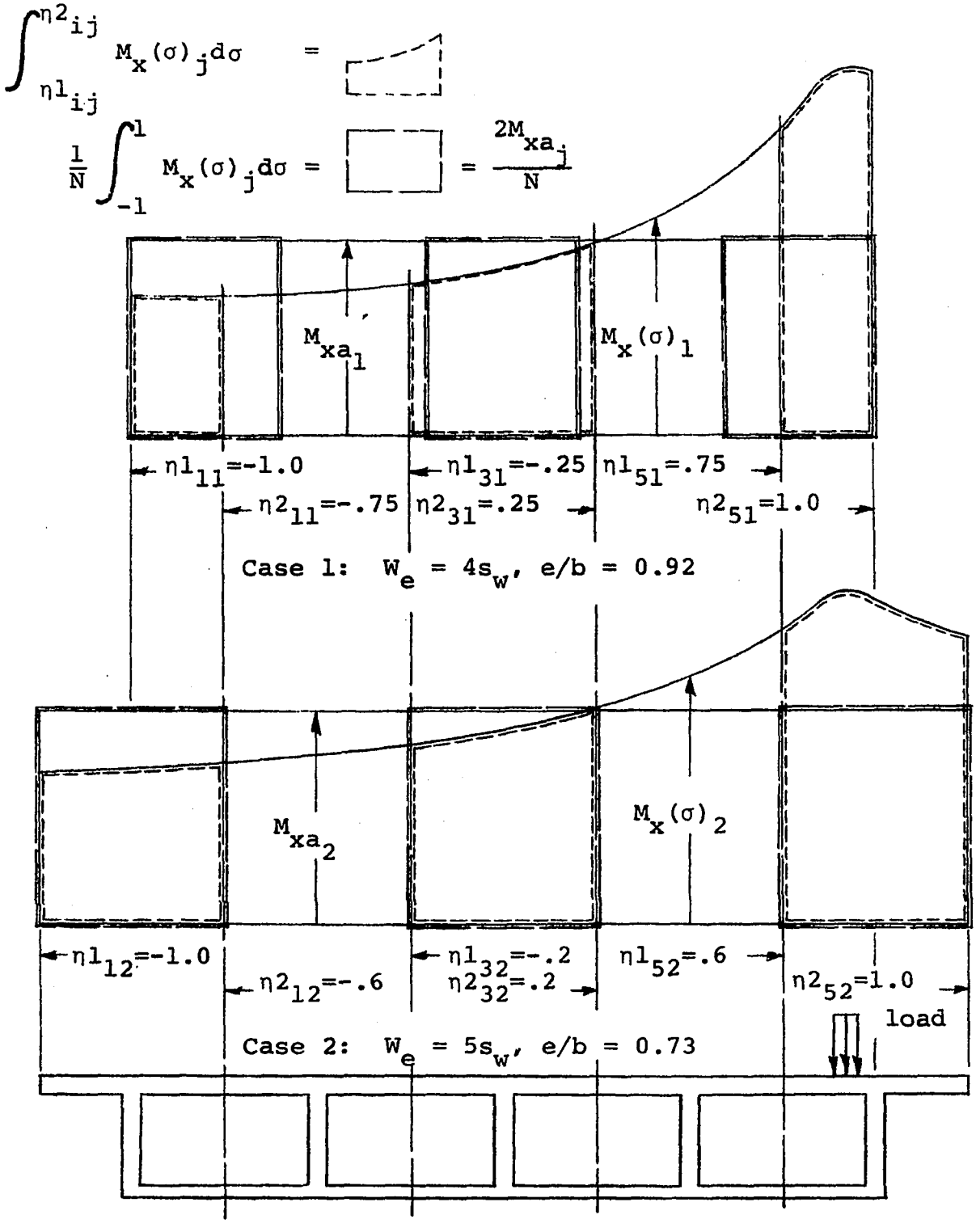

Figure 9. Variation of longitudinal bending moment coefficients per beam with effective width

than the interior beams, the effective width is used, and the aspect ratio becomes W_e/L.

The rigidity characteristics of the structure are represented by the parameter ϕ. ϕ appears in the solutions as the series term dependent variable ϕ_n. This correspondance is defined as

$$\phi_n = \phi(n\pi)^2 \quad .$$

The rigidity parameter, ϕ, is defined as

$$\phi = \psi \frac{i}{d^3} \left(\frac{d}{L}\right)^2$$

where ψ is a function of the internal geometry of the structure. In the case of no diaphragms, ψ is determined as follows:

$$\psi = \frac{1}{3(1+\nu)} \left(\frac{s_w}{d}\right) \left(\frac{d}{t_w}\right)^3 \left[\frac{(3r_t+2)(3r_b+2)-1}{6r_t r_b + r_t + r_b}\right] .$$

When diaphragms are used, ψ becomes

$$\psi = \left\{\frac{t_d}{s_d} + 3(1+\nu) \left(\frac{d}{s_w}\right) \left(\frac{t_w}{d}\right)^3 \left[\frac{6r_t r_b + r_t + r_b}{(3r_t+2)(3r_b+2)-1}\right]\right\}^{-1} .$$

The load width appears in the solutions as the ratio of the bridge width to the load width or b/f.

The effective width is defined such that the flexural rigidity remains constant within the effective width. This

definition results in the following expression for the effective width:

$$W_e = s_w \left(N - 2 + 2 \frac{I_e}{I_i} \right) .$$

Convergence Study

In order that the solutions derived thus far are mathematically and practically meaningful, the series representations for each of the quantities derived must be at least uniformly convergent. A mathematically rigorous proof of this convergence would be difficult and space consuming. In addition, a rigorous proof of convergence is beyond the scope of this study. However, for a qualitative indication of convergence, numerical evaluation of selected results for each of a finite number of series terms is mathematically and practically meaningful.

If a trend toward absolute convergence can be shown for a finite number of terms in the series evaluation of selected results, then convergence in the rigorous sense may reasonably be assumed. In particular, since the beam coefficients for shear, bending moment, and twisting moment are the most important quantities in the scope of the study, a numerical convergence study of these quantities is shown herein. Also, it can be seen that absolute convergence of the beam coefficients would indicate at least uniform convergence of the distributed

coefficients which appear under the integrals in the expressions for the beam coefficients.

For the qualitative convergence study, the three beam coefficients, $\bar{M}_{xb}$, $\bar{M}_{xyb}$, and $\bar{Q}_{xb}$ are evaluated for each series term, n, from n = 1 to n = 21 for selected parameters. The parameters used represent the extremes that may be expected for practical structures. The selection of the parameters is based on a study of the range of parameters used in this study. These ranges will be defined later. The case of an extremely long slender structure is shown in Figure 10 where the width and span are 35 and 110 feet respectively. For this span, the range of the stiffness parameter, ϕ, may be expected to be $0.0 \leq \phi \leq 0.3$. The extremes of this range are used in the coefficient evaluations where for each value of ϕ, a central loading and an eccentric loading is considered. In a similar manner, the case of a short wide bridge is considered where W = 63 feet and L = 50 feet. The results of this study are shown in Figure 11. In this case, however, the use of a shorter span requires the maximum practical value of ϕ to be 0.2. In all cases, only the maximum beam coefficients are shown since it may be expected that the convergence of the coefficients for the most highly loaded beam will be critical.

The most important result shown by the convergence study is that the various coefficients are all convergent. In addition, the results show the rate of convergence of the

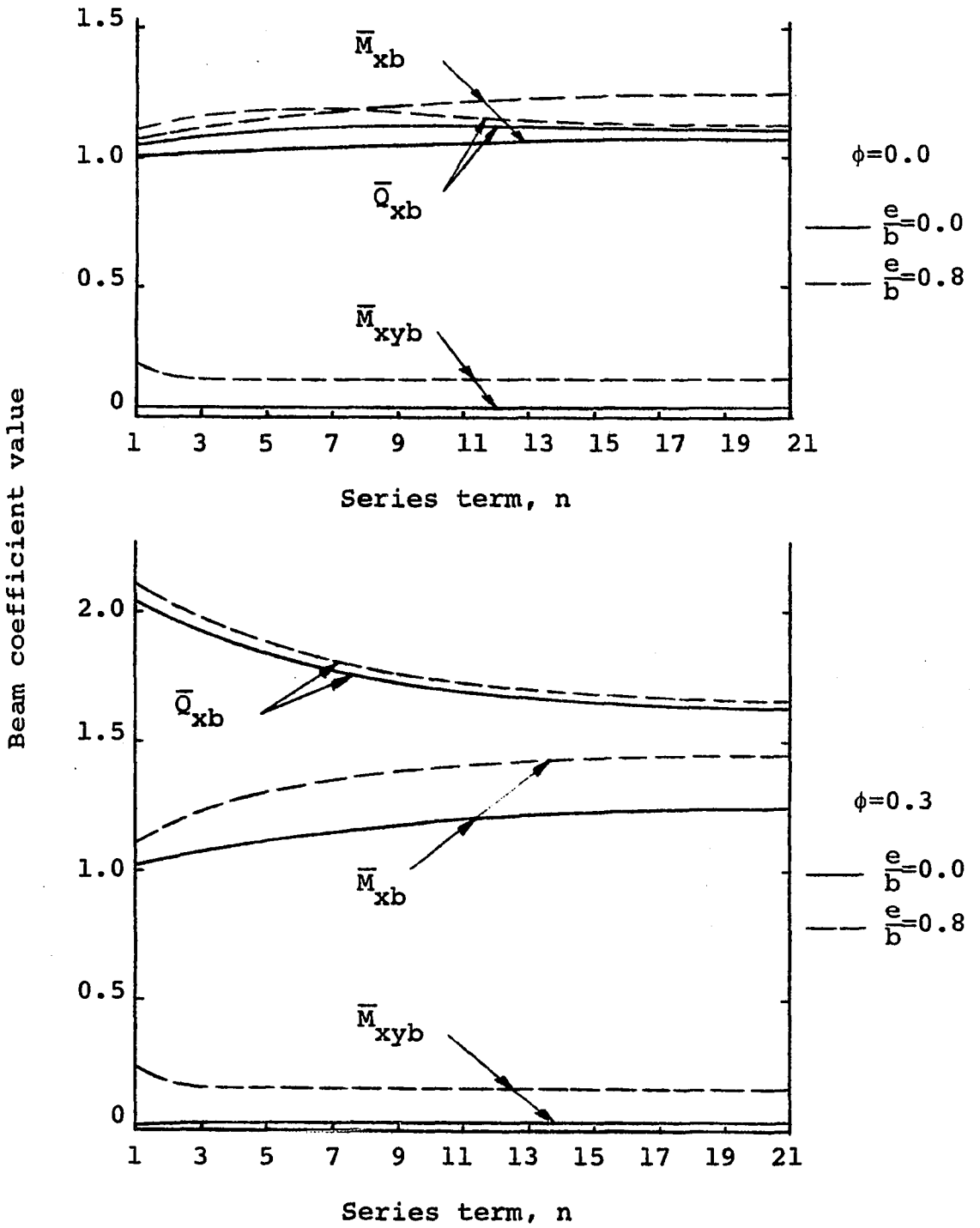

Figure 10. Convergence of maximum beam coefficients: W = 35 ft., L = 110 ft., c/a = 1.0

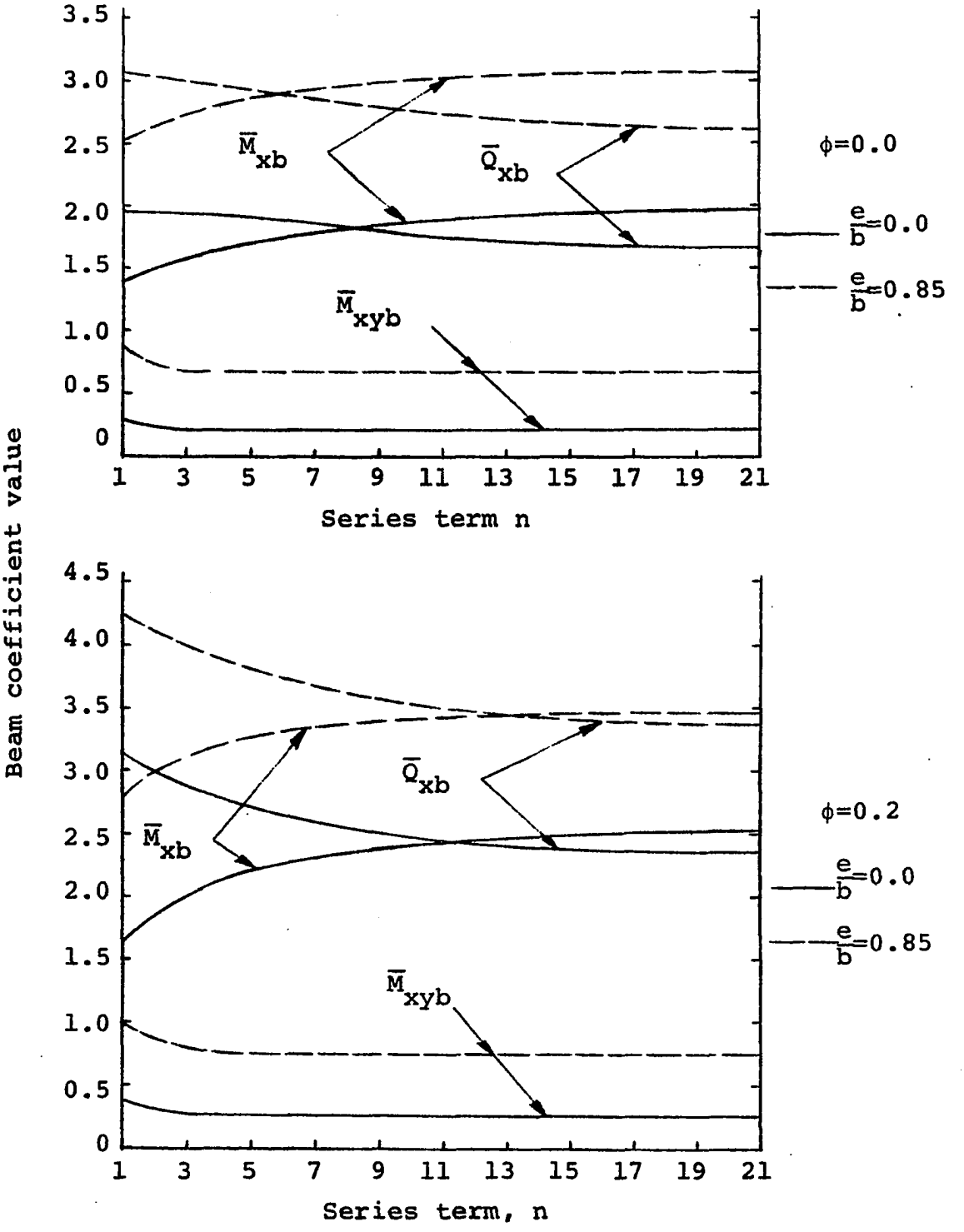

Figure 11. Convergence of maximum beam coefficients: W = 63 ft., L = 50 ft., c/a = 1.0

coefficients. Since all infinite series must be approximated by finite series for numerical evaluations, a practical maximum value of n must be determined such that the finite sums are within a specified small error interval about the infinite sum. It is seen that for all coefficients, convergence is nearly complete for n = 21. However, limited computer time necessitates the use of a smaller maximum n for computational purposes. The use of n = 13 as a maximum for finite sum evaluations gives results which are within approximately ±7% of the results for n = 21. Hence, it is assumed that 13 term finite sum results are within approximately ±10% of the infinite sum values since convergence is nearly complete for n = 21. An error interval of approximately ±10% is compatible with the object of this study. Therefore, for all succeeding numerical evaluations, the infinite series expressions are approximated by finite sum expressions where the maximum value of n is 13.

VERIFICATION OF THE PROPOSED ANALYSIS

Verification of the proposed analysis is shown herein through comparisons with experimental results and results predicted by other analytical procedures. The theories which are used for comparison are the folded plate analysis and the orthotropic plate theory. Comparisons with test results are restricted to results of full scale field tests.

Comparisons with Field Test Results

Full scale testing of concrete box girder highway bridges has been limited to an extensive test of one bridge. This test is described by Davis et al. (4). The structure tested is the Harrison Street Undercrossing, which is located in Oakland, California. The bridge has one simple span of 80 feet and is rectangular in plan. The overall width is 34 feet. There are five girders with the webs spaced at 7.25 feet. A cross-section of the structure is shown in Figure 12.

Instrumentation of the structure was very complete. Carlson strainmeters were placed at thirty locations in the top slab and the reinforcing steel was gaged extensively with electrical resistance strain gages. During testing, all strain gages were monitored on multi-channel oscillographs.

A complete live load testing program was carried out consisting of both static and dynamic load applications. For the

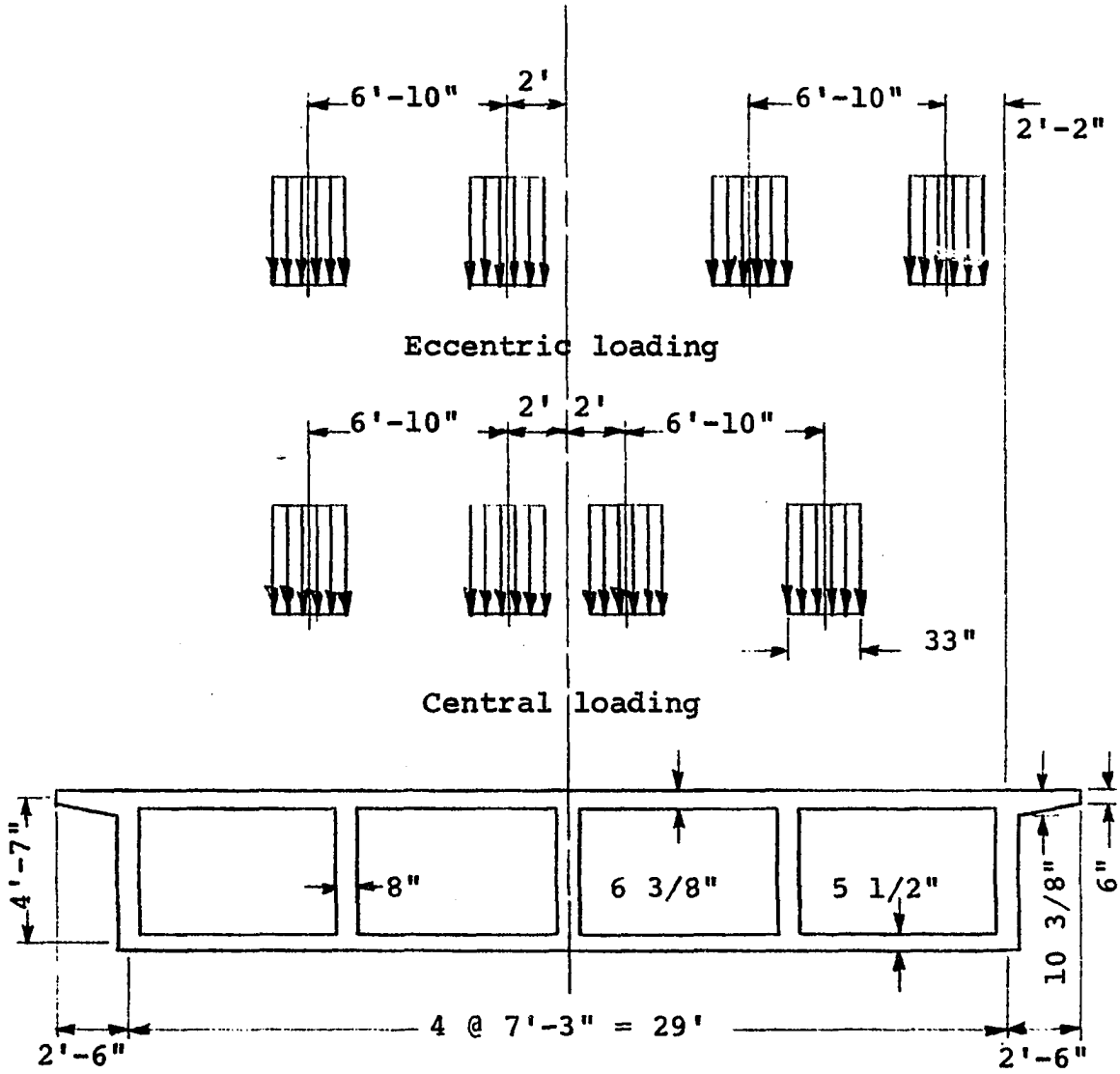

Figure 12. Cross-section and loading patterns, Harrison Street Undercrossing

static test portion, a single heavily loaded test vehicle moved across the span at crawl speeds of two to five miles per hour. In addition, the static testing was divided into three phases. In the first phase, testing was conducted on the structure without interior diaphragms or barrier curbs and railings. A single interior diaphragm was added at mid-span for the second phase, and barrier curbs and railings were added for the third phase.

Influence lines for strain at the various gage locations were found by allowing the test vehicle to occupy several transverse positions on the structure and plotting the measured strains as functions of the vehicle position. Strains for four hypothetical vehicle positions which cause maximum moment conditions in each of the girders for design loadings were then found. Upon superposition of the strains caused by two vehicle position combinations and conversion of the strain data to longitudinal beam bending moments, final total bending moments for each beam were found for each of the three critical load combinations.

The results of two of the critical combinations, maximum central and exterior girder moments, are reported herein for both phase one and phase two results. The transverse positions of the two load combinations are shown in Figure 12. In all results reported, actual beam moments are converted to longitudinal moment coefficients per beam.

For the predictions of moment coefficients by the proposed analysis, the effective width of the structure must be found and the stiffness parameter, ϕ, must be calculated for the case of no diaphragms and the case of one interior diaphragm. Using the expressions given in the previous chapter for the effective width and stiffness parameters, the effective width is found to be 32.2 feet and the stiffness parameters are 0.066 and 0.0063 for the case of no diaphragms and one diaphragm, respectively. For each load position corresponding to the experimental load positions, longitudinal beam bending moment coefficients are found using the proposed analysis. The appropriate combinations of these coefficients are then superimposed for comparison with the experimental results.

The comparisons are presented in both graphical and tabular form. Table 1 presents a tabular comparison of the experimental and analytically predicted coefficients and Figures 13 and 14 represent the comparisons graphically.

It may be seen from both representations of the comparisons that there is good agreement between the experimental results and analytical predictions. In particular, agreement is best for the more heavily loaded interior girders. Considering all cases, the maximum error for a predicted moment in an interior girder is a conservative 4.1% error. These comparisons indicate validification of the proposed analysis. However, since there is only one available field test result, further validification

Table 1. Comparison of longitudinal bending moment coefficients from the field test and proposed analysis

Girder	Test result	Predicted	% Error (exp. base)
Phase I: No interior diaphragm			
		Central loading	
1	0.785	0.737	-6.1
2	1.135	1.157	+1.9
3	1.175	1.212	+3.1
4	1.125	1.157	+2.8
5	0.780	0.737	-5.5
		Eccentric loading	
1	0.765	0.723	-5.5
2	1.105	1.136	+2.8
3	1.160	1.157	-0.3
4	1.155	1.175	+1.7
5	0.815	0.809	-0.7
Phase II: Interior diaphragm at mid-span			
		Central loading	
1	0.800	0.755	-5.6
2	1.140	1.152	+1.1
3	1.132	1.186	+4.1
4	1.135	1.152	+1.5
5	0.793	0.755	-4.8
		Eccentric loading	
1	0.785	0.740	-5.7
2	1.123	1.130	+0.6
3	1.123	1.151	+2.3
4	1.153	1.170	+1.5
5	0.816	0.809	-0.9

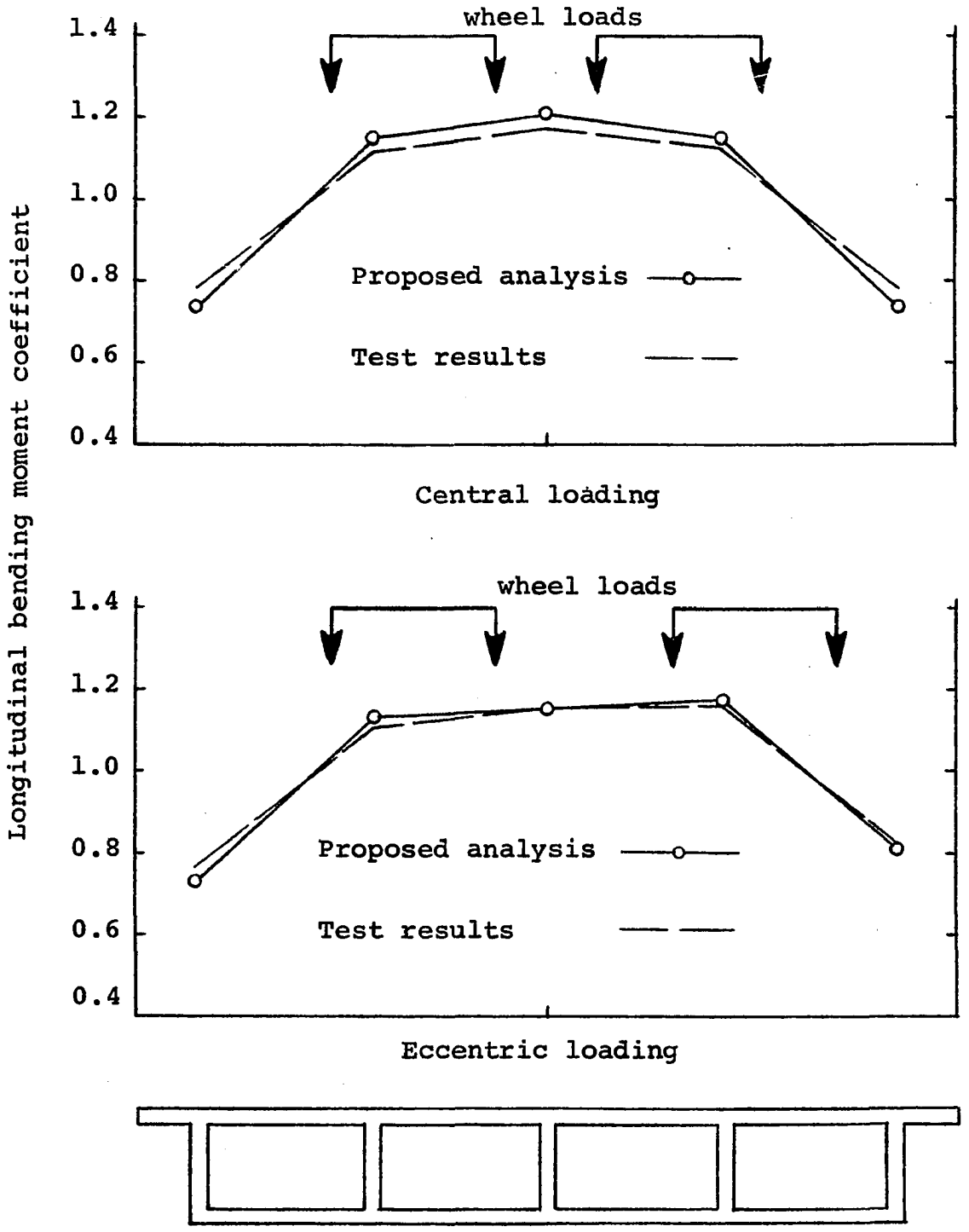

Figure 13. Longitudinal bending moment coefficients, Harrison Street Undercrossing - no diaphragms

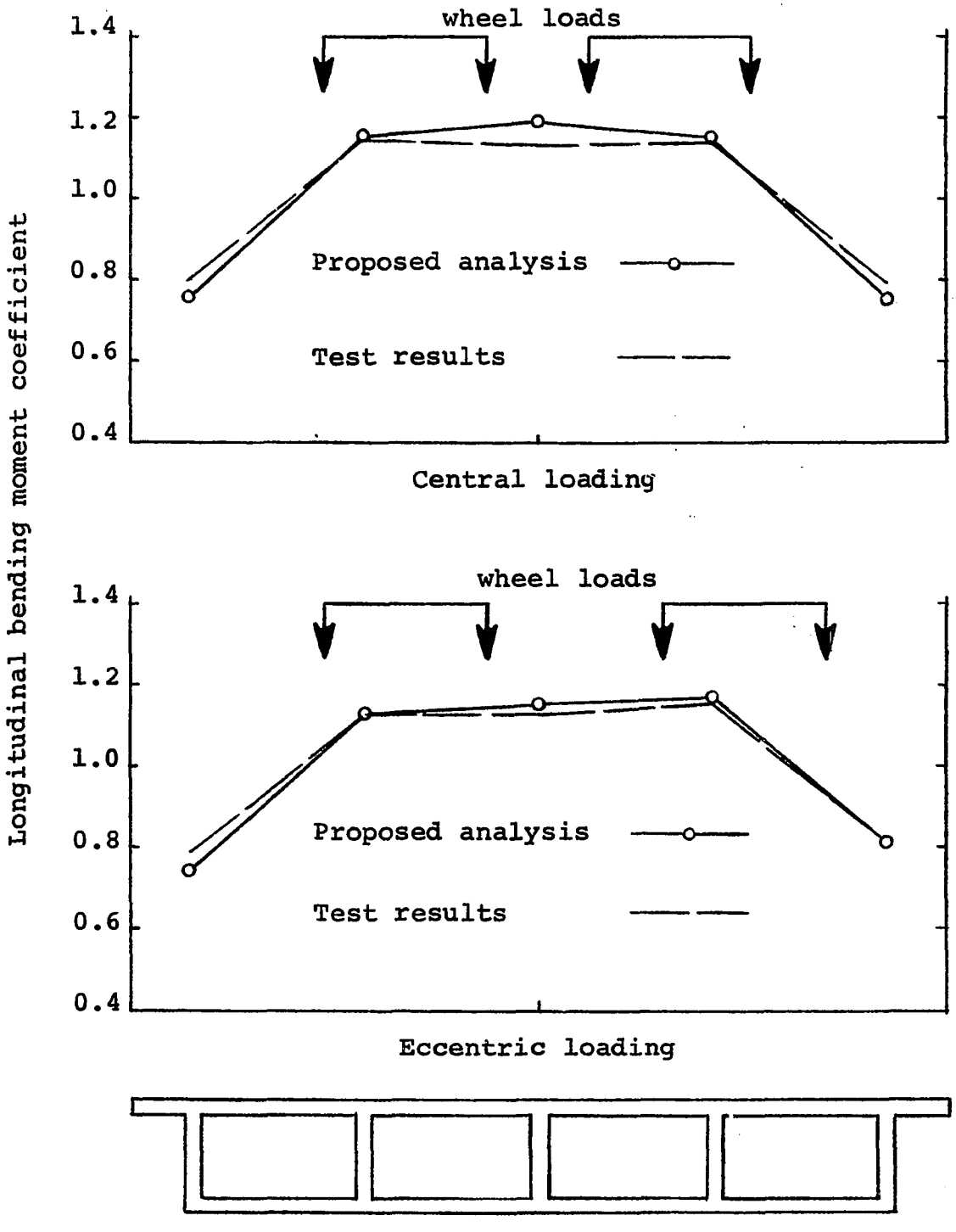

Figure 14. Longitudinal bending moment coefficients. Harrison Street Undercrossing - diaphragm located at mid-span

of the analysis is required and is obtained by means of comparisons of results derived from the proposed analysis with results predicted by other analytical methods already in use.

Comparisons with other Theoretical Procedures

As discussed in the section on review of previous studies, the most widely used analytical procedure for the analysis of box girder bridges is the folded plate method. In particular, the use of a modification of the theory of prismatic folded plate structures has been developed by Scordelis of the University of California at Berkeley (11) for the analysis of concrete box girder highway bridges. The direct stiffness solution was developed using a folded plate harmonic analysis based on an elasticity method (11). Scordelis used elastic plate theory for loads normal to the plane of the plates and two-dimensional plane stress theory for loads in the plane of the plates.

Using these theories, a computer program, MUPDI, was developed by Scordelis. This computer program can be used to analyze box girder bridges, with and without intermediate diaphragms, under concentrated or distributed loads anywhere on the bridge. An assumption inherent in this solution for the case of bridges with interior diaphragms is that the diaphragms are perfectly rigid in their plane and infinitely flexible normal to their plane.

Sanders and Elleby (9) used this theory in a general study of load distribution in short and intermediate length highway bridges. In particular, the theory was used as a basis of an extensive study of the parameters affecting the distribution of longitudinal bending moments in concrete box girder highway bridges. Some selected results of this study are used for comparisons with moment coefficients predicted by the proposed analysis for similar geometric and loading configurations.

The moment coefficients[a] derived by Sanders and Elleby for critical design loadings on four geometrically different bridges are compared herein. The cross-section of the bridges studied is shown in Figure 15. As illustrated, the section is composed of six cells and seven girders. The top and bottom flanges are 6.5 and 5.5 inches thick respectively, and the webs are 8.0 inches thick. The overall width of the structures is 51 feet and the width of the cells is 7.333 feet. The depth of the structures varies with span. Two ratios of the depth to the span are used: $d/L = 0.05$ and $d/L = 0.07$. Also two spans are studied: $L = 50$ feet and $L = 110$ feet. For the 50 foot span, three cases are studied: $d/L = 0.05$ where the number of diaphragms, N_d, is zero, and $d/L = 0.07$ where $N_d = 0$ and 2. The fourth structure studied has a span of 110 feet, and $d/L = 0.07$ where $N_d = 0$.

---

[a]Sanders, W. W., Jr., Ames, Iowa. Data from the computer analysis. Private communication. 1968.

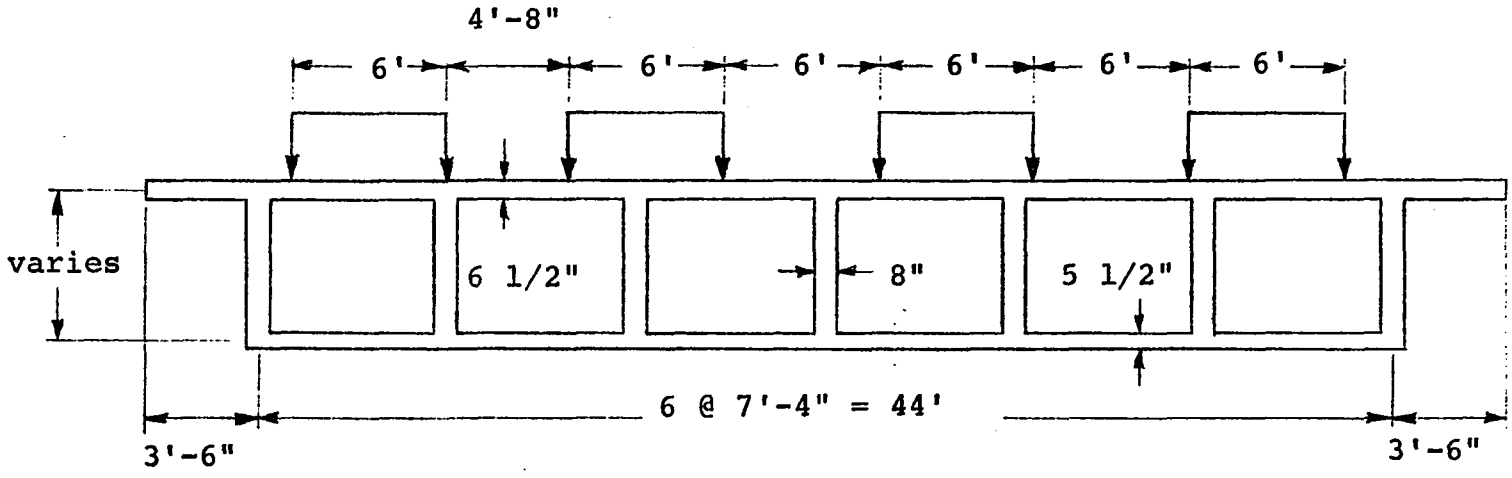

Figure 15. Cross-section and critical load pattern, structure used for folded plate theory comparisons

The critical loading, as shown in Figure 15, was determined by Sanders and Elleby by considering various combinations of possible design loads. The criteria used to determine the position of the loads was similar to that used to determine the load distribution equation for composite box girders in the American Association of State Highway Officials 1966-1967 Interim Specifications for Highway Bridges (14). The critical load or combination of loads is defined as causing the maximum possible bending moment in any girder for all combinations of possible design loads. The behavior of the four structures described above is described later for this critical loading.

For the plate procedure developed herein, the stiffness constant, ϕ, for each of these four structures would be:

for L = 50 feet, d/L = 0.05, and $N_d = 0$, $\phi = 0.0233$,

for L = 110 feet, d/L = 0.07, and $N_d = 0$, $\phi = 0.2380$,

for L = 50 feet, d/L = 0.07, and $N_d = 0$, $\phi = 0.0727$,

for L = 50 feet, d/L = 0.07, and $N_d = 2$, $\phi = 0.0054$.

Influence lines were generated for longitudinal bending moments per beam for the four structures with the parameter combinations shown above. These influence lines were then utilized to find bending moment coefficients per beam for the critical loading. The results were compared with the results found by Sanders and Elleby (9) using the folded plate analysis developed by Scordelis (11).

The comparisons of bending moments per beam for the four structures show no difference between the coefficients as

predicted by either theory when the results are represented by four significant digits. The moment coefficients per beam resulting from both procedures are reproduced in Table 2 and Figure 16.

As a final comparison with other analytical procedures, results for bending moments per unit width and deflections are compared with similar results found from orthotropic plate theory. The use of orthotropic plate theory for the analysis of highway bridge decks utilized the same philosophy of replacing the actual structure with an equivalent unit plate as is used in the proposed analysis. However, in orthotropic plate theory, the transverse shearing rigidity of the equivalent plate is considered large so that shearing deformations contribute negligibly toward the behavior of the structure or equivalent plate. Also, orthotropic plate theory considers the transverse and longitudinal flexural and torsional rigidities of the equivalent plate to be variable parameters. The development and presentation of equations for calculating distributed longitudinal bending moment coefficients and deflection coefficients by orthotropic plate theory for concentrated loads may be found in references 1, 8, and 9. The computer program used for the orthotropic plate theory comparison was derived from a previous thesis by the author (1) and is given in Appendix B.

For the purpose of comparing orthotropic plate theory results with results predicted by the proposed analysis,

Table 2. Distribution of moment coefficients for typical structures and critical loading - proposed analysis and folded plate theory[a]

Girder number	1	2	3	4	5	6	7
	L = 50 feet, d/L = 0.05, N_d = 0, ϕ = 0.0233						
Coefficient value	0.785	1.154	1.098	1.079	1.082	1.072	0.729
	L = 110 feet, d/L = 0.07, N_d = 0, ϕ = 0.2380						
Coefficient value	0.819	1.113	1.087	1.076	1.074	1.057	0.775
	L = 50 feet, d/L = 0.07, N_d = 0, ϕ = 0.0727						
Coefficient value	0.789	1.159	1.101	1.081	1.083	1.065	0.723
	L = 50 feet, d/L = 0.07, N_d = 2, ϕ = 0.0054						
Coefficient value	0.782	1.153	1.092	1.077	1.084	1.079	0.733

[a]Only one value is shown for both procedures since both results are identical for the significant figures shown.

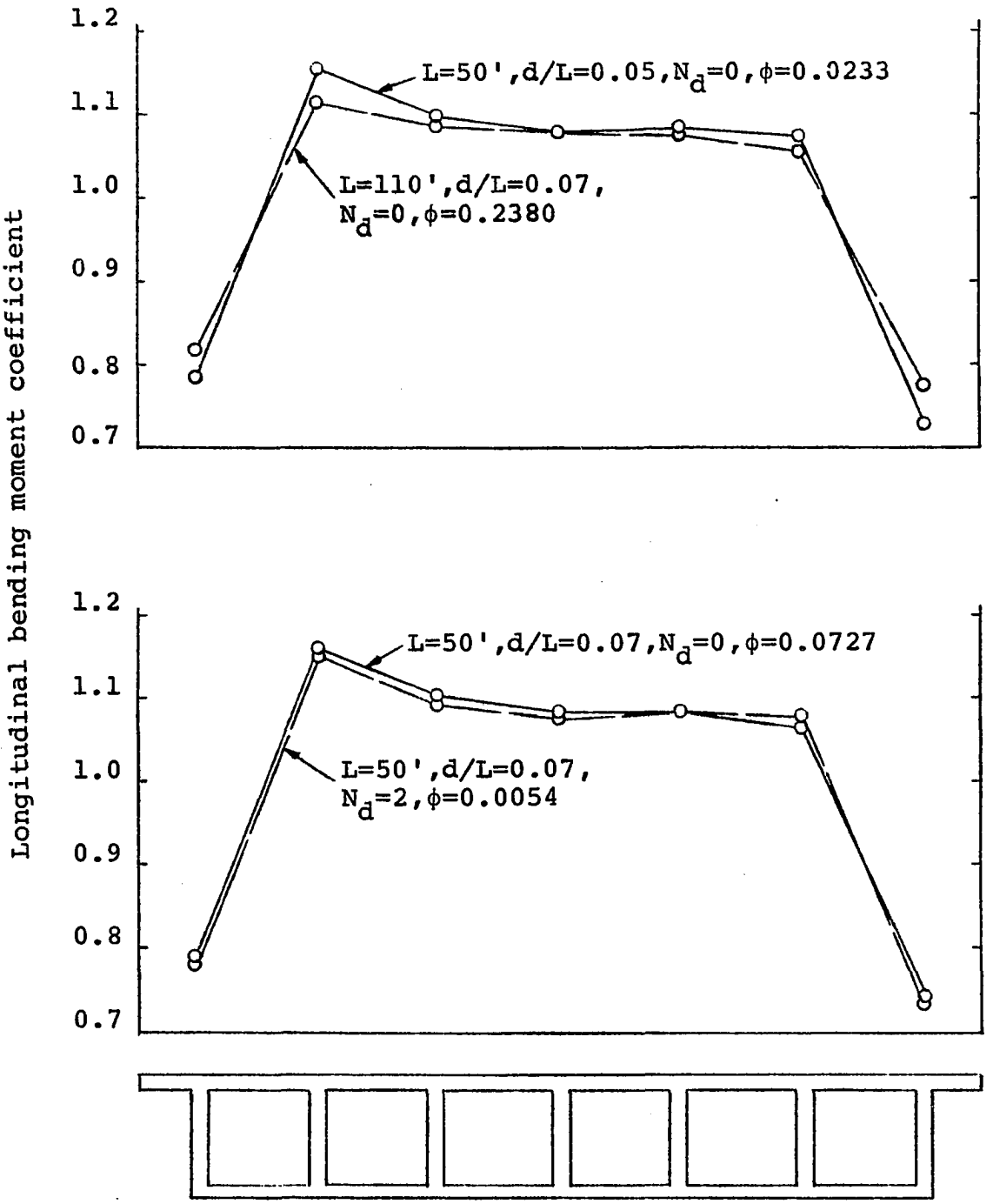

Figure 16. Distribution of longitudinal moment coefficients for critical loading, proposed analysis and folded plate theory

stiffness parameters are used such that both theories degenerate to a common or isotropic condition. For the case of orthotropic plate theory, the transverse and longitudinal flexural rigidities are set equal to the flexural rigidity of the shear anisotropic plate. Also, the transverse and longitudinal torsional rigidities of the orthotropic plate are set equal to the torsional rigidity of the shear anisotropic plate. For the shear anisotropic plate, the isotropic condition is found by setting the stiffness parameter, ϕ, equal to zero.

For the comparison, an equivalent plate 50 feet wide and 80 feet long is subjected to central and eccentric loads. The results of the comparison are shown in Figure 17. It is observed that a slight difference exists between the predicted coefficients in the vicinity of the loads. This discrepancy is clarified when it is observed that the loading on the orthotropic plate is concentrated whereas the loads on the shear anisotropic plate are distributed over a small line segment. In general, however, excellent agreement exists between results predicted by orthotropic plate theory and the proposed analysis.

Accuracy of the Proposed Analysis

The comparisons shown in this section serve to verify the proposed analysis by comparing results predicted by these analysis with two independent theoretical approaches and results derived from field tests on a full scale structure.

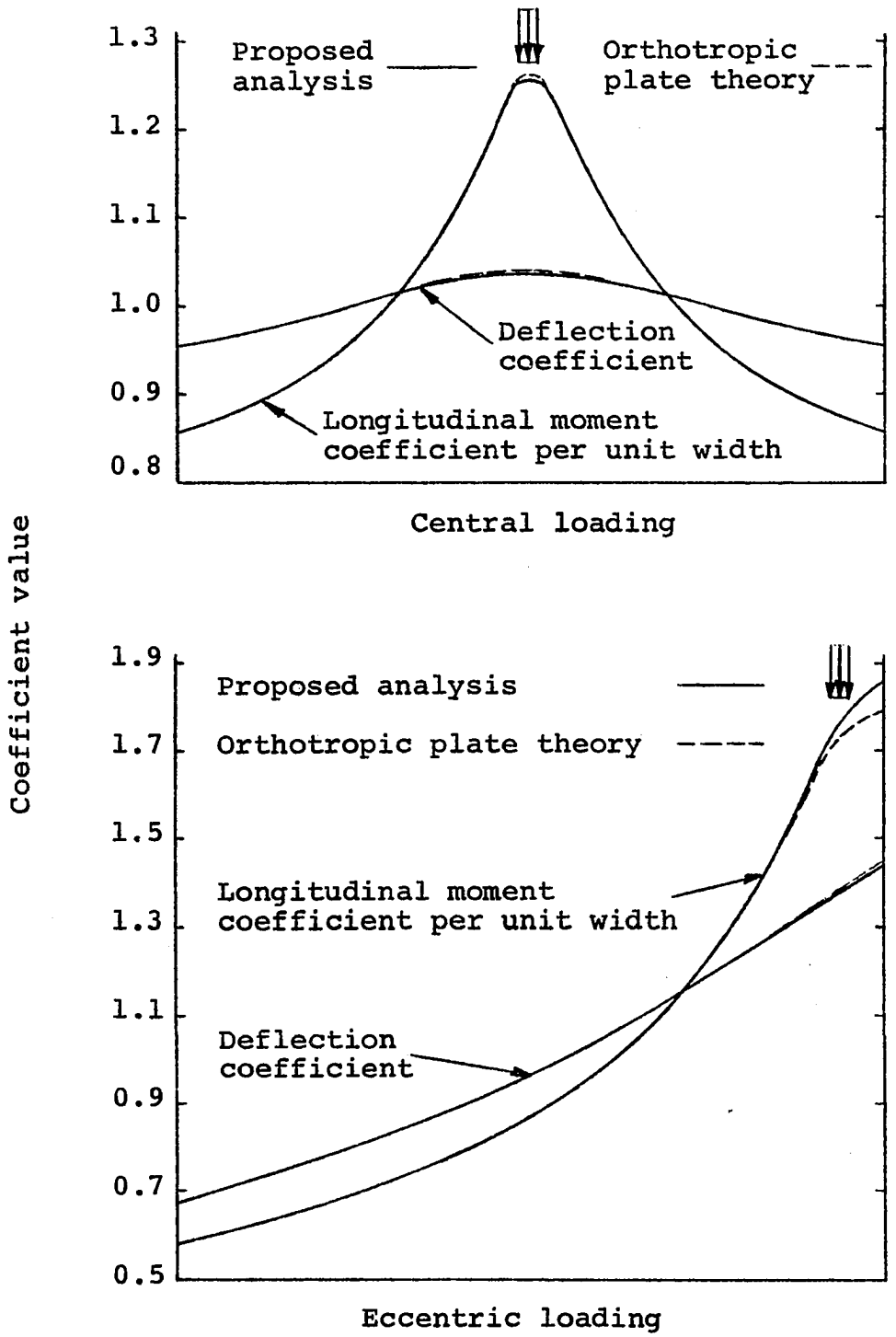

Figure 17. Coefficient comparison between proposed analysis and orthotropic plate theory

The most important result shown by the comparisons is that the proposed analysis predicts with good accuracy the distribution of longitudinal bending moments per beam as measured in full scale field tests. The complete agreement of results from the proposed analysis and folded plate theory tends to validify the analysis since folded plate theory is accepted as a valid method for the analysis of box girder highway bridges. Finally, the agreement of results predicted by the proposed analysis with similar results derived from orthotropic plate theory shows that the mathematics of the analysis procedure are correct since both plate solutions are based on different mathematical techniques.

It has been shown that the philosophy of the proposed analysis and longitudinal bending moments per beam predicted by the proposed analysis are valid. However, other results derived from the proposed analysis such as twisting moment, transverse moments, and shearing force coefficients are unproven. Since the derivation of the unproved quantities follows from the same basic equations for deflection and transverse unit shearing force, and since these derivations use the same techniques as the derivation of the proven moment coefficients, the results for quantities other than longitudinal bending moment and deflection coefficients are assumed to be correct.

BEHAVIORAL STUDY

The effect of variations of bridge geometry and stiffnesses on internal force quantities produced by the application of loads to the structure is studied herein. The magnitude and distribution of internal shears and moments are ascertained for variations of bridge geometry, stiffnesses, and external load positions. These results are presented such that recommendations may be made concerning the effect of commonly used design configurations on the possible optimization of the behavior of the structure for the various configurations. However, before presenting these results, the major variables and their ranges are outlined.

Range of Parameters

Scordelis (11) has presented a very complete summary of the major variables affecting the behavior of concrete box girder bridges and the range of these variables in a report summarizing a study of approximately 200 in-place California concrete box girder highway bridges. Sanders and Elleby (9) provided additional information concerning the major variables and their ranges. The major variables and their ranges, as given in the reports cited above, are:

1. Span length: The span lengths of the majority of simple span box girder bridges fall within the range of 50 to

130 feet. However, spans of the range 50 to 110 feet are the most common.

2. Overall width: The width of commonly built bridges varies from about 33 feet for two lanes to about 75 feet for six lanes. However, widths greater than about 61 feet are uncommon since separate structures are usually employed when the total number of lanes exceeds four.

3. Depth of cross-section: According to the sources cited above, the depth of the bridge is related to the span. The depth/span ratio ranges from 0.05 to 0.07 for reinforced concrete bridges, although a prestressed box girder bridge may have a ratio as low as 0.045.

4. Number of girders: The number of girders is equal to the number of cells plus one. The number of cells and the width of the cells are chosen such that the transverse spacing between the vertical webs of the girders is within the normal design range of from seven to nine feet. Thus, for the widths of bridges studied herein, the number of girders ranges from five to nine.

5. Number of diaphragms: The number of interior diaphragms commonly used in concrete box girder bridge construction varies from none to two. The most common configuration is one diaphragm, while bridges with more than two diaphragms are comparatively rare. Scordelis (11) found the usage of diaphragms in existing structures to be approximately 30, 55, and

10 per-cent for zero, one, and two diaphragms respectively. The cases of zero and two interior diaphragms are studied herein to give an indication of the full range of behavior that can generally be expected.

6. Thickness of webs and flanges: Practically all of the bridges studied by Scordelis (11) maintained nearly constant ranges of dimensions for web and flange thicknesses. These dimensions were 6.0 to 7.0 inches for the top flange, 5.5 to 6.0 inches for the bottom flange, and 8.0 to 12.0 inches for the webs. The most common dimensions were 6.5, 5.5, and 8.0 inches for the top flange, bottom flange, and webs respectively. These last dimensions were common to about 80 per-cent of the bridges studied.

7. Edge conditions: The most common edge configuration is a cantilevered top slab. However, edge slabs supported by inclined or curved side webs are being increasingly used. It may be seen, however, that these various conditions may be taken into account by resolving the overall width into an effective width as was presented in a previous section.

The method of analysis used in this study groups the variables just presented into three major governing parameters: the stiffness parameter, ϕ (equations 86, 89, and 91), aspect ratio, W/L, and the edge conditions or effective width, W_e (equation 92).

Values of the stiffness parameter are given in Table 3 for several combinations of the geometrical variables. The range of the variables conforms to the ranges just presented. Eight overall widths which vary from 33 to 75 feet inclusive were considered. The number of girders range from five for the narrowest bridge to nine for the widest bridge. In all cases, the thickness of the plate elements are 6.5, 5.5, and 8.0 inches for the top flange, bottom flange, and webs respectively. Stiffness parameters were calculated for the cases of zero and two diaphragms and d/L values of 0.05 and 0.07.

The variation of the stiffness parameter with the aspect ratio is shown in Figure 18 for various values of d/L and L. It can be seen from the figure that the calculated ϕ values for bridges with zero diaphragms are banded, and that the bands are dependent primarily on the value of d. For d/L = 0.07 and L = 110 feet, or d = 7.7 feet, ϕ ranges from about 0.22 to about 0.26. For d/L = 0.05 and L = 110 feet, or d = 5.5 feet, ϕ ranges from about 0.06 to about 0.08. Also, for d/L = 0.07 and L = 50 feet, or d = 3.5 feet, ϕ varies from about 0.07 to about 0.09. Finally, for d/L = 0.05 and L = 50 feet, or d = 2.5 feet, ϕ varies from about 0.02 to about 0.03. The reason for the apparent banding is that the web spacing has been limited to the range 6.5 to 9.5 feet. In all cases studied, the larger values of ϕ correspond to the greatest web spacings and the lower values of ϕ correspond to the smallest web spacings.

Table 3. Stiffness parameters for 0 and 2 diaphragm bridges

W (ft.)	N	s_w (ft.)	L (ft.)	d/L	ϕ (0 diaph.)	ϕ (2 diaph.)
33	5	6.50	50	0.05	0.0218	0.0035
			50	0.07	0.0673	0.0053
			110	0.05	0.0661	0.0039
			110	0.07	0.2175	0.0056
39	5	8.00	50	0.05	0.0252	0.0036
			50	0.07	0.0768	0.0054
			110	0.05	0.0737	0.0039
			110	0.07	0.2385	0.0057
45	5	9.50	50	0.05	0.0286	0.0036
			50	0.07	0.0862	0.0054
			110	0.05	0.0812	0.0039
			110	0.07	0.2594	0.0057
45	7	6.33	50	0.05	0.0214	0.0035
			50	0.07	0.0663	0.0053
			110	0.05	0.0652	0.0039
			110	0.07	0.2152	0.0056
51	7	7.33	50	0.05	0.0237	0.0035
			50	0.07	0.0726	0.0054
			110	0.05	0.0703	0.0039
			110	0.07	0.2292	0.0057
61	7	9.00	50	0.05	0.0275	0.0036
			50	0.07	0.0830	0.0054
			110	0.05	0.0787	0.0039
			110	0.07	0.2524	0.0057
61	9	6.75	50	0.05	0.0224	0.0035
			50	0.07	0.0689	0.0053
			110	0.05	0.0673	0.0039
			110	0.07	0.2210	0.0056
75	9	8.50	50	0.05	0.0263	0.0036
			50	0.07	0.0799	0.0054
			110	0.05	0.0762	0.0039
			110	0.07	0.2455	0.0057

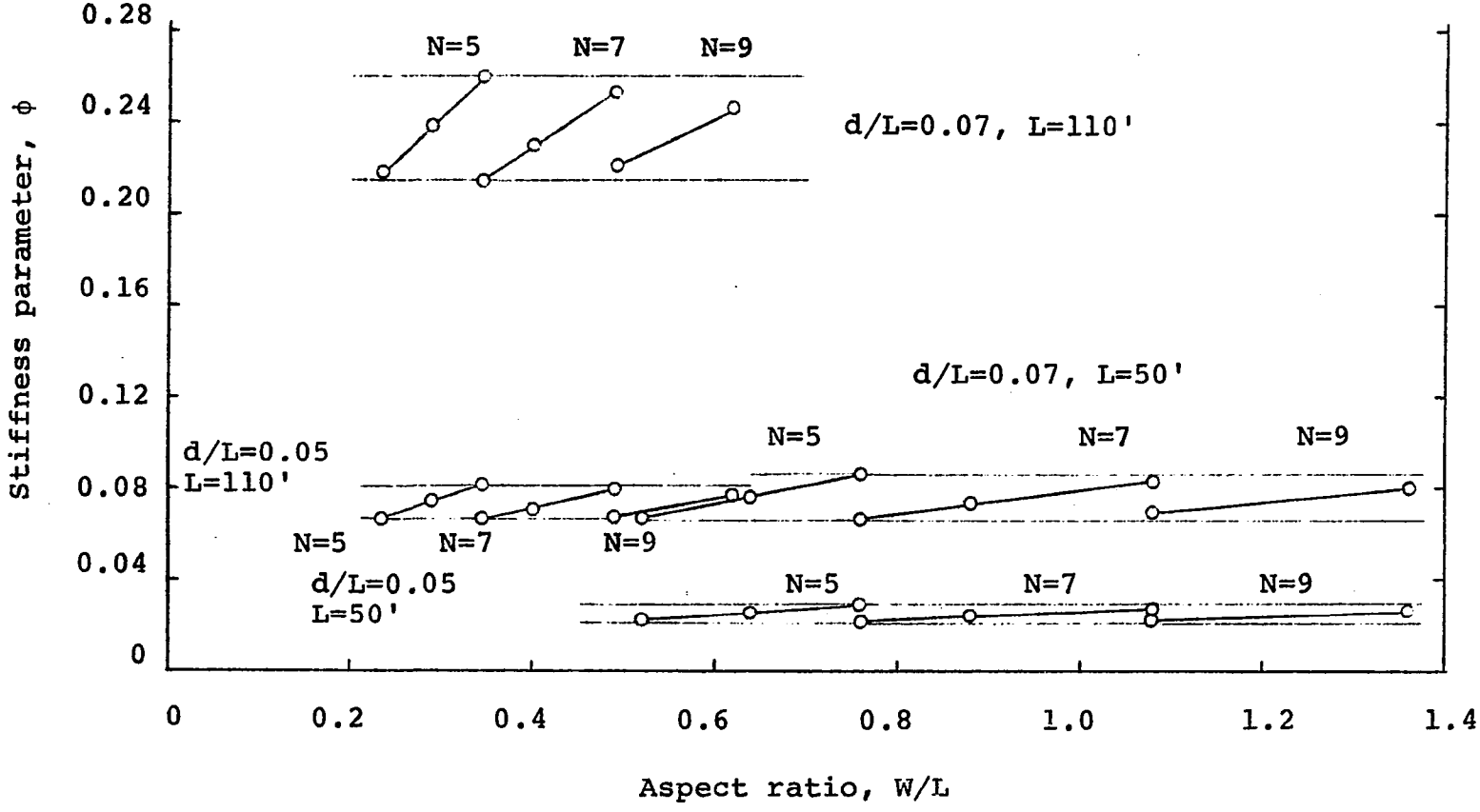

Figure 18. Stiffness parameters for bridges with no interior diaphragms

In Table 3, it can be seen that for the case of two diaphragms, ϕ is dependent primarily on d/L. For all cases where d/L = 0.05, ϕ = 0.0037±0.0002. For all cases where d/L = 0.07, ϕ = 0.0055±0.0002. Thus, the value of ϕ for the cases where two diaphragms are present is nearly determined completely by the shearing rigidity of the diaphragms.

From the preceding discussion, the physical significance of the parameter ϕ may be seen. For the case of no diaphragms, an increase in ϕ was accomplished by increasing the depth or web spacing. Thus, an increase in ϕ is accomplished by increasing the flexural rigidity and decreasing the transverse shearing rigidity of the structure. For the case of two diaphragms, ϕ is independent of the flexural rigidity. Thus, for large transverse shearing rigidity, an increase in ϕ is accomplished only by decreasing the transverse shearing rigidity.

The aspect ratio of the bridges studied above varies from 0.30 for W = 33 feet and L = 110 feet to 1.50 for W = 75 feet and L = 50 feet. However, it is felt that a total width of 75 feet is somewhat above a practical limit. A practical upper bound for the aspect ratio would be about 1.20. This would result from a short - wide bridge such as one with L = 50 feet and W = 60 feet.

Bridge design practice generally limits the width of cantilevered top edge flanges to one-half of the web spacing (13). The maximum effective width will occur for the greatest

width of edge flanges. In the case where the width of the edge flanges is equal to one-half of the web spacing and the thickness of the edge flanges is the same as the thickness of the interior top flange, the maximum effective width, as derived from equation 92, can be expected to be equal to about $s_w(N-0.5)$. The minimum effective width would occur in the case where there are no flanges extending beyond the outermost webs. In this case, the minimum effective width would be equal to $s_w(N-1.0)$. In the succeeding section, the extreme cases of effective width shown above are considered so that the behavior of the structure is ascertained for the entire range of edge conditions.

Parameter Study

Selected values of the governing parameters for practical bridge configurations have been taken from the ranges presented in the previous section for use in detailed behavioral studies. The parameter values have been selected so that they cover the full range of normal designs. In the case of the stiffness parameter, ϕ, and the aspect ratio, W/L, upper, lower, and intermediate values of these ranges were studied. To determine the effects of edge conditions, the full cantilevered and non-cantilevered top edge slab conditions were studied for each combination of the aspect ratio and the stiffness parameter.

The values of ϕ and W/L selected for study are:

Stiffness parameter, ϕ: Values of 0.0045, 0.06, and 0.24 were studied. 0.0045 represents the average value of ϕ for the condition of two intermediate diaphragms. It is seen that this value represents a practical minimum for common bridge configurations. As seen in Figure 18, $\phi = 0.006$ is representative of the majority of no-diaphragm bridges where depth varies between 2.5 and 5.5 feet. For the case of an extremely deep bridge without diaphragms, ϕ becomes a maximum. $\phi = 0.24$ is selected to represent this maximum for practical structures. This value, as seen from Figure 18, represents the average stiffness parameter for the 7.7 feet deep bridges studied.

Aspect ratio, W/L: Three aspect ratios, 0.318, 0.700, and 1.260, were studied for $\phi = 0.0045$ and 0.06. For $\phi = 0.24$, the two aspect ratios, 0.318 and 0.573, were studied. The choice of these ratios follows from the previous study of the range of parameters. For $\phi \leq 0.06$, the width and span ranges are 35 feet $\leq$ W $\leq$ 63 feet and 50 feet $\leq$ L $\leq$ 110 feet. Thus, it follows that $0.318 \leq W/L \leq 1.260$. In addition to the extreme values of W/L, the intermediate value of 0.700 was studied because of the large range of W/L. Since $\phi = 0.24$ occurs only for extremely deep bridges, it is seen from the previous study of parameter ranges that this stiffness parameter is obtainable only for long spans of about 110 feet. Thus, for 35 feet $\leq$ W $\leq$ 63 feet and L = 110 feet, it is seen that the range of

aspect ratios for $\phi = 0.24$ is $0.318 \leq W/L \leq 0.573$. An intermediate aspect ratio is not used in this case since the range of W/L obtainable for $\phi = 0.24$ is not great.

Widths are explicitly defined for each of the aspect ratios given above for the purpose of determining the number of girders in each structure studied. Based on the assumed limiting ranges of W and L given in a previous paragraph, it is seen that for W/L = 0.318, W must be equal to 35 feet. Similarly, for W/L = 1.260 where $\phi = 0.0045$ and 0.06, and for W/L = 0.573 where $\phi = 0.24$, W must be equal to 63 feet. For W/L = 0.700, the width was chosen to be an intermediate value of 49 feet where L = 70 feet. The number of girders, N, was determined so that the spacing between the vertical webs, s_w, was within the practical design range of 7 to 9 feet. Thus, for W/L = 0.318 where W = 35 feet, N = 5; for W/L = 0.700 where W = 49 feet, N = 7; and for W/L = 0.573 and 1.260 where W = 63 feet, N = 9.

Figure 19 illustrates the two edge conditions considered for each structure studied. For an actual bridge design where the width of roadway and number of girders are specified, these cases represent the limiting possibilities for the bridge cross-section. In Figure 19, case 1 represents the full cantilevered top edge flange condition and case 2 represents the condition where there are no cantilevered flanges. If the top and bottom flange thicknesses are nearly equal, the effective width, W_e,

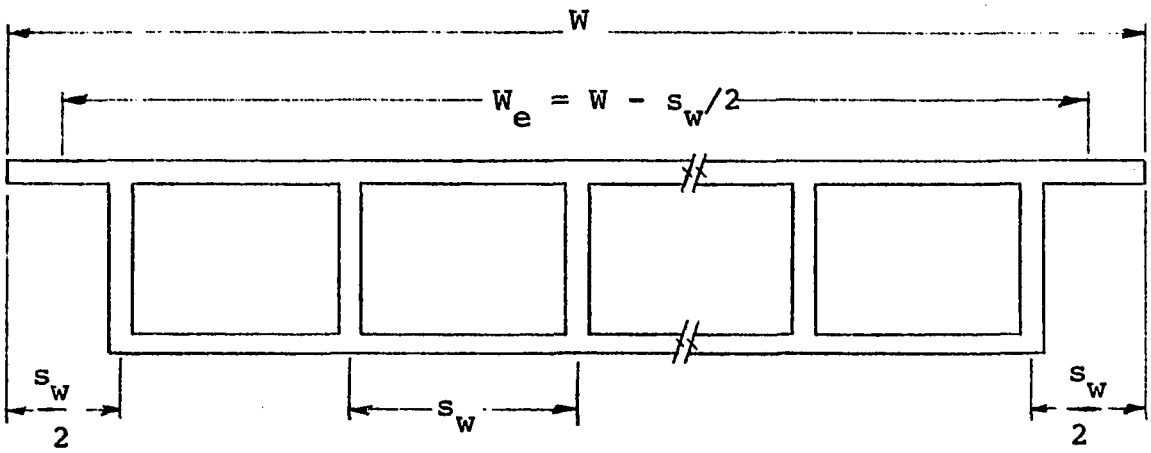

Configuration case 1, fully cantilevered top edge flange

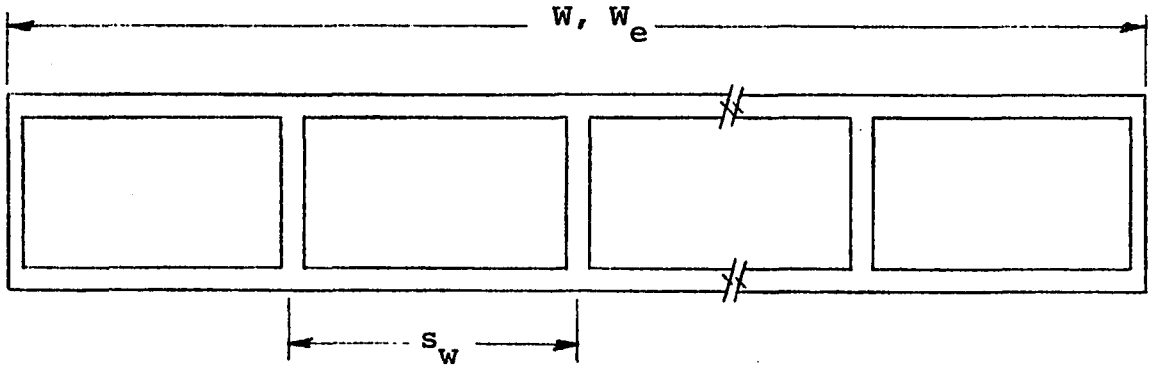

Configuration case 2, no cantilevered flanges

Figure 19. Edge configurations considered in parameter study

for case 1, as derived from equation 92, will be approximately $W - s_{w1}/2$, where s_{w1} is equal to the web spacing for case 1. For case 2, it is seen that $W_e = W$. Thus, if $W_e = W - s_w/2$, the effective widths and web spacings for each of the aspect ratios selected for the study of the effect of the cantilevered flange edge condition are:

for W/L = 0.318, W_e = 31.5 feet and s_w = 7.0 feet,

for W/L = 0.700, W_e = 45.5 feet and s_w = 7.0 feet, and

for W/L = 0.573 and 1.260, W_e = 59.5 feet and s_w = 7.0 feet. For case 2, the effective widths will be equal to the total widths. In this case, the web spacing is:

for W/L = 0.318 or W = 35 feet, s_w is 8.75 feet,

for W/L = 0.700 or W = 49 feet, s_w = 8.16 feet, and

for W/L = 0.573 and 1.260 or W = 63 feet, s_w = 7.88 feet.

Finally, the effect of the transverse position of the applied external loads was investigated. For each of various combinations of ϕ, W/L, and effective width, two load positions were used - a central load and an eccentric load. In the central loading case, the load was applied at the centerline of the structure, or at e/b = 0.0. In the eccentric loading cases, the centroid of the applied load is located 3.5 feet from the outside edge of the structures. Thus, for W = 35 feet, e/b = 0.800, for W = 49 feet, e/b = 0.857, and for W = 63 feet, e/b = 0.889. The load width, 2f, used approximates the width of a tandem truck wheel and was set at 2.5 feet. Thus, for

W = 35 feet, f/b = 0.071; for W = 49 feet, f/b = 0.051; and for W = 63 feet, f/b = 0.04.

In summary, three stiffness parameters were studied, ϕ = 0.0045, 0.06, and 0.24. For ϕ = 0.0045 and 0.06, the three aspect ratios, W/L = 0.318, 0.700, and 1.260, were used, and for ϕ = 0.24, the two aspect ratios, W/L = 0.318 and 0.573, were used. For each of the above combinations of parameters, the full cantilevered and non-cantilevered edge conditions were investigated. Finally, eccentric and central loading conditions were considered for every case studied.

Nine coefficients have been calculated for the various combinations of parameters, six coefficients per unit width and three coefficients per beam. The six coefficients per unit width, as given by equations 73 through 77 and 79, are: longitudinal bending moment, $\bar{M}_x$, transverse bending, $\bar{M}_y$, twisting moment, $\bar{M}_{xy}$, deflection, $\bar{w}$, longitudinal shearing force, $\bar{Q}_x$, and transverse shearing force, $\bar{Q}_y$. The three coefficients per beam, as given by equations 81 through 83, are: longitudinal bending moment, $\bar{M}_{xb}$, twisting moment, $\bar{M}_{xyb}$, and longitudinal shearing force, $\bar{Q}_{xb}$. Since all loads are applied at mid-span, $\bar{M}_x$, $\bar{M}_{xb}$, $\bar{M}_y$, $\bar{w}$, and $\bar{Q}_y$ are measured at mid-span. $\bar{Q}_x$, $\bar{Q}_{xb}$, $\bar{M}_{xy}$, and $\bar{M}_{xyb}$ are measured at the reaction, x = 0.

Results of the parameter study are presented for both the coefficients per unit width and the coefficients per beam. The distributed coefficients represent behavior which is dependent

only on ϕ, W/L, and the load eccentricity, e/b. It is seen that the transverse unit force quantities, $\bar{M}_y$ and $\bar{Q}_y$, and the deflection coefficient, $\bar{w}$, are representable only in the distributed form. However, the longitudinal bending moment, twisting moment, and longitudinal shearing force coefficients are representable in both distributed and beam forms. Results are presented as coefficients per beam for the purpose of determining the effect of edge conditions and to show the range of design forces that may be expected for the range of parameters considered.

Table 4 shows the extremum distributed coefficients for each of the combinations of parameters considered. Only the extremum values are shown since the effects of parameter variations are most easily seen by examining these values. However, the complete transverse distribution of the various coefficients is shown in Figures 20 & 21 for a typical combination of parameters for the purpose of qualitatively indicating the distributions. These figures show the distributions for the case where $\phi = 0.06$ and $W/L = 0.700$. Figure 20 represents a central load where $e/b = 0.0$, and Figure 21 represents an eccentric load where $e/b = 0.857$.

Complete results of the beam distribution coefficients are presented so that the effects of variations of edge beam geometry are ascertained. Tables 5 through 7 present all beam

Table 4. Extremum coefficients per unit width for the parameter studied

ϕ	W/L	e/b	Extremum coefficients per unit width					
			$\bar{M}_x$	$\bar{M}_y$	$\bar{M}_{xy}$	$\bar{w}$	$\bar{Q}_x$	$\bar{Q}_y$
0.0045	0.318	0.0	1.209	0.097	±0.033	1.028	1.276	±1.321
		0.800	1.513	-0.033	0.172	1.169	1.252	1.903
0.0045	0.700	0.0	1.664	0.380	±0.022	1.076	1.841	±2.823
		0.857	2.387	-0.136	0.421	1.686	1.797	3.860
0.0045	1.260	0.0	2.480	0.830	±0.130	1.297	2.754	±4.010
		0.889	3.706	-0.233	0.782	2.776	3.360	6.110
0.06	0.318	0.0	1.333	-0.064	±0.070	1.085	3.535	±0.444
		0.800	1.816	0.095	0.227	1.264	3.532	0.787
0.06	0.700	0.0	2.053	0.131	±0.172	1.324	6.564	±1.005
		0.857	3.004	0.174	0.530	2.019	6.731	1.655
0.06	1.260	0.0	3.308	0.304	±0.348	1.913	10.787	±1.723
		0.889	4.641	0.228	0.969	3.422	11.647	2.720
0.24	0.318	0.0	1.382	-0.138	±0.169	1.137	6.852	±1.850
		0.800	2.052	0.135	0.309	1.451	6.914	1.440
0.24	0.573	0.0	2.072	-0.314	±0.317	1.434	22.145	±0.333
		0.889	3.447	0.286	0.615	2.318	22.377	0.819

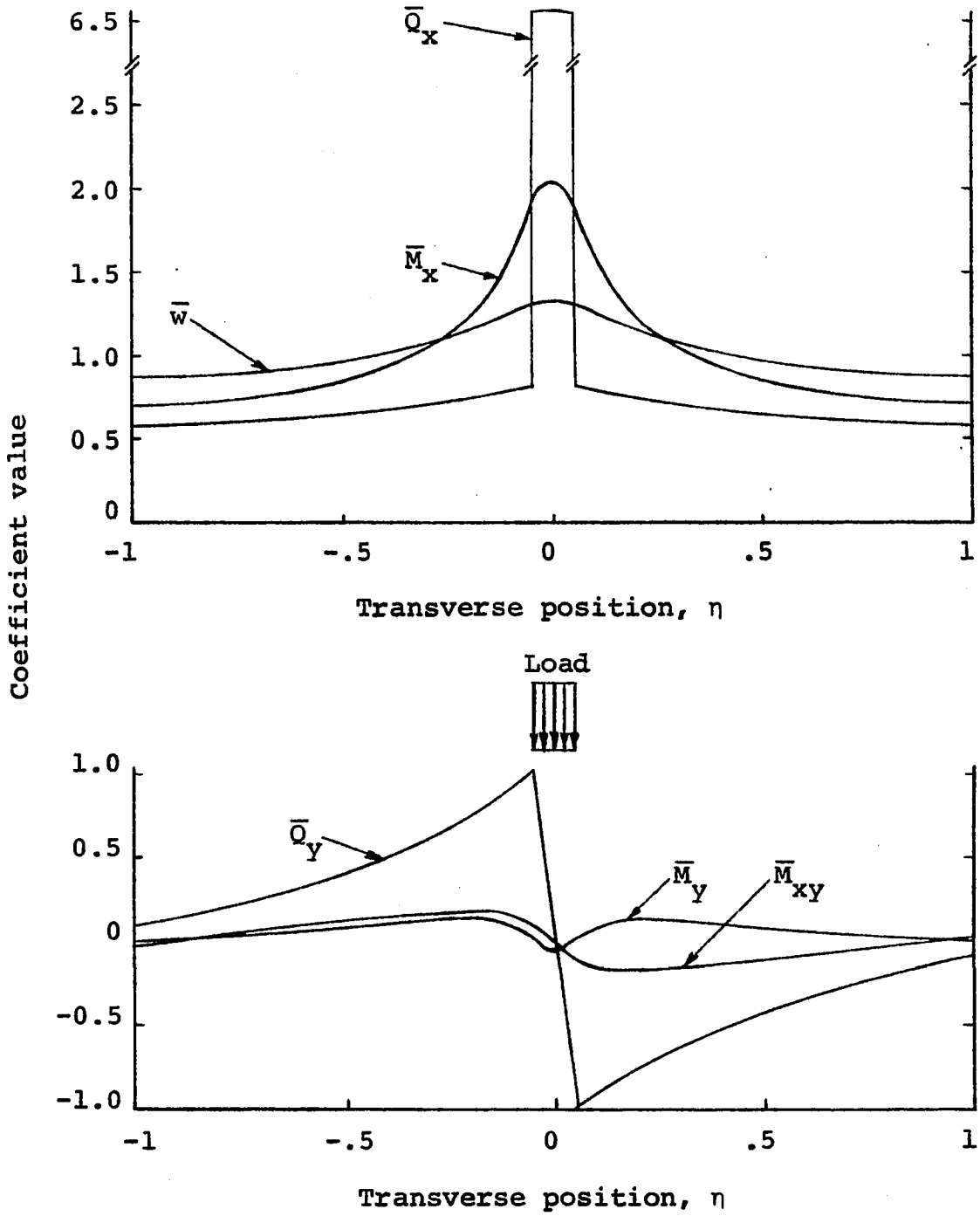

Figure 20. Coefficient per unit width distributions for a typical structure: ϕ = 0.06, W/L = 0.700, and e/b = 0.0

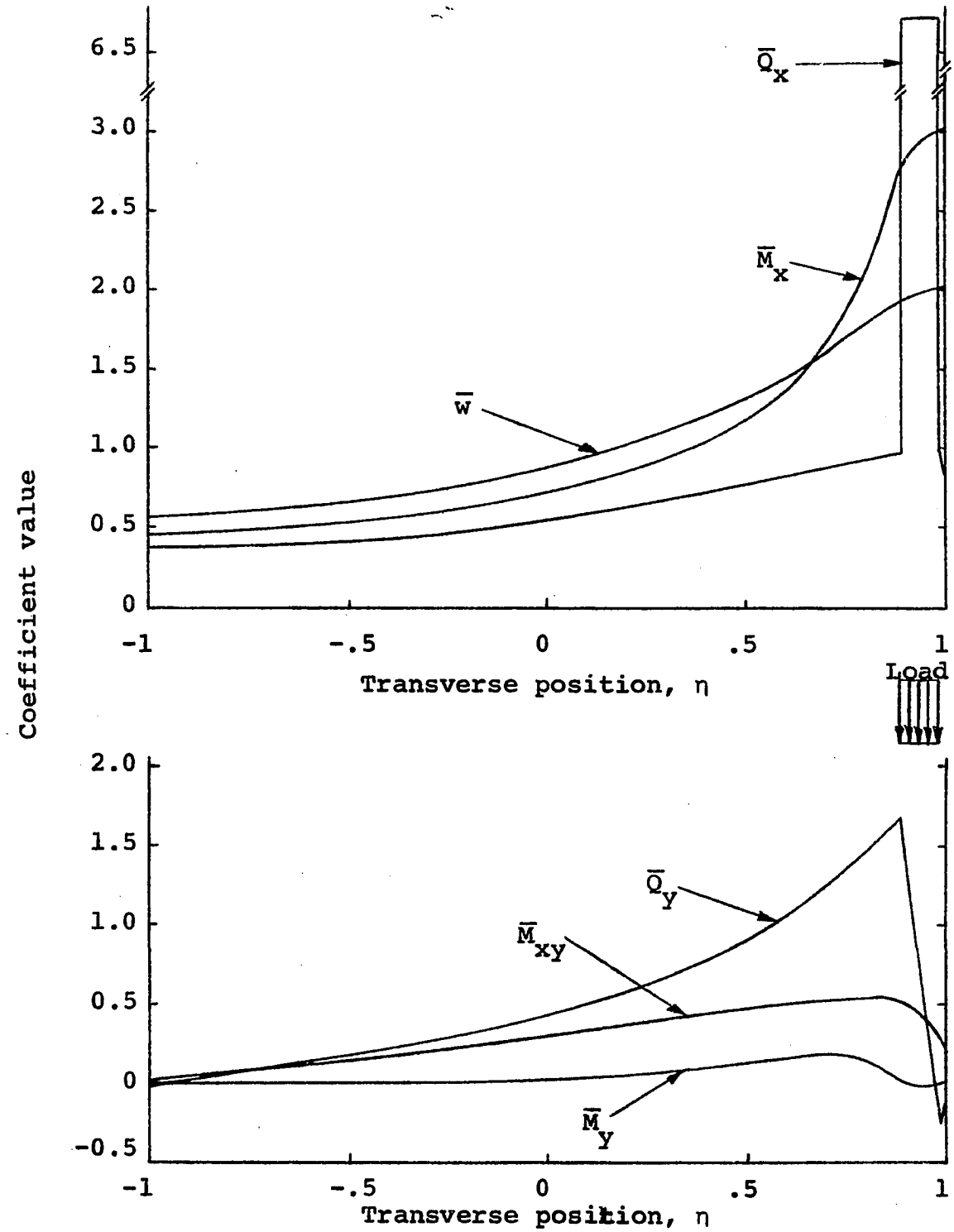

Figure 21. Coefficient per unit width distributions for a typical structure: $\phi = 0.06$, $W/L = 0.700$, and $e/b = 0.857$

Table 5. Beam coefficients for $\phi = 0.0045$

W/L	e/b	Beam number	$\bar{M}_{xb}$ Case 1	$\bar{M}_{xb}$ Case 2	$\bar{M}_{xyb}$ Case 1	$\bar{M}_{xyb}$ Case 2	$\bar{Q}_{xb}$ Case 1	$\bar{Q}_{xb}$ Case 2
0.318	0.0	1	0.771	0.572	-0.022	-0.018	0.787	0.589
		2	1.094	1.208	-0.015	-0.019	1.062	1.191
		3	1.272	1.440	0.0	0.0	1.303	1.439
0.318	0.800	1	0.678	0.498	0.079	0.056	0.794	0.595
		2	0.943	1.038	0.125	0.135	1.053	1.181
		3	1.020	1.146	0.147	0.167	1.049	1.183
		4	1.193	1.433	0.168	0.197	1.059	1.259
		5	1.166	0.886	0.140	0.106	1.046	0.783
0.700	0.0	1	0.672	0.479	-0.001	0.002	0.727	0.520
		2	0.945	0.998	0.018	0.028	1.009	1.076
		3	1.108	1.175	0.021	0.033	1.063	1.151
		4	1.549	1.696	0.0	0.0	1.402	1.507
0.700	0.857	1	0.448	0.310	0.119	0.079	0.632	0.435
		2	0.652	0.669	0.199	0.199	0.830	0.849
		3	0.742	0.774	0.258	0.270	0.873	0.907
		4	0.877	0.945	0.322	0.348	0.973	1.055
		5	1.086	1.213	0.381	0.414	1.109	1.246
		6	1.465	1.830	0.422	0.453	1.237	1.516
		7	1.730	1.258	0.333	0.231	1.346	0.992
1.260	0.0	1	0.532	0.361	0.066	0.049	0.582	0.397
		2	0.776	0.785	0.135	0.146	0.835	0.841
		3	0.927	0.949	0.165	0.193	1.006	1.030
		4	1.237	1.299	0.127	0.159	1.218	1.309
		5	2.057	2.210	0.0	0.0	1.718	1.846

Table 5. Continued

W/L	e/b	Beam number	$\bar{M}_{xb}$		$\bar{M}_{xyb}$		$\bar{Q}_{xb}$	
			Case 1	Case 2	Case 1	Case 2	Case 1	Case 2
1.260	0.889	1	0.191	0.125	0.076	0.048	0.273	0.172
		2	0.300	0.288	0.138	0.128	0.347	0.326
		3	0.381	0.372	0.203	0.196	0.391	0.368
		4	0.502	0.509	0.291	0.294	0.505	0.499
		5	0.686	0.719	0.406	0.420	0.717	0.747
		6	0.949	1.038	0.537	0.567	1.035	1.146
		7	1.353	1.536	0.675	0.705	1.473	1.692
		8	2.038	2.589	0.771	0.780	1.921	2.410
		9	2.600	1.823	0.611	0.390	2.339	1.640

Table 6. Beam coefficients for $\phi = 0.06$

W/L	e/b	Beam number	$\bar{M}_{xb}$		$\bar{M}_{xyb}$		$\bar{Q}_{xb}$	
			Case 1	Case 2	Case 1	Case 2	Case 1	Case 2
0.318	0.0	1	0.722	0.529	-0.004	-0.006	0.560	0.419
		2	1.091	1.189	0.040	0.045	0.766	0.858
		3	1.374	1.564	0.0	0.0	2.347	2.448

Table 6. Continued

W/L	e/b	Beam number	$\bar{M}_{xb}$ Case 1	$\bar{M}_{xb}$ Case 2	$\bar{M}_{xyb}$ Case 1	$\bar{M}_{xyb}$ Case 2	$\bar{Q}_{xb}$ Case 1	$\bar{Q}_{xb}$ Case 2
0.318	0.800	1	0.601	0.442	0.038	0.023	0.549	0.402
		2	0.859	0.941	0.144	0.121	0.729	0.803
		3	0.966	1.088	0.177	0.211	0.742	0.837
		4	1.226	1.516	0.226	0.276	0.776	1.298
		5	1.349	1.014	0.148	0.070	2.203	1.660
0.700	0.0	1	0.579	0.407	-0.004	-0.002	0.493	0.348
		2	0.861	0.890	0.091	0.091	0.703	0.739
		3	1.138	1.190	0.163	0.188	0.799	0.862
		4	1.843	2.025	0.0	0.0	3.010	3.101
0.700	0.857	1	0.379	0.256	0.037	0.020	0.345	0.229
		2	0.544	0.544	0.121	0.109	0.481	0.477
		3	0.628	0.644	0.211	0.214	0.546	0.557
		4	0.775	0.833	0.317	0.314	0.658	0.706
		5	1.023	1.167	0.433	0.482	0.815	0.922
		6	1.541	2.048	0.532	0.594	1.009	1.804
		7	2.110	1.508	0.331	0.129	3.145	2.305
1.260	0.0	1	0.414	0.277	0.014	0.005	0.346	0.230
		2	0.626	0.618	0.121	0.108	0.535	0.526
		3	0.828	0.828	0.245	0.252	0.709	0.715
		4	1.316	1.363	0.347	0.385	0.975	1.038
		5	2.631	2.830	0.0	0.0	3.867	3.981

Table 6. Continued

W/L	e/b	Beam number	$\bar{M}_{xb}$ Case 1	$\bar{M}_{xb}$ Case 2	$\bar{M}_{xyb}$ Case 1	$\bar{M}_{xyb}$ Case 2	$\bar{Q}_{xb}$ Case 1	$\bar{Q}_{xb}$ Case 2
1.260	0.889	1	0.136	0.087	0.019	0.010	0.117	0.071
		2	0.206	0.191	0.061	0.051	0.171	0.153
		3	0.269	0.253	0.112	0.102	0.220	0.202
		4	0.377	0.371	0.183	0.177	0.309	0.300
		5	0.555	0.573	0.287	0.290	0.460	0.471
		6	0.828	0.905	0.440	0.465	0.691	0.752
		7	1.277	1.482	0.661	0.718	1.040	1.191
		8	2.145	2.945	0.902	0.975	1.509	2.605
		9	3.207	2.193	0.590	0.209	4.489	3.256

Table 7. Beam coefficients for $\phi = 0.24$

W/L	e/b	Beam number	$\bar{M}_{xb}$ Case 1	$\bar{M}_{xb}$ Case 2	$\bar{M}_{xyb}$ Case 1	$\bar{M}_{xyb}$ Case 2	$\bar{Q}_{xb}$ Case 1	$\bar{Q}_{xb}$ Case 2
0.318	0.0	1	0.700	0.507	0.017	0.009	0.255	0.189
		2	1.092	1.184	0.113	0.126	0.351	0.392
		3	1.417	1.618	0.0	0.0	3.789	3.838

Table 7. Continued

W/L	e/b	Beam number	$\bar{M}_{xb}$		$\bar{M}_{xyb}$		$\bar{Q}_{xb}$	
			Case 1	Case 2	Case 1	Case 2	Case 1	Case 2
0.318	0.800	1	0.488	0.355	-0.017	-0.019	0.221	0.157
		2	0.765	0.825	0.082	0.082	0.314	0.339
		3	0.942	1.060	0.190	0.232	0.346	0.389
		4	1.300	1.627	0.285	0.363	0.389	1.308
		5	1.505	1.133	0.159	0.023	3.730	2.807
0.573	0.0	1	0.530	0.362	0.008	-0.001	0.218	0.151
		2	0.787	0.799	0.102	0.093	0.303	0.314
		3	0.945	0.965	0.203	0.213	0.328	0.342
		4	1.282	1.341	0.294	0.325	0.361	0.385
		5	1.912	2.066	0.0	0.0	6.581	6.615
0.573	0.889	1	0.245	0.161	-0.057	-0.043	0.110	0.070
		2	0.386	0.376	-0.020	-0.033	0.175	0.169
		3	0.470	0.466	0.050	0.042	0.216	0.213
		4	0.578	0.591	0.131	0.132	0.262	0.269
		5	0.732	0.770	0.228	0.243	0.320	0.336
		6	0.947	1.037	0.337	0.375	0.385	0.417
		7	1.294	1.476	0.459	0.522	0.464	0.512
		8	1.939	2.444	0.572	0.662	0.549	2.235
		9	2.408	1.679	0.304	0.006	6.517	4.779

coefficients ($\bar{M}_{xb}$, $\bar{M}_{xyb}$, and $\bar{Q}_{xb}$) for all of the combinations of parameters studied. Results for $\phi = 0.0045$ are given in Table 5, $\phi = 0.06$ in Table 6, and $\phi = 0.24$ in Table 7. In the case of central loads, only the results for beams 1 through $(N + 1)/2$ are presented since $\bar{M}_{xb}$ and $\bar{Q}_{xb}$ are symmetric and $\bar{M}_{xyb}$ is antisymmetric about the central beam.

In addition to the results presented in Tables 5 through 7, values of $\bar{M}_{xb}$ and $\bar{Q}_{xb}$ are presented in graphical form for selected combinations of parameters so that the effect of individually varying parameters may be qualitatively examined. Figures 22 through 27 represent the transverse distribution of $\bar{M}_{xb}$ and $\bar{Q}_{xb}$ for these parameter variations. So that the effect of the stiffness parameter, ϕ, is ascertained, $\bar{M}_{xb}$ and $\bar{Q}_{xb}$ are plotted in Figures 22 through 24 for constant combinations of W/L and edge conditions. In these figures, the edge condition is configuration case 1, as shown in Figure 19, and the W/L values are: W/L = 0.318, shown in Figure 22, W/L = 0.700, shown in Figure 23, and W/L = 1.260, shown in Figure 24. Figures 25 through 27 present the transverse distribution of $\bar{M}_{xb}$ and $\bar{Q}_{xb}$ for constant combinations of ϕ and W/L where the edge conditions are varied. In Figure 25, low values of 0.0045 and 0.318 are respectively used for ϕ and W/L. In Figure 26, the intermediate values, $\phi = 0.06$ and W/L = 0.700, are used, and in Figure 27, the high values, $\phi = 0.24$ and W/L = 0.537, are used.

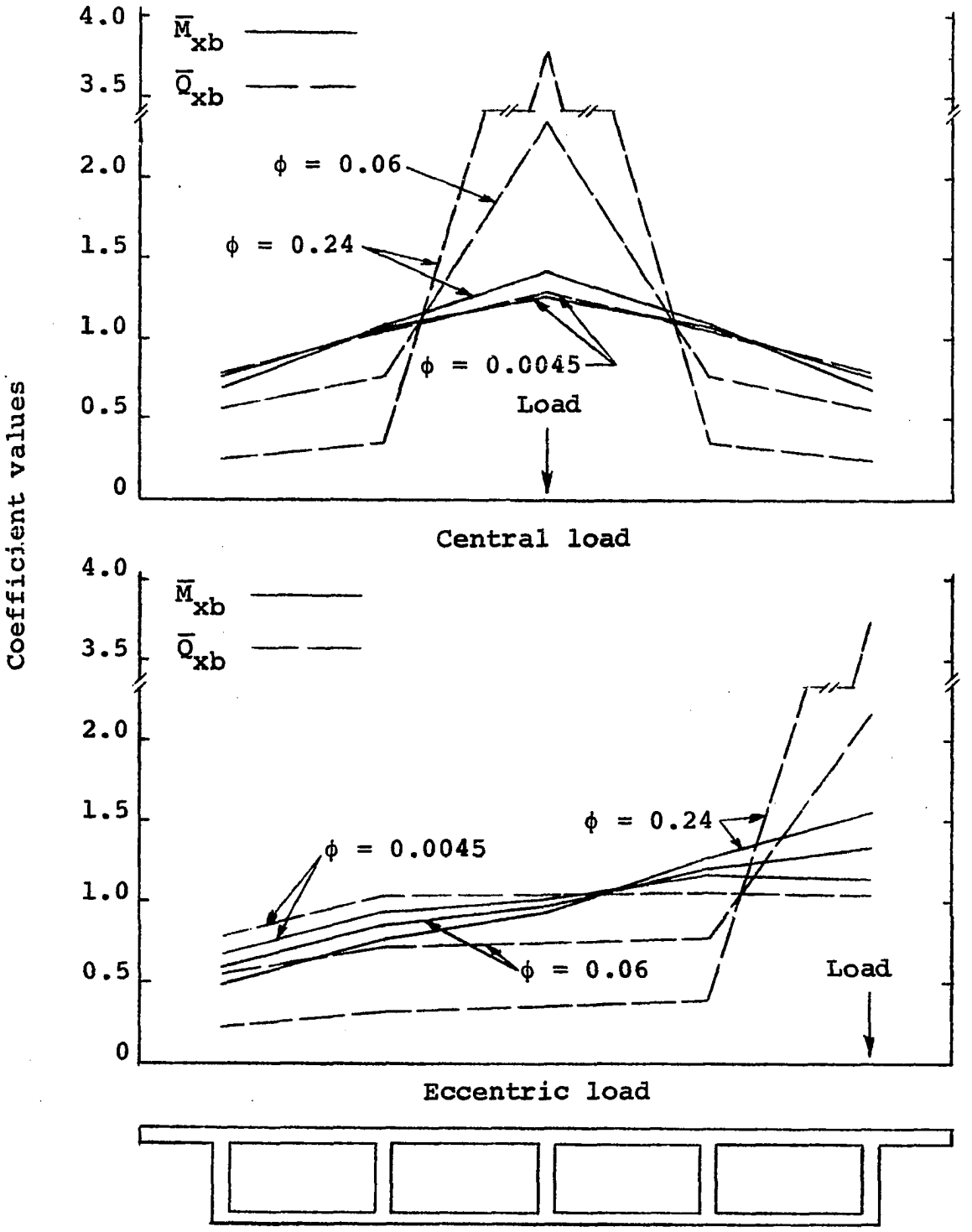

Figure 22. Comparison of beam coefficients for variations of the stiffness parameter ϕ, W/L = 0.318

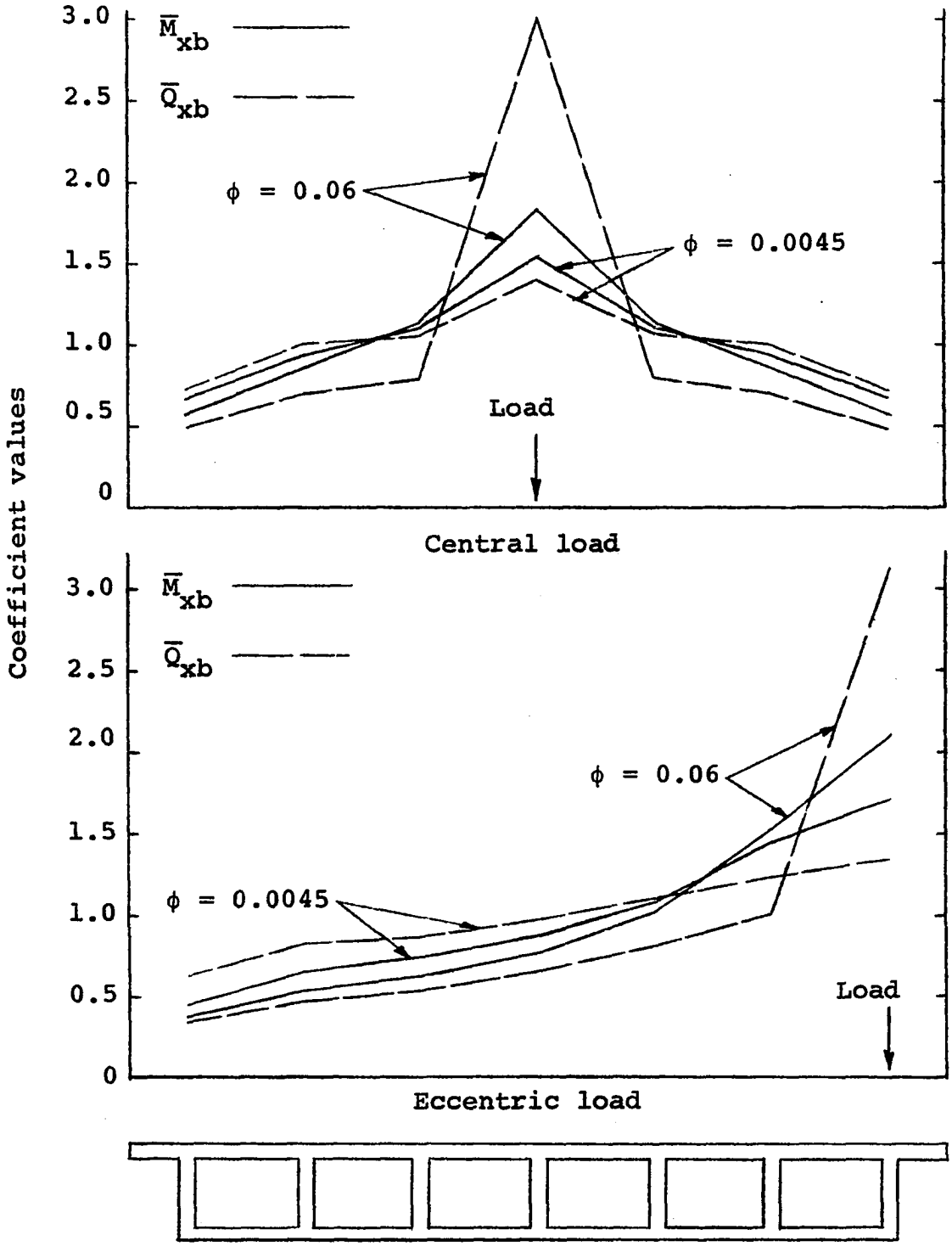

Figure 23. Comparison of beam coefficients for variations of the stiffness parameter ϕ, W/L = 0.700

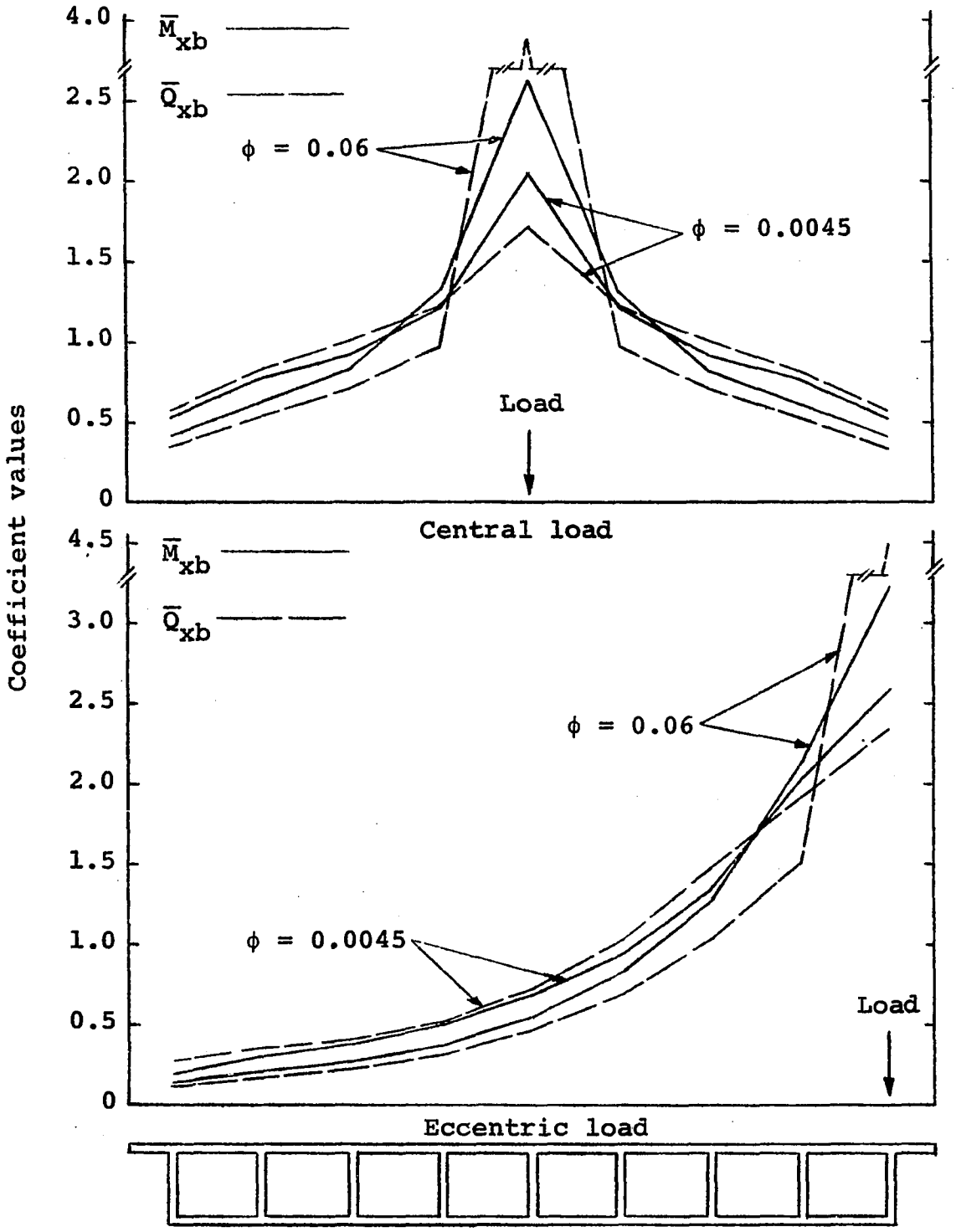

Figure 24. Comparison of beam coefficients for variations of the stiffness parameter ϕ, W/L = 1.260

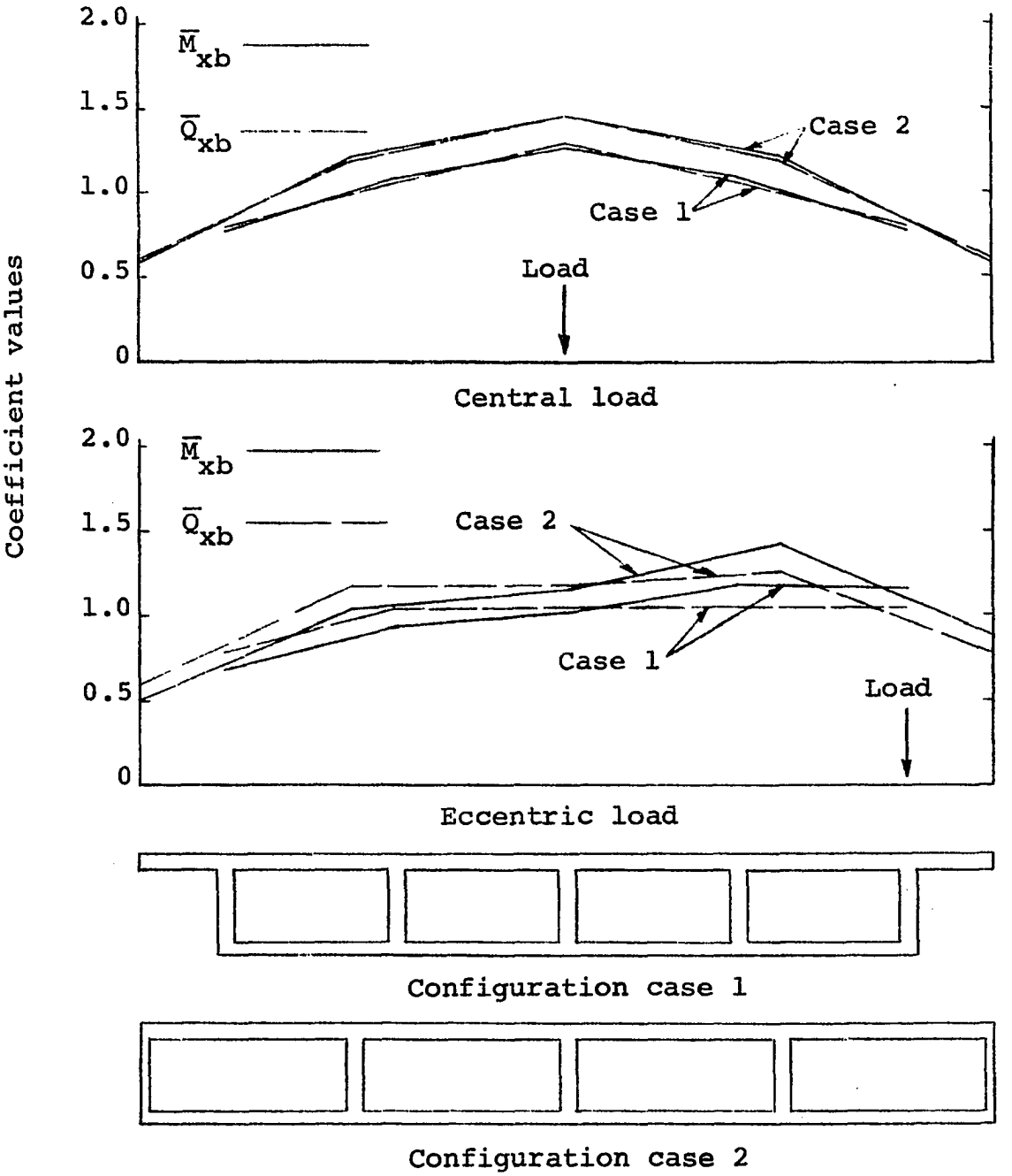

Figure 25. Comparison of beam coefficients for variations of configuration, ϕ = 0.0045 and W/L = 0.318

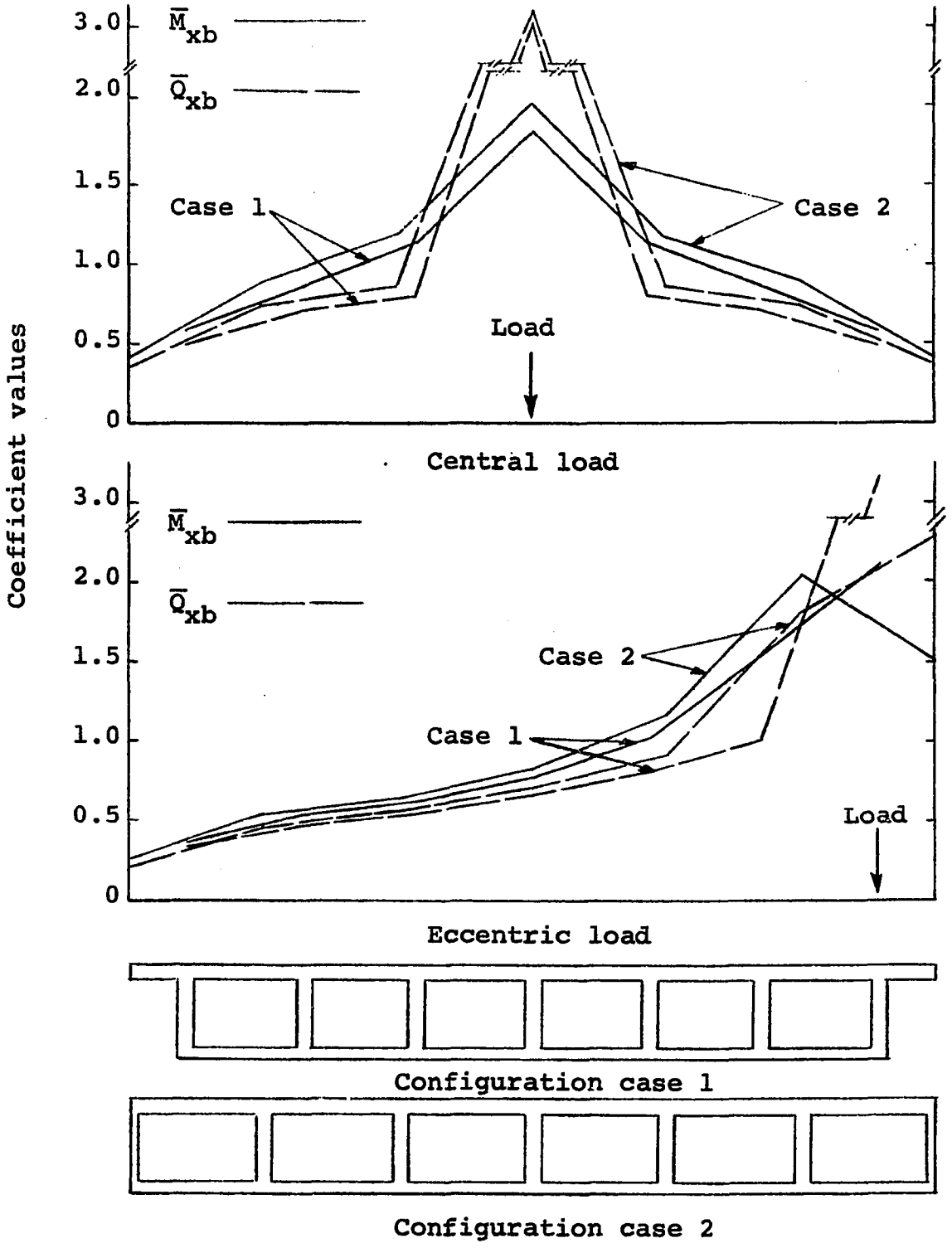

Figure 26. Comparison of beam coefficients for variations of configuration, $\phi = 0.06$ and $W/L = 0.700$

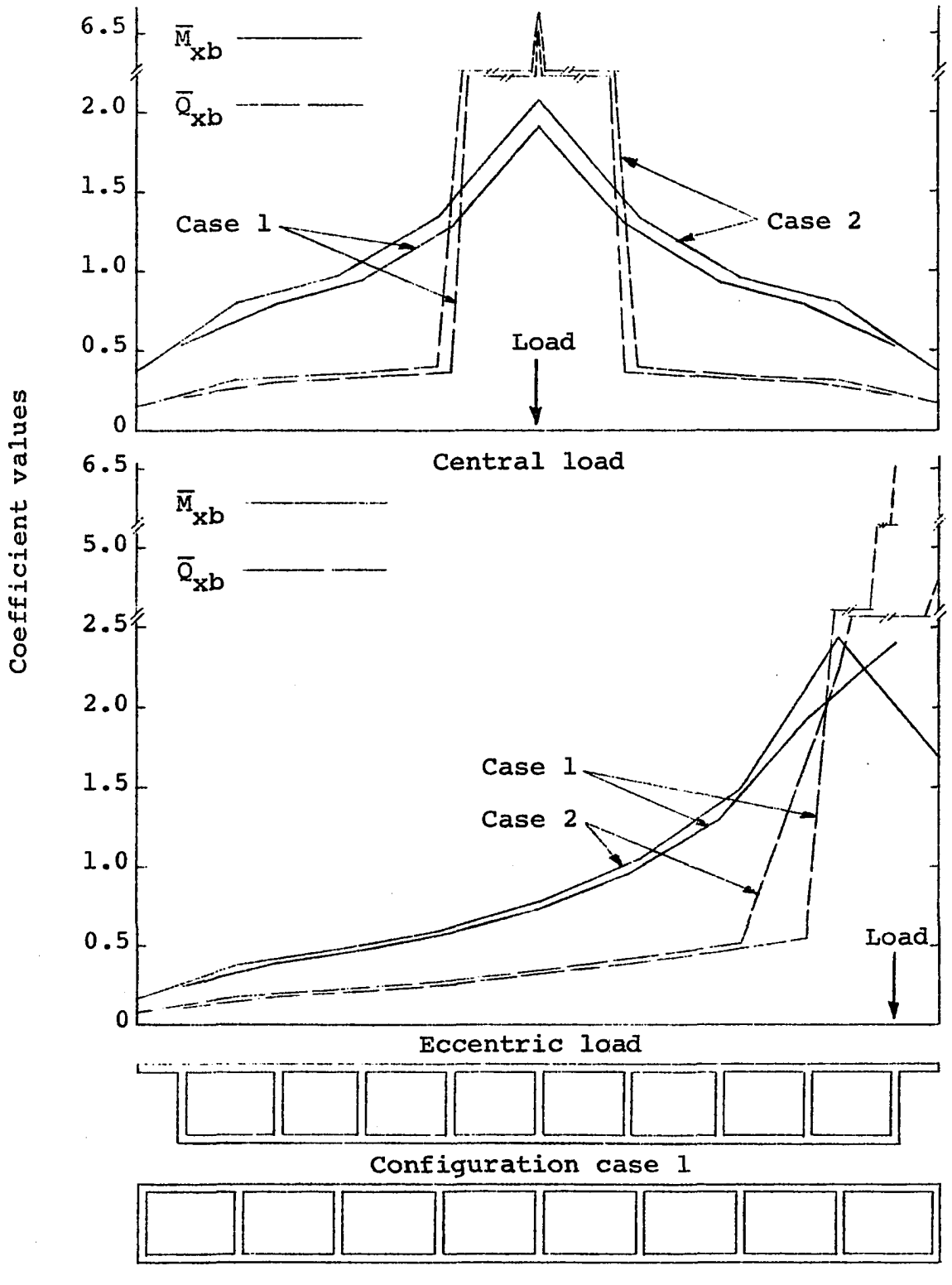

Figure 27. Comparison of beam coefficients for variations of configuration, ϕ = 0.24 and W/L = 0.573

In summary, the parameter study presented herein completely describes the behavior of box girder bridges for the range of parameters that are found for practical structures. The extremum coefficients per unit width, as given in Table 4, serve to show the variation of maximum and minimum coefficients for the full range of stiffnesses and aspect ratios when the edge condition is not a variable. Tables 5 through 7 present the beam coefficients, $\bar{M}_{xb}$, $\bar{M}_{xyb}$, and $\bar{Q}_{xb}$, for variations of ϕ, W/L, and edge condition. Figures 22 through 24 present $\bar{M}_{xb}$ and $\bar{Q}_{xb}$ for varying ϕ when W/L and edge conditions are constant. Figures 25 through 27 present $\bar{M}_{xb}$ and $\bar{Q}_{xb}$ for variable edge conditions when ϕ and W/L are held constant.

Results of the Parameter Study

A discussion of the ranges of the various coefficients and the effect of variations of the parameters on the coefficients are included in this section. The transverse coefficients, $\bar{M}_y$ and $\bar{Q}_y$, and the deflection coefficient, $\bar{w}$, are represented only as distributed quantities, or as coefficients per unit width. Thus, the following discussion of $\bar{M}_y$, $\bar{Q}_y$, and $\bar{w}$ is based on the parameter study results presented in Table 4. The longitudinal bending moment, longitudinal shear force, and twisting moment coefficients are examined in the coefficient per beam form. Thus, Tables 5 through 7 and Figures 22 through 27 are used as a basis for the discussion of $\bar{M}_{xb}$, $\bar{Q}_{xb}$, and $\bar{M}_{xyb}$. The ranges

of the coefficients and the effect of variations of the parameters on the coefficients are:

1. Transverse bending moment coefficient per unit length $\bar{M}_y$: The range of $\bar{M}_y$ extrema is -0.314 to 0.830. The upper and lower limits of this range are obtained when W/L is maximum and when the load eccentricity, e/b, is zero. The minimum extremum, -0.314, occurs for $\phi = 0.24$. Conversely, the maximum extremum, 0.830, is obtained for $\phi = 0.0045$. Thus, maximum and minimum $\bar{M}_y$ extrema occur when W/L is large and e/b is small. Also, $\bar{M}_y$ extrema tend to increase as ϕ decreases.

2. Transverse shear force coefficient per unit length, $\bar{Q}_y$: The range of $\bar{Q}_y$ is -4.010 to 6.110. The limits of this range are obtained for $\phi = 0.0045$ and W/L = 1.260. The minimum value occurs for e/b = 0.0 and the maximum value for e/b = 0.889. Also, the $\bar{Q}_y$ extrema increase in absolute value for increasing W/L and decreasing ϕ. In addition, except for the case when $\phi = 0.24$, absolute maximum $\bar{Q}_y$ extrema are obtained for large load eccentricities, and the absolute minimum $\bar{Q}_y$ extrema are obtained for small load eccentricities.

3. Deflection coefficient, $\bar{w}$: The range of deflection coefficient extrema is 1.028 to 3.422. The minimum value of this range is obtained for $\phi = 0.0045$, W/L = 0.318, and e/b = 0.0. Conversely, the maximum $\bar{w}$ extremum is obtained for large ϕ, W/L, and e/b. Thus, as ϕ, W/L, and e/b increase, the $\bar{w}$ extrema tend to increase.

4. Twisting moment coefficient per beam, $\bar{M}_{xyb}$: The range of $\bar{M}_{xyb}$ is -0.022 to 0.975. The minimum value is obtained for ϕ = 0.0045, W/L = 0.318, e/b = 0.0, and the full cantilevered top edge slab or configuration case 1 (Figure 19). The maximum value of $\bar{M}_{xyb}$ is obtained for ϕ = 0.06, W/L = 1.260, e/b = 0.889, and configuration case 2 or the non-cantilevered top edge flange condition (Figure 19). In general, $\bar{M}_{xyb}$ increases for increasing ϕ, W/L, and e/b. Also, edge beam twisting moment coefficients tend to be smaller for configuration case 2, and interior $\bar{M}_{xyb}$ tend to be smaller for configuration case 1.

5. Longitudinal bending moment coefficient per beam, $\bar{M}_{xb}$: The range of maximum $\bar{M}_{xb}$ is 1.193 to 3.207. The minimum value of this range is found when ϕ = 0.0045, W/L = 0.318, e/b = 0.800, and the edge condition is configuration case 1. The maximum $\bar{M}_{xb}$ is obtained for ϕ = 0.06, W/L = 1.260, e/b = 0.889, and the edge condition is configuration case 1. It is seen that as ϕ, W/L, and e/b increase, the longitudinal bending moment coefficient per beam maximum values increase. The effect of edge condition is dependent on the load position. For central loads, configuration case 2 tends to produce maximum $\bar{M}_{xb}$. Conversely, for eccentric loads, configuration case 1 tends to result in maximum $\bar{M}_{xb}$.

6. Longitudinal shear force coefficient per beam, $\bar{Q}_{xb}$: The range of maximum $\bar{Q}_{xb}$ is 1.059 to 6.615. For the minimum value of this range, the parameters are: ϕ = 0.0045,

W/L = 0.318, e/b = 0.800, and edge configuration case 2. For the maximum value, the parameters are: ϕ = 0.24, W/L = 0.573, e/b = 0.0, and edge configuration case 2. The maximum values of $\bar{Q}_{xb}$ are seen to increase for an increase in either ϕ or W/L. Also, configuration case 2 tends to produce maximum $\bar{Q}_{xb}$ values. However, the effect of the load position on maximum $\bar{Q}_{xb}$ values is seen to be dependent on the value of W/L. In general, for low values of W/L, maximum $\bar{Q}_{xb}$ values are found for central loads. Conversely, for higher W/L values, $\bar{Q}_{xb}$ becomes a maximum for eccentric loads.

From the results of the parameter study and the summary of the ranges of the coefficients, the parameter which has the greatest influence on the behavior of the structures studied is the aspect ratio, W/L. For all coefficients except $\bar{Q}_y$ where ϕ = 0.24, an increase of W/L results in an increase of the absolute values of the various coefficient extrema. The exception to this trend, decreasing $\bar{Q}_y$ for increasing W/L when ϕ = 0.24, may be attributed to the very great increase of $\bar{Q}_x$ when W/L is increased from 0.318 to 0.941 for ϕ = 0.24. Thus, a much greater portion of the total vertical shear force is carried longitudinally for large ϕ and W/L than is the case when ϕ is small and W/L is large. The effect of the variation of W/L on the distributions of $\bar{M}_{xb}$ and $\bar{Q}_{xb}$ is illustrated by Figures 22 through 24. It is seen that for constant ϕ and e/b, the distribution curves do not change their relative positions,

but do significantly increase their values when W/L is increased.

The stiffness parameter, ϕ, is also seen to have a significant affect on the various coefficients. The transverse coefficients per unit length, $\bar{M}_y$ and $\bar{Q}_y$, are seen to decrease for increasing ϕ. This result intuitively follows since ϕ is a measure of the transverse shearing rigidity of the structure so that as ϕ increases, the transverse shearing rigidity of the structure decreases. Thus, it follows that a decrease in rigidity would result in a corresponding decrease in the transverse coefficients, $\bar{M}_y$ and $\bar{Q}_y$. For all coefficients except $\bar{M}_y$ and $\bar{Q}_y$, increasing ϕ results in the increase of the coefficients' extremum values. The effect of variations of ϕ on the distribution of $\bar{M}_{xb}$ and $\bar{Q}_{xb}$ for constant W/L and e/b is illustrated in Figures 22 through 24. Increasing ϕ causes an increase in the difference between maximum and minimum values of the beam coefficients for any given distribution curve. Hence, increasing ϕ results in poorer distributions of the beam coefficients, $\bar{M}_{xb}$ and $\bar{Q}_{xb}$. In addition, it is observed that for a uniform increase in ϕ, a greater change occurs in the distributions of $\bar{M}_{xb}$ and $\bar{Q}_{xb}$ when W/L is large. Finally, it is seen from the figures that variations of ϕ affect the distribution $\bar{Q}_{xb}$ to a much greater extent than the $\bar{M}_{xb}$ distributions.

A qualitative examination of the effect of edge beam geometry on the distributions of $\bar{M}_{xb}$ and $\bar{Q}_{xb}$ follows from the

study presented in Figures 25 through 27. For centrally applied loads, or e/b = 0.0, the full cantilevered top edge flange condition, or configuration case 1, results in better distribution of $\bar{M}_{xb}$ and $\bar{Q}_{xb}$. That is, less variation exists between the maximum and minimum coefficient values for a given combination of parameters. However, for eccentric loads, the effect of the edge condition on the distribution of $\bar{M}_{xb}$ and $\bar{Q}_{xb}$ is dependent on W/L and ϕ. In general, it is observed that for ϕ and W/L small, configuration case 1 results in better distribution of $\bar{M}_{xb}$ and $\bar{Q}_{xb}$. Conversely, for ϕ and W/L large, the non-cantilevered top edge flange condition or configuration case 2 results in better $\bar{M}_{xb}$ and $\bar{Q}_{xb}$ distributions. Also, it is seen that as W/L increases, the relative difference between the distributions as found from either configuration diminishes. This follows since greater widths and, hence, a greater number of beams results from the large W/L values. For a large value of the number of beams, N, the coefficient per beam values approach the coefficients per unit width values. Thus, for W/L large, the coefficient per beam values approach the common coefficient per unit width values for variations of edge beam geometry.

In summary, it has been shown that an increase of the aspect ratio, W/L, generally results in poorer distribution of all of the coefficients studied. The exception to this trend occurs for very large values of ϕ. It was shown that for ϕ = 0.24, the distribution of $\bar{Q}_y$ was improved for an increase in W/L.

Increasing the stiffness parameter, ϕ, had the effect of improving the distribution of $\bar{Q}_y$ and $\bar{M}_y$. However, for all other coefficients, an increase in ϕ resulted in poorer distributions. Edge beam configuration case 1 was shown to result in better distributions of the beam coefficients in the case of centrally applied loads. For eccentric loads, edge beam configuration case 2 resulted in better beam coefficient distributions when ϕ and W/L were large. For the case of eccentric loading and ϕ and W/L small, configuration case 1 resulted in better distributions.

Design Considerations

The results just presented lead to the following recommendations concerning the proportioning of the governing parameters for the most favorable load distribution. Usually in practical design circumstances, the overall geometry or width and span of the structure are governed by factors other than load distribution. However, it is seen from the behavioral study that the least possible W/L ratio should be used for the most optimum distribution of all of the forces, moments, and deflections existing in the structure.

The variation of the stiffness parameter, ϕ, has been shown to have a significant effect on the load distribution, especially on the distribution of longitudinal shear forces.

It has been noted that decreasing ϕ results in more favorable distributions of all of the coefficients except the transverse moment and shear force coefficients, $\bar{M}_y$ and $\bar{Q}_y$. From Table 4, it is seen that the transverse moment coefficient extrema are small even in the case where ϕ is small. Also, the transverse shear force coefficient extrema do not become large until ϕ becomes small, or equal to about 0.0045, and the aspect ratio, W/L, is large. Thus, to obtain a favorable transverse shear force distribution, a minimum value of $\phi = 0.01$ is recommended when W/L is greater than about 0.7. This value of ϕ would be obtained in a practical structure having one interior diaphragm and an intermediate d/L ratio of about 0.06. From the relationships developed for the calculation of the stiffness parameter, it is seen that for bridges without interior diaphragms, the most effective method of reducing ϕ is to reduce the depth of the structure, d, or to use the minimum permissible d/L ratio. Other less effective methods for the reduction of ϕ would be the use of small web spacings or the use of thicker webs. The use of interior diaphragms significantly decreases ϕ. If interior diaphragms are used, it has been shown that ϕ is primarily dependent on the depth-span ratio. Thus, if interior diaphragms are present and a decrease in ϕ is desired, then d/L must be decreased.

The edge beam configuration has been shown to affect the distribution of the beam coefficients. However, the effect is

dependent on the load position and W/L. Since the governing load configuration is usually determined so that the loads are in their most eccentric position (9), recommendations for the most optimum edge beam configuration are based on the effect of eccentric loads. Therefore, it is recommended that for W/L less than about 0.5, the edge beam configuration should correspond to configuration case 1. For W/L greater than about 0.5, the amount of top flange cantilevering should be decreased as W/L decreases.

In summary, the best load distribution is usually obtained in a bridge with:

1. the smallest practical W/L ratio,
2. a small value of the stiffness parameter ϕ:

for bridges with no interior diaphragms, the smallest flexural rigidity - transverse shearing rigidity ratio, and for bridges with diaphragms, the largest transverse shearing rigidity,

3. edge configuration case 1 if $W/L<0.5$, and if $W/L\geq 0.5$, an edge configuration with less top edge flange cantilevering.

It should be noted that certain forces and moments do not follow these general statements, but they can be used as design guides.

SUMMARY AND CONCLUSIONS

Summary

A procedure has been developed for the complete determination of the load distribution in simply supported concrete box girder highway bridges. Expressions have been presented for the complete determination of the moments, shearing forces, and deflections in the structure due to externally applied vertical concentrated loads.

The procedure developed was used for an extensive study of the behavior of the range of commonly built concrete box girder highway bridges. The behavior of the bridges studied was found to depend on three parameters: the ratio of the width to the span of the bridge, W/L, a stiffness parameter reflecting the relative flexural and torsional rigidities of the structure, ϕ, and an effective width, W_e, which is a function of the bridge's edge beam geometry. The ranges of the internal forces, moments, and deflections for the bridges studied are presented, and the effect of variations of the governing parameters on these quantities is discussed. The results of the behavioral study were used to discuss optimum design configurations so that a more uniform distribution of the internal force quantities may be obtained.

The computer programs used for the determination of the load distribution results are given in the appendices. The

program developed for the complete determination of load distribution in concrete box girder highway bridges is shown in Appendix A, and the program used for the determination of longitudinal moments and deflections in orthotropic plates is shown in Appendix B.

Conclusions

The concept of replacing the actual cellular structure of a concrete box girder highway bridge by a uniform plate with structural properties equivalent to those of the actual bridge has been shown to be a valid method of analysis. The use of this analysis results in an accurate and comparatively simple method for the complete determination of load distribution in concrete box girder highway bridges. The accuracy of the method has been demonstrated in the section of the study concerned with the verification of the proposed analysis. The simplicity of the use of the analysis results from the requirement that only the three parameters, W/L, ϕ, and W_e, need be specified for the complete description of the behavior of the structure.

From the behavioral study, the following conclusions were drawn:

1. The parameter found to have the most significant effect on the distribution of the internal force and deflection quantities is the aspect ratio, W/L. An increase in W/L results

in poorer distribution of all of the quantities considered.

2. The stiffness parameter, ϕ, significantly affects the distribution of the force and deflection quantities. Except for the transverse bending moment and shear force, an increase in ϕ results in poorer distribution of forces, moments, and deflections. Thus, by decreasing the flexural rigidity to transverse rigidity ratio, better distribution of forces and deflections generally occurs.

3. The edge beam configuration, which is represented by the effective width parameter, W_e, influences the distribution of the internal forces and deflections. However, the influence of W_e is not as great as the influence of W/L and ϕ, on the load distribution. For W/L less than about 0.5, the fully cantilevered top edge flange condition generally results in better load distribution. For W/L greater than about 0.5, decreasing the amount of top flange cantilevering in proportion to the increase of W/L generally results in the most optimum load distribution.

Recommendations for Further Research

The scope of this study has been limited to the analysis of simply supported concrete box girder highway bridges. In addition, only non-skew bridges (bridges with rectangular plan) were included in the scope. However, continuous, skew, and horizontally curved concrete box girder bridges are being

increasingly used for highway structures. Thus, it would be desirable to obtain solutions to the governing equations of the equivalent plate for the boundary conditions representing these structures. The complexity of these boundary conditions may rule out an analytical solution of the governing equations. However, the equations could be easily converted to finite difference operators, and the solutions could thus be found by numerical procedures.

In conclusion, the foundations for the analysis of more complex box girder bridges have been presented and proven. Further applications of the theory to more complicated bridge configurations could prove to be a valuable technique for the analysis of these structures.

LITERATURE CITED

1. Arendts, J. G. Study of experimental and theoretical load distribution in highway bridges. Unpublished M.S. thesis. Library, Iowa State University of Science and Technology, Ames, Iowa. 1968.

2. Campbell-Allen, D. and Lee, H. C. The influence of diaphragms on the behavior of multi-box concrete bridge girders. School of Civil Engineering, The University of Sydney, Sydney, Australia, Research Report R72. 1966.

3. Cheng, S. On the theory of bending of sandwich plates. U.S. National Congress of Applied Mechanics Proceedings 4: 511-518. 1962.

4. Davis, R. E., Kozak, J. J. and Scheffey, C. F. Structural behavior of a box girder bridge. Bridge Department, California Highway Transportation Agency, Sacramento, California. 1965.

5. Langhaar, H. L. Energy methods in applied mechanics. John Wiley and Sons, New York, New York. 1962.

6. Little, G. The distribution of a load in a box-section bridge from tests on a xylonite model. Cement and Concrete Association Reprint 18. 1954.

7. Little, G. and Rowe, R. E. Load distribution in multi-webbed bridge structures from tests on plastic models. Cement and Concrete Association Technical Report TRA/185. 1955.

8. Rowe, R. E. Concrete bridge design. John Wiley and Sons, New York, New York. 1962.

9. Sanders, W. W., Jr. and Elleby, H. A. Distribution of wheel loads on highway bridges. Unpublished research report. Engineering Research Institute, Iowa State University of Science and Technology, Ames, Iowa. 1968.

10. Scordelis, A. C. Analysis of continuous box girder bridges. Department of Civil Engineering, University of California, Berkeley, Structures and Materials Research Report SESM-67-25. 1967.

11. Scordelis, A. C. Analysis of simply supported box girder bridges. Department of Civil Engineering, University of California, Berkeley, Structures and Materials Research Report SESM-66-17. 1966.

12. Scordelis, A. C. and Meyer, C. Wheel load distribution in concrete box girder bridges. Department of Civil Engineering, University of California, Berkeley, Structures and Materials Research Report SESM-69-1. 1969.

13. Standard specifications for highway bridges. Ninth edition. American Association of State Highway Officials, Washington, D.C. 1965.

14. Standard specifications for highway bridges, 1966-1967 interim specifications. American Association of State Highway Officials, Washington, D.C. 1967.

15. Timoshenko, S. P. and Woinowsky-Krieger, S. Theory of plates and shells. Second edition. McGraw-Hill, New York, New York. 1959.

16. Wright, R. N., Abdel-Samad, S. R. and Robinson, A. R. Analysis and design of closed-section girder bridges with diaphragms. Department of Civil Engineering, University of Illinois, Urbana, Illinois. 1967.

ACKNOWLEDGMENTS

The author wishes to express appreciation to his major professor, Dr. W. W. Sanders, Jr., for his guidance and encouragement throughout this study and the writer's graduate program.

This study was sponsored by the Engineering Research Institute of Iowa State University. Its support of the writer during the conduct of the investigation is gratefully acknowledged.

APPENDIX A: COMPUTER PROGRAM FOR THE DETERMINATION OF LOAD DISTRIBUTION BY THE EQUIVALENT PLATE ANALYSIS

```
C      COMPLETE SOLUTION FOR LOAD DISTRIBUTION IN A SIMPLY
C      SUPPORTED CONCRETE BOX GIRDER HIGHWAY BRIDGE
C
       DIMENSION EBRAT(10),BAB(10),DCOF(17),BCOF(10),XV(17)
       DIMENSION XM(17),YM(17),XYM(17),DEF(17),XSH(17),YSH(17)
       DIMENSION XMB(10),XYMB(10),XVB(10),YV(17)
       DIMENSION CHEK(10)
       DOUBLE PRECISION ET1(3),ET2(3),C(3,4),DELT(3),A(12,12),
      1BB(12),AA(144)
       DOUBLE PRECISION SH,CH
       DOUBLE PRECISION CNU,PNU,CS,ZET,BET,PHN,PPH,CLAM,PPH1,
      1SB,CB,HB,HSHB,HCHB,SHB,CHB,ETT1,ETT2,CONMBN,CBE1,CBE2,
      2SBE1,SBE2,DCBE,DSBE,EDCBE,EDSBE,BTW,BREA,ET,BE,SBE,CBE,
      3XM1,YM1,XYM1,DEF1,SHX1,SH1,V1,VX1
       EQUIVALENCE (A(1,1),AA(1))
     1 FORMAT(8F10.2)
     2 FORMAT(3I10)
     3 FORMAT(10F5.2)
   200 FORMAT('1   ',47X,'** BOX GIRDER BRIDGE RESULTS **')
   201 FORMAT('0',40X,'STIFFNESS PARAMETER =',1PE20.4)
   202 FORMAT('0',40X,'WIDTH =                ',F20.2)
   203 FORMAT('0',40X,'SPAN =                 ',F20.2)
   204 FORMAT('0',40X,'NO. OF SERIES TERMS =',I20)
   205 FORMAT('0',40X,'LOAD POSITION',I2,'     E/B =',F10.3)
   207 FORMAT('0',67X,'** Y/B **')
   208 FORMAT('0QUANTITY')
   210 FORMAT('1',60X,'COEFFICIENTS PER BEAM'/)
   211 FORMAT('0BEAM NUMBER     ',10I10)
   212 FORMAT('0BEAM X-MOM. COEF. ',10F10.3)
   213 FORMAT('0BEAM X-MOM. COEF. SUM   =',F10.3)
   214 FORMAT('0VALUES OF LONG. SHEAR AT THE DISCONTINUITIES='
      1,4F10.3)
   217 FORMAT('0',40X,'IER =',I5///)
   219 FORMAT('0',60X,'**CONSTANTS**'/)
   220 FORMAT('0',28X,'  A(',I1,')=',1PD10.2,'     B(',I1,
      1')=',1PD10.2,'     M(',I1,')=',1PD10.2,'     N(',I1,
      2')=',1PD10.2)
   221 FORMAT('0BEAM XY-MOM. COEF.',10F10.3)
   222 FORMAT('0BEAM SHEAR  COEF. ',10F10.3)
   223 FORMAT('0BEAM SHEAR  COEF. SUM   =',F10.3)
   224 FORMAT('0BEAM XY-MOM.COEF. SUM   =',F10.3)
   230 FORMAT('0XMOM. COEF.',17F7.3)
   231 FORMAT('0YMOM. COEF.',17F7.3)
   232 FORMAT('0XYMOM.COEF.',17F7.3)
```

```
  233 FORMAT('0DEFL. COEF.',17F7.3)
  234 FORMAT('0XSHR. COEF.',17F7.3)
  235 FORMAT('0YSHR. COEF.',17F7.3)
  236 FORMAT('0XREA. COEF.',17F7.3)
  237 FORMAT('0YREA. COEF.',17F7.3)
    8 READ(1,1) PH,RNU,WID,CLEN,XARAT,XARAT1,CARAT,DBRAT
      IF(WID) 9,999,9
    9 READ(1,2) NN,NG,NEB
      READ(1,3) (BAB(LL),LL=2,NG)
      NG1=NG+1
      BAB(1)=-1.
      BAB(NG1)=1.
      READ(1,3) (EBRAT(LL),LL=1,NEB)
C
C     INITIAL CALCULATIONS
C
      PI=3.14159
      CNU=RNU
      PNU=1.0D0-CNU
      B=WID/2.
      DELT(1)=0.0D0
      DELT(2)=1.0D0
      DELT(3)=0.0D0
      BDRAT=1./DBRAT
      GN=NG
      TTM=GN*BDRAT*CLEN/(PI*WID)
      TTD=BDRAT/PNU
C
C     LOAD LOOP
C
      DO 150 JJJ=1,NEB
      CS=EBRAT(JJJ)+DBRAT
      ZET=EBRAT(JJJ)-DBRAT
      DEN=0.
      DEND=0.
      DENXS=0.
      DENYS=0.
      DO 7 J=1,10
      CHEK(J)=0.
      XMB(J)=0.
      XYMB(J)=0.
    7 XVB(J)=0.
      DO 10 J=1,17
      XM(J)=0.
      YM(J)=0.
      XYM(J)=0.
      DEF(J)=0.
      XSH(J)=0.
      XV(J)=0.
      YV(J)=0.
```

```
   10 YSH(J)=0.
C
C      PRIMARY SERIES LOOP
C
       H=-1.
       HM=-1.
       DO 100 I=1,NN,2
       H=H*HM
       CCC=I
       BET=CCC*PI*B/CLEN
       ALPH=BET/B
       PHN=PH*(CCC*PI)**2
       PPH=PHN+1.0D0
       CLAM=(PHN*(1.+CNU)-PNU)/2.
       TSH=H/CCC
       TM=TSH/CCC
       TMB=TM/CCC
       TD=TMB/CCC
       TRE=H/ALPH
       SXAR=SIN(CCC*PI*XARAT/2.)
       CXAR=COS(CCC*PI*XARAT1/2.)
C
C      LOAD SIMULTANEOUS EQUATION COEFFICIENT ARRAY
C
       DO 11 II=1,12
       BB(II)=0.0D0
       DO 11 JJ=1,12
   11  A(II,JJ)=0.0D0
       PPH1=CLAM-PHN+1.0D0
       SB=SH(BET)
       CB=CH(BET)
       A(1,1)=-SB
       A(1,2)=CB
       A(1,3)=CLAM*BET*SB-PPH*CB
       A(1,4)=-CLAM*BET*CB+PPH*SB
       A(2,1)=CB
       A(2,2)=-SB
       A(2,3)=-(CLAM*BET*CB+PPH1*SB)
       A(2,4)=CLAM*BET*SB+PPH1*CB
       A(11,9)=SB
       A(11,10)=CB
       A(11,11)=A(1,3)
       A(11,12)=-A(1,4)
       A(12,9)=CB
       A(12,10)=SB
       A(12,11)=-A(2,3)
       A(12,12)=A(2,4)
       DO 20 L=1,2
       GO TO (12,13),L
   12  II=3
```

```
      JJ=-4
      HB=BET*ZET
      GO TO 14
   13 II=7
      JJ=4
      HB=BET*CS
   14 SHB=SH(HB)
      CHB=CH(HB)
      HSHB=HB*SHB
      HCHB=HB*CHB
      A(II,5)=-SHB
      A(II,6)=-CHB
      A(II,7)=-CLAM*HSHB
      A(II,8)=-CLAM*HCHB
      A(II+1,5)=-CHB
      A(II+1,6)=-SHB
      A(II+1,7)=-CLAM*(HCHB+SHB)
      A(II+1,8)=-CLAM*(HSHB+CHB)
      A(II+2,5)=SHB
      A(II+2,6)=CHB
      A(II+2,7)=CLAM*HSHB-PPH*CHB
      A(II+2,8)=CLAM*HCHB-PPH*SHB
      A(II+3,7)=-SHB
      A(II+3,8)=-CHB
      II3=II+3
      DO 16 NR=II,II3
      DO 16 NC=5,8
   16 A(NR,JJ+NC)=-A(NR,NC)
   20 CONTINUE
      BB(3)=PNU
      BB(5)=CNU
      BB(7)=PNU
      BB(9)=CNU
      CALL DSIME(BB,AA,12,12,1,.000001,IER)
      KL=-4
      DO 22 KK=1,3
      KL=KL+4
      DO 22 LL=1,4
      KLL=KL+LL
   22 C(KK,LL)=BB(KLL)
C
C     INITIATE TRANSVERSE LOOP
C
      PAREN=2.0D0*CLAM-PHN-1.0D0
      DO 30 KIK=1,21
      IF(KIK-5) 600,605,610
  600 GO TO (601,601,607,607),KIK
  601 ET=ZET
      GO TO (602,603),KIK
  602 LL=1
```

```
      GO TO 611
  603 LL=2
      GO TO 611
  605 ET=-1.125D0
      GO TO 610
  607 ET=CS
      GO TO (30,30,608,609),KIK
  608 LL=2
      GO TO 611
  609 LL=3
      GO TO 611
  610 CONTINUE
      ET=ET+.125D0
  611 CONTINUE
      BE=BET*ET
      SBE=SH(BE)
      CBE=CH(BE)
      IF(KIK-5) 613,612,612
  612 CONTINUE
      IF(ET-ZET) 23,24,24
   23 LL=1
      GO TO 27
   24 IF(ET-CS) 25,25,26
   25 LL=2
      GO TO 27
   26 LL=3
   27 XM1=C(LL,1)*SBE+C(LL,2)*CBE+C(LL,3)*(CLAM*BE*SBE+CNU*
     1PPH*CBE)+C(LL,4)*(CLAM*BE*CBE+CNU*PPH*SBE)+DELT(LL)
      YM1=C(LL,1)*SBE+C(LL,2)*CBE+C(LL,3)*(CLAM*BE*SBE-PPH*
     1CBE)+C(LL,4)*(CLAM*BE*CBE-PPH*SBE)-DELT(LL)*CNU
      XYM1=C(LL,1)*CBE+C(LL,2)*SBE+C(LL,3)*(CLAM*BE*CBE-PNU*
     1PPH*SBE/2.)+C(LL,4)*(CLAM*BE*SBE-PNU*PPH*CBE/2.)
      DEF1=C(LL,1)*SBE+C(LL,2)*CBE+C(LL,3)*CLAM*BE*SBE+
     1C(LL,4)*CLAM*BE*CBE+DELT(LL)*PNU
  613 CONTINUE
      SHX1=C(LL,3)*CBE+C(LL,4)*SBE+DELT(LL)
      IF(KIK-5) 615,614,614
  614 CONTINUE
      SH1=C(LL,3)*SBE+C(LL,4)*CBE
      V1=C(LL,1)*CBE+C(LL,2)*SBE+C(LL,3)*(CLAM*BE*CBE+PPH1*
     1SBE)+C(LL,4)*(CLAM*BE*SBE+PPH1*CBE)
      VX1=C(LL,1)*SBE+C(LL,2)*CBE+C(LL,3)*(CLAM*BE*SBE+PAREN*
     1CBE)+C(LL,4)*(CLAM*BE*CBE+PAREN*SBE)-DELT(LL)
      J=KIK-4
      XM(J)=XM(J)+TM*XM1*SXAR
      YM(J)=YM(J)-TM*YM1*SXAR
      XYM(J)=XYM(J)+TM*XYM1*CXAR
      DEF(J)=DEF(J)+TD*DEF1*SXAR
      XSH(J)=XSH(J)+TSH*SHX1*CXAR
      YSH(J)=YSH(J)+TSH*SH1*SXAR
```

```
      XV(J)=XV(J)-TSH*VX1*CXAR
      YV(J)=YV(J)+TSH*V1*SXAR
  615 IF(KIK-5) 616,30,30
  616 CHEK(KIK)=CHEK(KIK)+TSH*SHX1*CXAR
   30 CONTINUE
      DEN=DEN+TM*SXAR
      DENO=DENO+TO*SXAR
      DENXS=DENXS+TSH*CXAR
      DENYS=DENYS+TSH
C
C     CALCULATE BEAM COEFFICIENTS
C
      DO 50 L=1,NG
      ETT1=BAB(L)
      ETT2=BAB(L+1)
      IF(ETT1-ZET) 32,40,40
   32 IF(ETT2-ZET) 33,33,35
   33 L1=1
      L2=1
      ET1(1)=ETT1
      ET2(1)=ETT2
      GO TO 48
   35 IF(ETT2-CS) 36,36,38
   36 L1=1
      L2=2
      ET1(1)=ETT1
      ET2(1)=ZET
      ET1(2)=ZET
      ET2(2)=ETT2
      GO TO 48
   38 L1=1
      L2=3
      ET1(1)=ETT1
      ET2(1)=ZET
      ET1(2)=ZET
      ET2(2)=CS
      ET1(3)=CS
      ET2(3)=ETT2
      GO TO 48
   40 IF(ETT1-CS) 41,44,44
   41 IF(ETT2-CS) 42,42,43
   42 L1=2
      L2=2
      ET1(2)=ETT1
      ET2(2)=ETT2
      GO TO 48
   43 L1=2
      L2=3
      ET1(2)=ETT1
      ET2(2)=CS
```

```
      ET1(3)=CS
      ET2(3)=ETT2
      GO TO 48
   44 L1=3
      L2=3
      ET1(3)=ETT1
      ET2(3)=ETT2
   48 CONMBN=0.0D0
      BTW=0.0D0
      BREA=0.0D0
      DO 49 LL=L1,L2
      CBE1=CH(BET*ET1(LL))
      CBE2=CH(BET*ET2(LL))
      SBE1=SH(BET*ET1(LL))
      SBE2=SH(BET*ET2(LL))
      DCBE=CBE2-CBE1
      DSBE=SBE2-SBE1
      EDCBE=ET2(LL)*CBE2-ET1(LL)*CBE1
      EDSBE=ET2(LL)*SBE2-ET1(LL)*SBE1
      CONMBN=CONMBN+C(LL,1)*DCBE+C(LL,2)*DSBE+C(LL,3)*(CLAM*
     1BET*EDCBE+(CNU*PPH-CLAM)*DSBE)+C(LL,4)*(CLAM*BET*EDSBE
     2+(CNU*PPH-CLAM)*DCBE)+DELT(LL)*(ET2(LL)-ET1(LL))*BET
      BTW=BTW+C(LL,1)*DSBE+C(LL,2)*DCBE+C(LL,3)*(CLAM*BET*
     1EDSBE-PHN*DCBE)+C(LL,4)*(CLAM*BET*EDCBE-PHN*DSBE)
      BREA=BREA+C(LL,3)*DSBE+C(LL,4)*DCBE+
     2DELT(LL)*BET*(ET2(LL)-ET1(LL))
   49 CONTINUE
      XMB(L)=XMB(L)+TMB*CONMBN*SXAR
      XYMB(L)=XYMB(L)+TMB*BTW*CXAR
      XVB(L)=XVB(L)+TM*BREA*CXAR
   50 CONTINUE
      IF (I-9) 100,501,501
  501 CONTINUE
      WRITE(3,200)
      WRITE(3,201) PH
      WRITE(3,202) WID
      WRITE(3,203) CLEN
      WRITE(3,204) I
      WRITE(3,217) IER
      WRITE(3,219)
      DO 91 KK=1,3
   91 WRITE(3,220) KK,C(KK,1),KK,C(KK,2),KK,C(KK,3),KK,
     1C(KK,4)
      WRITE(3,205) JJJ,EBRAT(JJJ)
      WRITE(3,207)
      WRITE(3,208)
      DO 92 LL=1,17
   92 DCOF(LL)=BDRAT*XM(LL)/DEN
      WRITE(3,230) (DCOF(LL),LL=1,17)
      DO 93 LL=1,17
```

```
 93 DCOF(LL)=BDRAT*YM(LL)/DEN
    WRITE(3,231) (DCOF(LL),LL=1,17)
    DO 94 LL=1,17
 94 DCOF(LL)=BDRAT*XYM(LL)/DEN
    WRITE(3,232) (DCOF(LL),LL=1,17)
    DO 95 LL=1,17
 95 DCOF(LL)=TTD*DEF(LL)/DEND
    WRITE(3,233) (DCOF(LL),LL=1,17)
    DO 96 LL=1,17
 96 DCOF(LL)=BDRAT*XSH(LL)/DENXS
    WRITE(3,234) (DCOF(LL),LL=1,17)
    DO 103 LL=1,4
103 BCOF(LL)=BDRAT*CHEK(LL)/DENXS
    WRITE(3,214) (BCOF(LL),LL=1,4)
    DO 97 LL=1,17
 97 DCOF(LL)=BDRAT*YSH(LL)/DENYS
    WRITE(3,235) (DCOF(LL),LL=1,17)
    DO 98 LL=1,17
 98 DCOF(LL)=BDRAT*XV(LL)/DENXS
    WRITE(3,236) (DCOF(LL),LL=1,17)
    DO 99 LL=1,17
 99 DCOF(LL)=BDRAT*YV(LL)/DENYS
    WRITE(3,237) (DCOF(LL),LL=1,17)
    WRITE(3,210)
    WRITE(3,211) (LL,LL=1,NG)
    TOT=0.
    DO 90 III=1,NG
    BCOF(III)=XMB(III)*TTM/DEN
 90 TOT=TOT+BCOF(III)
    WRITE(3,212) (BCOF(LL),LL=1,NG)
    WRITE(3,213) TOT
    TOT=0.
    DO 101 IB=1,NG
    BCOF(IB)=TTM*XYMB(IB)/DEN
101 TOT=TOT+BCOF(IB)
    WRITE(3,221) (BCOF(LL),LL=1,NG)
    WRITE(3,224) TOT
    TOTSH=0.
    DO 105 IB=1,NG
105 TOTSH=TOTSH+XVB(IB)
    TOT=0.
    DO 106 IB=1,NG
    BCOF(IB)=GN*XVB(IB)/TOTSH
106 TOT=TOT+BCOF(IB)
    WRITE(3,222) (BCOF(LL),LL=1,NG)
    WRITE(3,223) TOT
100 CONTINUE
150 CONTINUE
    GO TO 8
999 STOP
```

```
      END
C
C
C
C     HYPERBOLIC SINE FUNCTION SUBROUTINE
C
      DOUBLE PRECISION FUNCTION SH(U)
      DOUBLE PRECISION DEXP
      DOUBLE PRECISION U
      SH=(DEXP(U)-DEXP(-U))/2.0D0
      RETURN
      END
C
C
C
C     HYPERBOLIC COSINE FUNCTION SUBROUTINE
C
      DOUBLE PRECISION FUNCTION CH(U)
      DOUBLE PRECISION DEXP
      DOUBLE PRECISION U
      CH=(DEXP(U)+DEXP(-U))/2.0D0
      RETURN
      END
C
C
C
C     SIMULTANEOUS EQUATION SOLUTION SUBROUTINE
C
      SUBROUTINE DSIME(R,A,M,MM,N,EPS,IER)
      DIMENSION A(1),R(1)
      DOUBLE PRECISION R,A,PIV,TB,TOL,PIVI
      DOUBLE PRECISION DABS
      IF(M)23,23,1
C
C     SEARCH FOR GREATEST ELEMENT IN MATRIX A
C
    1 IER=0
      PIV=0.
      M2=(M-1)*MM+M
      NM=N*MM
      DO 3 L1=1,M
      DO 3 L2=1,M
      L=MM*(L1-1)+L2
      TB=DABS(A(L))
      IF(TB-PIV)3,3,2
    2 PIV=TB
      I=L
    3 CONTINUE
      TOL=EPS*PIV
C
```

```
C       START ELIMINATION LOOP
C
        LST=1
        DO 17 K=1,M
C
C       TEST ON SINGULARITY
C
        IF(PIV)23,23,4
     4  IF(IER)7,5,7
     5  IF(PIV-TOL)6,6,7
     6  IER=K-1
     7  PIVI=1./A(I)
        J=(I-1)/MM
        I=I-J*MM-K
        J=J+1-K
        DO 8 L=K,NM,MM
        LL=L+I
        TB=PIVI*R(LL)
        R(LL)=R(L)
     8  R(L)=TB
        IF(K-M)9,18,18
C
C       COLUMN INTERCHANGE IN MATRIX A
C
     9  LEND=LST+M-K
        IF(J)12,12,10
    10  II=J*MM
        DO 11 L=LST,LEND
        TB=A(L)
        LL=L+II
        A(L)=A(LL)
    11  A(LL)=TB
C
C       ROW INTERCHANGE AND PIVOT ROW REDUCTION IN MATRIX A
C
    12  DO 13 L=LST,M2,MM
        LL=L+I
        TB=PIVI*A(LL)
        A(LL)=A(L)
    13  A(L)=TB
        A(LST)=J
C
C       ELEMENT REDUCTION AND NEXT PIVOT SEARCH
C
        PIV=0.
        LST=LST+1
        J=0
        DO 16 II=LST,LEND
        PIVI=-A(II)
        IST=II+MM
```

```
      J=J+1
      DO 15 L=IST,M2,MM
      LL=L-J
      A(L)=A(L)+PIVI*A(LL)
      TB=DABS(A(L))
      IF(TB-PIV)15,15,14
   14 PIV=TB
      I=L
   15 CONTINUE
      DO 16 L=K,NM,MM
      LL=L+J
   16 R(LL)=R(LL)+PIVI*R(L)
   17 LST=LST+MM
C
C     BACK SUBSTITUTION AND BACK INTERCHANGE
C
   18 IF(M-1)23,22,19
   19 IST=M2+MM
      LST=M+1
      LST2=MM+1
      DO 21 I=2,M
      II=LST-I
      IST=IST-LST2
      L=IST-MM
      L=A(L)+.5
      DO 21 J=II,NM,MM
      TB=R(J)
      LL=J
      DO 20 K=IST,M2,MM
      LL=LL+1
   20 TB=TB-A(K)*R(LL)
      K=J+L
      R(J)=R(K)
   21 R(K)=TB
   22 RETURN
C
C     ERROR RETURN
C
   23 IER=-1
      RETURN
      END
```

APPENDIX B: COMPUTER PROGRAM FOR THE DETERMINATION OF LONGITUDINAL MOMENTS AND DEFLECTIONS IN ORTHOTROPIC PLATES

```
C      ORTHOTROPIC PLATE SOLUTION FOR MOMENTS AND DEFLECTIONS
C
       DIMENSION XM(17),DEF(17),DCOF(17),EBRAT(10)
     1 FORMAT(3F10.2)
     2 FORMAT(2I10)
     3 FORMAT(8F10.2)
   200 FORMAT('1   ',47X,'**  ORTHOTROPIC PLATE  **')
   201 FORMAT('0',40X,'STIFFNESS PARAMETER =',1PE20.4)
   202 FORMAT('0',40X,'WIDTH =                ',F20.2)
   203 FORMAT('0',40X,'SPAN =                 ',F20.2)
   204 FORMAT('0',40X,'NO. OF SERIES TERMS =',I20)
   205 FORMAT('0',40X,'LOAD POSITION',I2,'     E/B =',F10.3)
   207 FORMAT('0',67X,'** Y/B **')
   208 FORMAT('0QUANTITY')
   214 FORMAT('0DEFL. COEF.',17F7.3)
   218 FORMAT('0MOM. COEFF.',17F7.3)
   998 READ(1,1) ALF,WID,CLEN
       IF(ALF) 999,999,5
     5 READ(1,2) NTERM, NEB
       READ(1,3) (EBRAT(LL),LL=1,NEB)
C
C      INITIAL CALCULATIONS
C
       PI=3.14159
       THET=WID/(2.*CLEN)
       RT1=SQRT((1.+ALF)/2.)
       RT2=SQRT((1.-ALF)/2.)
       RT3=SQRT((1.+ALF)/(1.-ALF))
       RT4=SQRT(1.-ALF**2)
       RT5=SQRT(2.*(1.+ALF))
       RT6=2.*ALF/SQRT(2.*(1.-ALF))
       SIG=THET*PI
       PH=SIG*RT1
       GAM=THET*RT1
       DEL=THET*RT2
       ET=SIG*RT2
       CONK=SIG/RT5
C
C      LOAD LOOP
C
       DO 30 JJJ=1,NEB
       DEND=0.
       DENM=0.
       DO 7 L=1,17
       XM(L)=0.
       DEF(L)=0.
     7 DCOF(L)=0.
       PS=PI*EBRAT(JJJ)
C
C      PRIMARY SERIES LOOP
```

```
C
      HNEG=-1.0
      DO 25 L=1,NTERM,2
      HNEG=-HNEG
      OR=L
      SIOR=SIN(OR*PI/2.)
      SIOR=HNEG*SIOR
      DENM=DENM+SIOR/OR**2
      DEND=DEND+SIOR/OR**4
      SE=SIN(OR*ET)
      CE=COS(OR*ET)
      SHPH=SH(OR*PH)
      CHPH=CH(OR*PH)
      CHC1=CHPH*CE
      SHS2=SHPH*SE
      SHC3=SHPH*CE
      CHS4=CHPH*SE
      PAR1=RT1*SE-RT2*CE
      PAR2=RT1*CE+RT2*SE
      PAR3=ALF*SE+RT4*CE
      PAR4=ALF*CE-RT4*SE
      PAR5=CHPH-SHPH
      BRAK3=-SHC3+RT3*CHS4
      BRAK4=-CHC1+RT3*SHS2
      BRAK5=SHS2+RT3*CHC1
      BRAK6=CHS4+RT3*SHC3
      BRAK9=RT5*CHC1+RT6*SHS2
      BRAK10=RT5*SHC3+RT6*CHS4
      BRAK11=RT6*SHC3-RT5*CHS4
      BRAK12=RT6*CHC1-RT5*SHS2
      CONG=(2.*ALF+1.)*RT2*SHPH*CHPH
      CONH=(2.*ALF-1.)*RT1*SE*CE
      CONM=CONG-CONH
      CONN=CONG+CONH
      SHGPS=SH(OR*GAM*PS)
      CHGPS=CH(OR*GAM*PS)
      SDPS=SIN(OR*DEL*PS)
      CDPS=COS(OR*DEL*PS)
      CHS5=CHGPS*SDPS
      SHS6=SHGPS*SDPS
      CHC7=CHGPS*CDPS
      SHC8=SHGPS*CDPS
      BRAK1=CHC7*PAR1-SHS6*PAR2
      BRAK2=SHC8*PAR1-CHS5*PAR2
      BRAK7=CHC7*PAR3-SHS6*PAR4
      BRAK8=SHC8*PAR3-CHS5*PAR4
      CONA=PAR5*(BRAK1*BRAK3+BRAK7*BRAK9)
      CONB=PAR5*(BRAK2*BRAK4+BRAK8*BRAK10)
      CONC=PAR5*(BRAK2*BRAK5+BRAK8*BRAK11)
      CONF=PAR5*(BRAK1*BRAK6+BRAK7*BRAK12)
```

```
C
C       TRANSVERSE LOOP
C
        BET=-1.125
        DO 20 J=1,17
        BET=BET+.125
        GAB=BET    *GAM*PI
        DEB=BET    *DEL*PI
        EP=ABS(BET    *PI-PS)
        GAEP=GAM*EP
        DEEP=DEL*EP
        CHMGB=CH(OR*GAB)
        SHMGB=SH(OR*GAB)
        CMDB=COS(OR*DEB)
        SMDB=SIN(OR*DEB)
        CONK1=(CH(OR*GAEP)-SH(OR*GAEP))*(COS(OR*DEEP)+RT3*
       1SIN(OR*DEEP))
        BRAKK=CONA*CHMGB*CMDB/CONM+CONB*SHMGB*CMDB/CONN-CONC*
       1CHMGB*SMDB/CONN-CONF*SHMGB*SMDB/CONM+CONK1
        XM(J)=XM(J)+SIOR*BRAKK/OR
        DEF(J)=DEF(J)+SIOR*BRAKK/OR**3
   20   CONTINUE
        WRITE(3,200)
        WRITE(3,201) ALF
        WRITE(3,202) WID
        WRITE(3,203) CLEN
        WRITE(3,204) L
        WRITE(3,205) JJJ,EBRAT(JJJ)
        WRITE(3,207)
        WRITE(3,208)
        DO 21 LL=1,17
   21   DCOF(LL)=CONK*XM(LL)/DENM
        WRITE(3,218) (DCOF(LL),LL=1,17)
        DO 22 LL=1,17
   22   DCOF(LL)=CONK*DEF(LL)/DEND
        WRITE(3,214) (DCOF(LL),LL=1,17)
   25   CONTINUE
   30   CONTINUE
        GO TO 998
  999   STOP
        END
C
C
C
C       HYPERBOLIC SINE FUNCTION SUBROUTINE
C
        FUNCTION SH(U)
        SH=(EXP(U)-EXP(-U))/2.
        RETURN
        END
```

```
C
C
C
C     HYPERBOLIC COSINE FUNCTION SUBROUTINE
C
      FUNCTION CH(U)
      CH=(EXP(U)+EXP(-U))/2.
      RETURN
      END
```